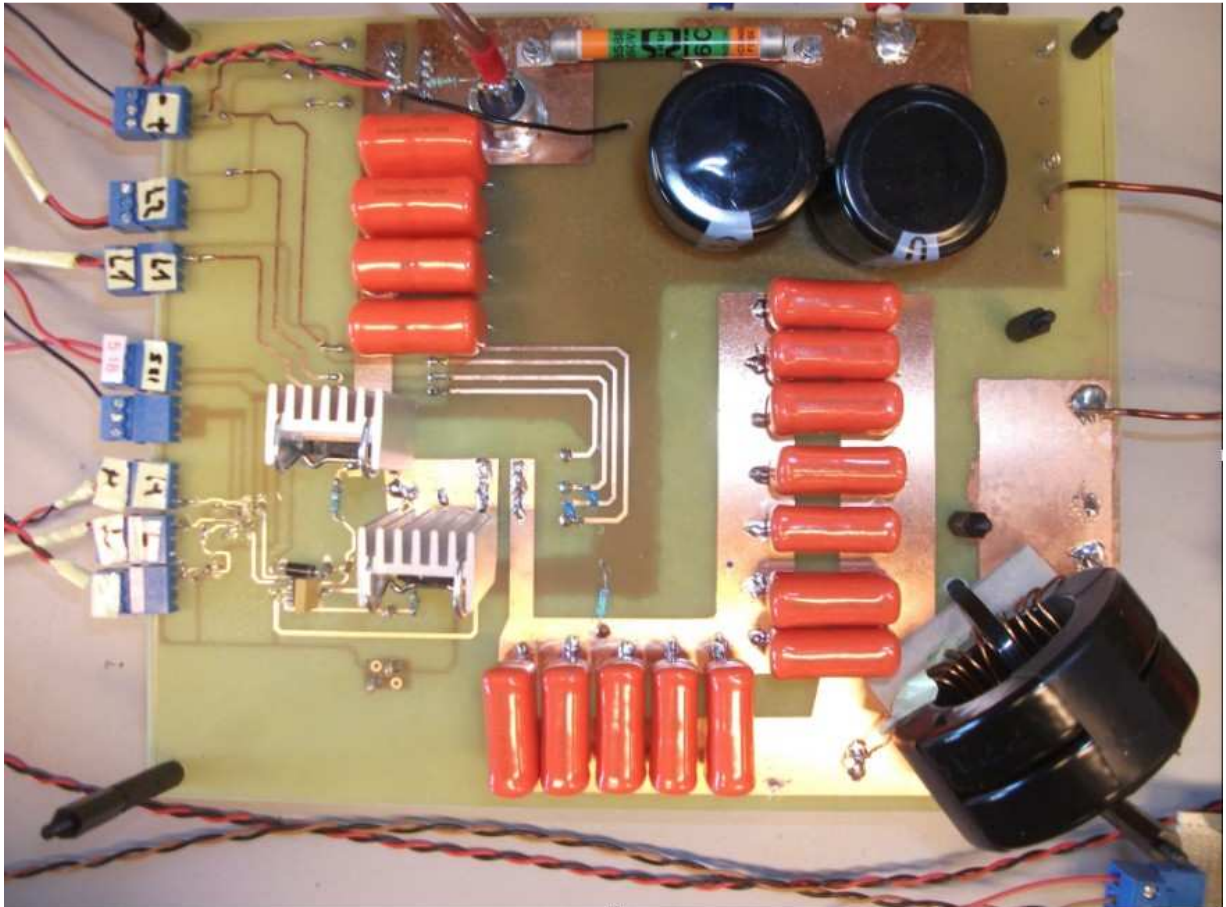


## Portable cancer treatment system using induction heating

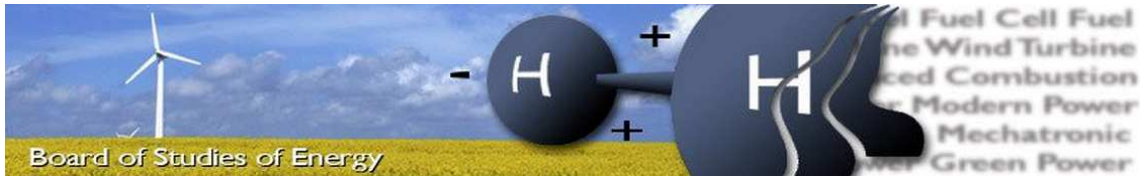


Master thesis, June 2012

Department of Energy Technology - Pontoppidanstræde 101

Aalborg University, Denmark





Title: Portable cancer treatment system using induction heating

Semester: Master Thesis

Project period: 4<sup>th</sup> September 2011 to 31<sup>st</sup> May 2012

ECTS: 50

Supervisors: Stig Munk Nielsen, Aalborg University

Johnny Wahl Jensen, Danfoss Drives A/S

Project group: WPS-1052

#### SYNOPSIS:

Andrés Suarez Gonzalez

Ángel Ruiz De Vega

This master thesis presents a resonant converter for future use in cancer treatment. This therapy is called Hyperthermia and takes advantage of the induction heating to burn the cancer cells. One high frequency inductor will produce the induction heating getting fed by an electronic converter. The topology of the converter is half bridge and the inductor is installed inside a resonant tank. The proposed converter is simulated and implemented in the laboratory. The current produced by the inductor is controlled by the switching frequency of the MOSFETS and this is obtained by a PWM signal produced by a microcontroller. To control the whole loop a digital controller was implemented inside the microcontroller, measuring the current in the output of the inductor and taking a reference from the user, it will produce a corrective signal that will generate an adequate PWM signal for the specifications in the reference. Moreover a crowbar protection circuit is designed with a digital control that will disconnect the system in case that a failure comes up. All the setup is implemented in the laboratory. Test results from the setups are discussed in the report.

Copies: 3

Pages: 83

Appendix: 4

Supplements: CD-ROM

**By signing this document, each member of the group confirms that all participated in the project work and thereby all members are collectively liable for the content of the report.**



# SUMMARY

---

The main focus of the thesis is to design, simulate and implement in the laboratory the resonant converter. The resonant converter topology used for the present thesis is half bridge with resonant tank. This resonant tank is made by means of capacitors and one inductor which is denominated during all the report as work coil. Through this work coil flows high current at high frequency which provides an electromagnetic field. This electromagnetic field is used in order to heat the tumor cells. If the tumor is localized and is not on the superficial tissues of the patient some metal seeds, called work piece in the introduction of the present thesis, must be used in order to conduct the electromagnetic field, and thus, generated the desired heat in order to destroy the cancer cells.

This treatment is known as hyperthermia and the goal for the future is to use the converter designed at the present thesis in this medical application. The medical and bioengineering references used in this thesis mention that the working frequencies for hyperthermia applications is in the range of radio frequency and microwave. Radio frequency was the selected switching frequency.

The present report is divided into nine chapters. First six chapters are focused in a brief explanation about hyperthermia therapy, design and explanation of the function of the resonant converter, desing of the control system and microcontroller programming, design of the inductors and design and explanation of the crowbar protection circuit respectively. The next two chapters are about the tests which were run at the laboratory about crowbar protection system and the converter. Along these chapters are discussed the different problems related to the development of the thesis and the solutions that were implanted in order to solve the problems and achieve the goals. Finally the last chapter the conclusions and future work.

Simulations: The resonant converter was simulated by means of LTspice. Several measurements have been taken like voltage and current through the power mosfets, current at the impedance matching and also current at the work coil.

The control system of the converter, which was implemented in the microcontroller, was previously simulated by means of MATLAB/SIMULINK-PLECS. Moreover these programmes were used to simulate likely malfunction events at the converter.

# PREFACE

---

This present Master Thesis, entitled "Portable cancer treatment using induction heating", is written by group WPS4-1052 formed by two students in the 4th Master semester at the Institute of Energy Technology, Aalborg University, Denmark. The project period is from 4<sup>th</sup> September 2011 to 31<sup>st</sup> May 2012. The report consists of two parts, a main part and an appendix part. The project has been carried out within the area of Power Electronics.

The references to studied literature are shown in form of a number, placed into brackets. The format of equation is (X,Y), where X is number of chapter and Y is the number of equation in that chapter. The figures are numbered Figure X.Y, in which X,Y are having the same significance as for the equations.

The appendixes are labeled with capital letters, put in alphabetical order. The enclosed CD contains the report in Adobe PDF format, documentations used throughout the report, Simulink and LTspice Models.

The authors would like to give special thanks to their supervisors Stig Munk Nielsen and Jonnhy Wahl Jensen for their support and valuable information provided throughout the project development period and having always shown especial interest about the knowledge achieved by authors. The authors are grateful for the help offered by Walter Neumayr at the laboratories facilities and also to their colleague Emmanouil Dimopoulos for sharing with them his experience in the area of Power Electronics.

Special mention should be done to the author's families for all the patient, support and affection given during this period, doing the study abroad easier.

# TABLE OF CONTENTS

---

1.	Introduction .....	1
1.1.	Hyperthermia .....	1
1.1.1.	Types of hyperthermia .....	1
1.1.2.	Types of application of the treatment with hyperthermia .....	2
1.1.3.	EMF generated and absorption in the body .....	2
1.1.4.	Frequency election .....	3
1.2.	Problem definition .....	4
1.3.	Objectives and limitations.....	4
1.4.	Project outline .....	5
2.	Converter Designing.....	7
2.1.	Half bridge topology.....	7
2.2.	Resonant Circuit .....	7
2.2.1.	Series Parallel Resonant Inverter .....	7
2.2.1.1.	Impedance matching.....	8
2.2.2.	Parameter Calculation.....	10
2.2.2.1.	Parallel Circuit .....	10
2.2.2.2.	Series Circuit.....	10
2.2.3.	Simulation Results .....	11
2.3.	Switching mosfet.....	11
2.3.1.	Bootstrap drive.....	12
2.3.2.	Bootstrap elements calculations.....	13
2.4.	Mosfet and driver losses .....	14
2.4.1.	Calculation of mosfet driver losses .....	14
2.4.2.	Calculation of power mosfet losses .....	15
2.4.3.	Simulation and calculation of power mosfet loss .....	17
2.4.4.	Maximum operating point at working conditions .....	19
2.4.5.	Simulation and calculation of power mosfet loss with low quality factor at the work coil 20	
2.5.	Heat sink design .....	22
3.	Control Designing .....	25

3.1.	Frequency analysis .....	25
3.2.	Control Design .....	26
3.3.	Control Implementation and Simulation .....	28
3.3.1.	Discrete Correlation .....	33
4.	Microcontroller Programming .....	35
4.1.	Control Loop Considerations .....	35
4.2.	Main structure .....	35
4.2.1.	Init User Inputs .....	36
4.2.2.	Init ADC .....	36
4.2.3.	Init PWM .....	37
4.3.	Interrupts .....	37
4.3.1.	A/D Interrupt .....	37
4.3.2.	Switch Interrupt .....	38
4.4.	PID Control and PWM signal Generator .....	39
4.4.1.	PID Control .....	39
4.4.2.	PWM function .....	41
4.5.	Simulation results .....	42
4.6.	Conclusions .....	42
5.	Inductor Designing .....	43
5.1.	Core Inductor Procedure .....	43
5.1.1.	Power Losses .....	44
5.2.	Air Coil Inductor Procedure .....	46
5.2.1.	Core Inductor Procedure .....	46
6.	Protection system .....	49
6.1.	Study of malfunction events .....	49
6.1.1.	Short-circuit high side mosfet .....	50
6.1.2.	Short-circuit low side mosfet .....	51
6.1.3.	Short-circuit both mosfets .....	52
6.1.4.	Conclusion from simulations .....	52
6.2.	General system protection .....	53
6.2.1.	Overcurrent .....	53
6.2.2.	Watchdog .....	53
6.3.	Crowbar protection design .....	53
6.3.1.	SCR .....	54

6.3.2.	Fuse .....	55
6.3.3.	Inductor .....	57
6.3.4.	Discharging path.....	57
6.4.	Short circuit current .....	58
6.4.1.	Calculation of resistance of the track of PCB .....	58
6.4.2.	Dynamic impedance of SCR.....	58
6.4.3.	ESR, fuse and cable resistance .....	59
6.4.4.	Short circuit current .....	59
6.5.	Logic circuit-Trigger signal.....	59
6.5.1.	Turning off mosfet.....	61
6.5.2.	Timing chart.....	61
7.	Laboratory work- Digital control circuit and crowbar protection circuit.....	63
7.1.	Digital control-First design .....	63
7.1.1.	Results of first digital control .....	64
7.1.2.	Triggering SCR.....	64
7.1.3.	Conclusions.....	66
7.2.	Digital control-SCR.....	67
7.2.1.	Digital control-longer pulse width.....	67
7.2.2.	Triggering SCR. ....	67
7.2.3.	Conclusions.....	70
7.3.	Test above 50 volts.....	71
7.3.1.	Triggering SCR.....	71
7.4.	Test- SCR+inductor .....	73
7.4.1.	SCR-inductor test.....	73
7.4.2.	Fuse .....	73
8.	Laboratory work: Converter .....	75
8.1.	Setup .....	75
8.2.	Testing work coil .....	76
8.2.1.	Frequency deviation - Explanation.....	79
8.2.2.	Validation of new frequency with laboratory parameters .....	79
9.	Conclusions and future work .....	81
9.1.	Future work.....	81
	Bibliography .....	852
	Appendix A List of components .....	85

Appendix B Selecting capacitor for inverter.....	87
Appendix C Dspic program .....	91
Appendix E Inductor design.....	985

# LIST OF FIGURES

---

Figure 1-1 Hyperthermia treatments.....	1
Figure 1-2 Spectrum of frequencies.....	3
Figure 1-3 Inductive heating scheme (3).....	4
Figure 2-1 Schematic of the circuit implemented.....	8
Figure 2-2 Resonant circuit without impedance matching.....	9
Figure 2-3 Resonant circuit with impedance matching .....	9
Figure 2-4 Current and voltage waveforms in the MOSFET without impedance matching .....	9
Figure 2-5 Current and voltage waveforms in the MOSFET with impedance matching.....	9
Figure 2-6 Current output in the work coil .....	11
Figure 2-7 Voltage and current output waveforms of the half-bridge converter.....	11
Figure 2-8 $V_s$ _floating reference for high side mosfet.....	12
Figure 2-9 Bootstrap circuit implemented with mosfet driver and power mosfets. (14).....	12
Figure 2-10 Gate-source voltage against total gate charge of the power mosfets (15) .....	15
Figure 2-11 Switching characteristics (linearized). A.Switching signal. B.Switch waveforms. ...	15
Figure 2-12 Schematic of the circuit simulated in LTspice.....	17
Figure 2-13 Results of the simulations (Voltage-red and current-blue) .....	18
Figure 2-14 Result of power loss and current at high side mosfet .....	18
Figure 2-15 Results of the simulations (Voltage-red and current-blue) .....	21
Figure 2-16 Result of power loss and current at high side mosfet .....	21
Figure 2-17 Cross section profile of semiconductor device (10).....	22
Figure 2-18 Equivalent circuit based on thermal resistance (10) .....	22
Figure 2-19 Heat sink with and without thermal grease (18) .....	23
Figure 3-1 Current paths in the resonant circuit.....	25
Figure 3-2 Bode Diagram of the resonant current.....	25
Figure 3-3 Bode Diagram of the resonant current for different values of Q .....	26
Figure 3-4 Block diagrams of the controller and the plant .....	27
Figure 3-5 Schematic of the system implemented .....	28
Figure 3-6 SIMULINK implementation of the system.....	29
Figure 3-7 PLECS model of the converter.....	29
Figure 3-8 SIMULINK model of the Controller .....	29
Figure 3-9 Values of reference and measured current of the controller.....	30
Figure 3-10 Traces of the output current and frequency range .....	31
Figure 3-11 Current Waveform and frequency for a zero current reference .....	32
Figure 4-1 Schematic of the microcontroller functions inside the system .....	35
Figure 4-2 Flow-chart of function Main .....	36
Figure 4-3 Flow-chart of the operation mode.....	38
Figure 4-4 Flow-chart of the PID function.....	41
Figure 4-5 Scope waveform with 140kHz.....	41
Figure 4-6 Scope waveform with 160kHz.....	41
Figure 4-7 Scope signals of the PWM waveforms.....	42
Figure 4-8 Image of the microcontroller programmed.....	42
Figure 5-1 Arbitrary terminal waveforms (30) .....	44

Figure 5-2 Core Loss Density Curves of the Core Material (31) .....	44
Figure 5-3 Different configurations of air coil inductors (32) .....	46
Figure 5-4 Plot of all the possible values of the inductor.....	47
Figure 5-5 Picture of the work coil .....	48
Figure 6-1 Implemented circuit for short-circuit simulation.....	49
Figure 6-2 Current when occurring short circuit at high side mosfet .....	50
Figure 6-3 Current when occurring short circuit at low side mosfet .....	51
Figure 6-4 Current when occurring short circuit at both mosfets .....	52
Figure 6-5 Hall sensors in the circuit .....	53
Figure 6-6 Crowbar protection circuit.....	54
Figure 6-7 SCR triggering characteristics (35) .....	55
Figure 6-8 Prospective current against pre-arcing time of fuse (36) .....	56
Figure 6-9 Discharging path (red).....	57
Figure 6-10 SCR on state electrical characteristics (35) .....	58
Figure 6-11 Schematic of digital control .....	60
Figure 6-12 Logic control- turn off mosfets .....	61
Figure 6-13 Timing chart .....	62
Figure 7-1 First digital control .....	63
Figure 7-2 Digital control signals .....	64
Figure 7-3 Schematic of the setup build in the laboratory .....	65
Figure 7-4 Trigger and SCR signals (5V).....	65
Figure 7-5 Trigger and SCR signals (10V).....	66
Figure 7-6 Trigger and SCR signals (30V).....	66
Figure 7-7 Schematic of new delay circuit .....	67
Figure 7-8 New pulse width .....	67
Figure 7-9 Trigger and SCR signals (5V).....	68
Figure 7-10 Trigger and SCR detailed signals (5V).....	68
Figure 7-11 Trigger and SCR signals_new R_gate (5V).....	69
Figure 7-12 Pulse width with R-gate=20 .....	69
Figure 7-13 Current and voltage across SCR applying 10 and 20 V.....	70
Figure 7-14 Current and voltage across SCR applying 30 and 40 V.....	70
Figure 7-15 Current and voltage across SCR applying 50 V .....	70
Figure 7-16 Schematic of the setup build in the laboratory .....	71
Figure 7-17 Current and voltage across SCR applying 50 V .....	72
Figure 7-18 Figure 7-19 Current and voltage across SCR applying 30 and 40 V .....	72
Figure 7-20 Figure 7-21 Current and voltage across SCR applying 150 and 200 V .....	72
Figure 7-22 Width of short circuit current .....	73
Figure 7-23 Fuse blown up .....	73
Figure 8-1 Setup buildt in the laboratory.....	75
Figure 8-2 Setup built in the laboratory II.....	76
Figure 8-3 General setup.....	76
Figure 8-4 Current at work coil (140.7KHz).....	77
Figure 8-5 Current at work coil (138.3).....	77
Figure 8-6 Current at work coil (148 KHz).....	78
Figure 8-7 Current at work coil (149.3KHz).....	78

Figure 8-8 Detailed current at work coil (149.3KHz).....	79
Figure 8-9 simulated schematic .....	80
Figure 8-10 Simulated current at work coil.....	80
Figure B. 1 Voltage against frequency.....	87
Figure B. 2 Alternating voltage limit depending on frequency .....	88
Figure B. 3 Variation of voltage and frequency depending on temperature.....	89
Figure B. 4 Dissipation factor for different dielectrics .....	90
Figure B. 5 Moisture absorption for different dielectrics .....	90
Figure C. 1 Equivalent circuit with parasitic inductance .....	91
Figure C. 2 Equivalent circuit with parasitic inductance and DC-Link .....	92
Figure C. 3 Setup built in the laboratory .....	93
Figure C. 4 Voltage and current with thin film capacitor .....	93
Figure C. 5 Voltage and current with electrolytic capacitor.....	93

# LIST OF TABLES

---

Table 2.1 Rise and fall times of power mosfet SPA11N60C3 .....	18
Table 2.2 Rise and fall times of power mosfet TK40J60U .....	19
Table 2.3 Electrical characteristics of power mosfet TK40J60U .....	19
Table 5.1 Obtained values of the work coil.....	47
Table 8.1 Parameter values of the components at the simulation.....	80

# 1.Introduction

*This chapter presents an introduction to the report. Medical basics principles are briefly described in first section, followed by the problem definition, objectives and limitations and finally the project outline.*

## 1.1. Hyperthermia

One of the biggest disadvantages of the treatment of cancer is the painful effects caused in the patients. Many researches have been dedicated in order to avoid or, at least, reduce this suffering. At this point is where the Hyperthermia has been developed (1).

Hyperthermia is a good alternative technique to the cancer treatment because it is one of the less invasive techniques. Also is an appropriate treatment when the volume of the tumor makes difficult surgery or the function preservation of the organ is needed. It can be used as a lonely treatment or in combination with radiotherapy or chemotherapy.

The process is also attractive because is relatively easy to implement: Particles of metal are heated through a magnetic field produced by a high frequency current. These particles of metal are installed close to the tumor in order to burn the cancer cells. It is well known that cancer tissues are more sensitive to temperature than the normal cells; in fact, cancer cells are killed when heated to more than 42.5 °C for a certain period of time (2). The hyperthermia working principle takes advantages of latter statement and by means of electromagnetic field (EMF) generated.

The EMF is generated by a converter and usually a work coil. This arrangement should produce high frequency currents. The converter and work coil should be properly tuned, focused and placed at the right distance, thus produces a temperature increment at the desired point: where the tumor is located. In short, the appropriate increment of the temperature produces the kill of the cancer tissue.

The main drawback is that cannot be used for some types of cancer like colorectal cancer, soft tissue sarcomas, head and neck nodules, deep-seated tumors... (3).

### 1.1.1. Types of hyperthermia

The temperature generated and time exposed for the patient to the EMF depends on some factors, such as, location of the cancer, volume of the tumor or types of application of the treatment (local, external, internal, whole body). Next table defines the range of temperature and time to remove the cancer tissue causing no damage or minimal damage to health cells and tissues (3).

Treatment	Temperature Range	Time Range
Long-term low temperature hyperthermia	40-41 °C	6-72 hr
Moderate-temperature hyperthermia	42-45 °C	15-60 min
High temperature hyperthermia or thermal ablation	>50 °C	4-6 min

**Figure 1-1 Hyperthermia treatments**

### **1.1.2. Types of application of the treatment with hyperthermia**

As it was said before, there are some types of application of the treatment and different technologies to destroy the cancer tissue (1).

- Local hyperthermia: Applied for small tumors. In this case higher temperature than in other types of hyperthermia is needed to kill all the cancer cells. If the tumor is located near the body surface, it is only necessary the converter which provides the high frequency currents, but if the tumor is located deeper (normally inside the liver, kidneys or lungs) a thin needle, probe, antenna or capacitive/inductive mediators such as ferromagnetic rods or thermo seeds (4) should be placed to confine the EM energy and kill through the heat the cancerous cells.
- Regional hyperthermia: it used to heat a part of the body, such as organ, limb or body cavity. Usually it is not used as lonely technique but it is combined with chemotherapy or radiotherapy.
- Whole body hyperthermia: it is under study and it is considered to be used as a complement of chemotherapy to do the treatment more effective for patients with metastatic cancer.

### **1.1.3. EMF generated and absorption in the body**

The EMF generated by the converter should be within a frequency range. The frequencies used for hyperthermia are inside the margins of radiofrequency (hundreds of KHz to few MHz) and microwaves (hundreds of MHz to 10 GHz). These frequencies belong to the non-ionizing frequencies as can be seen in the Figure 1-2.

Although radiofrequency waves do not belong to the group of ionizing frequencies, it should be taking into account that the time of exposition is an important parameter. Exposition to frequencies over 100 KHz could produce significant absorption of energy and undesired effects in the body when the exposition is longer than it should be. The time and energy absorbed in a safety range are defined in some guidelines. In the case of Europe, the reference is the International Commission on Non-Ionizing Radiation Protection (ICNIRP).

For hyperthermia the guideline used is "Guidelines for limiting exposure to time-varying electric, magnetic, and electromagnetic fields (up to 300 GHz)". In this guideline is explained which parameters depends on the energy absorption in the body. These parameters are briefly explained in following points:

- Frequency: it excites the cells and generates heat.
- Intensity of the beam: factor to determine how much energy is available to be transferred.
- Duration of exposure: the longer duration of exposure, the greater amount of energy that will be absorbed (5).

All previous parameters must be studied by medical professionals, and they will be the only one who will decide how much will be the intensity of the beam and the duration of the exposure.

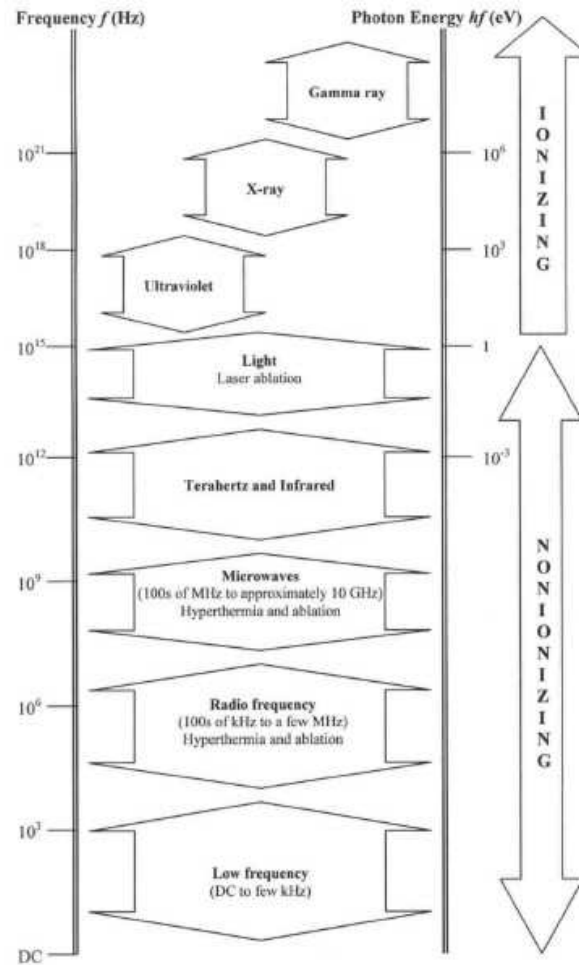


**Figure 1-2 Spectrum of frequencies**

#### 1.1.4. Frequency election

In order to choose the adequate frequency of the current at the work coil, some of the large amount of papers and books related to hyperthermia treatment were used as a reference to design and implement the converter in the laboratory. Next paragraph shows 3 references which mentioned that radiofrequency and microwave are suitable waves for hyperthermia treatment.

In (1) is mentioned that “heat is usually applied using high frequency energy waves from a source outside the body (such as microwave or ultrasound source). By contrast, in order to treat deeper tumors within the body, the RF wave is used. Moreover microwave techniques are used by means of antennas inserted into hollow tubings, ferromagnetic seed implants for delivering thermal energy to deep seated tumors. These frequencies allow the tumor to be heated to higher temperatures than external techniques”. In (6) is also mentioned that radiofrequency treatment is suitable to heat deep tumor. In (7), at chapter 93 radiofrequency hyperthermia in cancer therapy, it is deeply explained in medical terms the effects and how to apply the correct treatment by means of radiofrequency waves.

Therefore, the chosen frequency was inside the range of radiofrequency. The value of the switching frequency will be around 140 KHz.

## 1.2. Problem definition

In the last decades medicine is not only focused in the cure of diseases, also in the fast recovery and minimal invasion of the patient. Hyperthermia makes the cancer treatment easier for the patient. It removes all the pain that patient has to support with chemotherapy and radiotherapy. Moreover it improves the quality of life because it does not produce possible psychology effects, as the head drop. As it is well known, if the patient is positive with the treatment the probability to get better soon increased (8).

So hyperthermia is a good alternative therapy because it produces minimal effects in the patient. In order to achieve that objective, there are various devices to produce EMF necessary to heat the tumor, but this project is only focused in inductive heating. Next figure shows the how can be applied the hyperthermia treatment by means of the induction heating.

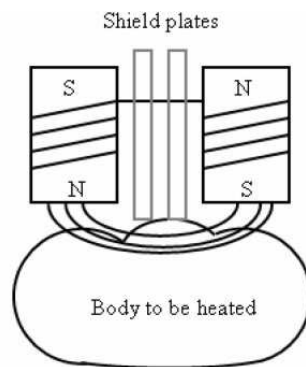


Figure 1-3 Inductive heating scheme (3)

The time-varying magnetic field produced by a converter penetrates the body and causes an eddy current. Such as a result, Joule's heat is produced and the piece of metal is warmed so it is possible kill the tumor.

The purpose of this project is developed a converter, which will be able to produce high frequency currents in order to heat a piece of metal sited inside of the magnetic field produced by a work coil when the mentioned high frequency currents pass through it.

## 1.3. Objectives and limitations

The objectives of this thesis are:

- Design the converter which will be used for portable cancer treatment.
- Simulations of the converter.
- Build in the laboratory the prototype of the converter.
- Design and build in the laboratory a protection system for the converter.
- Achieve in the work coil the resonant current.

The thesis is limited by several different factors:

- No animal, no human will be used to test the converter.
- No piece of metal will be used to test the converter.

## 1.4. Project outline

The report structured in nine chapters.

- The first chapter may be seen as an introduction of hyperthermia therapy for not medical experts. The chapter is followed up by the problem definition and the objectives of the current thesis. The limitations are also presented.
- The second chapter different facts related to the converter design. In the first part of the chapter is explained the behaviour and the design considerations about the topology of the converter. The second part of the chapter shows different aspects as switching design, losses at the switching devices and thermal management.
- The third chapter addresses the frequency analysis of the converter and the its response, depending on the quality factor of the work coil. Taking that into consideration a control system was implemented and explained inside this chapter. Finally a simulation of that implementation is shown and explained.
- The Microcontroller programming and configuration is explained and developed inside the chapter four. All the functions needed to obtain the PWM signal for the converter are explained inside with a brief explanation of the programming tools required for this implementation.
- The inductors design procedure is explained in chapter five. A brief explanation is shown inside the chapter, being the MATLAB scripts required for the designing inside the appendixes.
- The sixth chapter describes the protection designed to protect the converter in case of malfunction. The calculations and how it operates is also included in this chapter.
- In seventh chapter is presented different tests run in the laboratory. First test are related to the first designs for the converter and the explanation about why they did not work adequately. Along the chapter also is described the adopted solutions and final result of the new implementations.
- Eight chapter shows the results related to the currents at the work coil.
- Ninth chapter: Conclusions and future work



## 2. Converter Designing

*In this chapter a brief description of the topology chose for the converter is explained. Moreover, the switching design, power losses of the mosfets and heat sink design is also explained.*

### 2.1. Half bridge topology

The topology chose for the inverter was a half bridge. This topology is commonly used in induction heating systems, whenever the required output power is within the range small to medium power capacity (9). The main advantages are the simple constitution of the circuit, the low number of components, and thus, the low cost, but the most important is that as a single-phase inverter is easily controllable.

This inverter is supplied by DC voltage and provides as an output square waveform. The chosen switches for this inverter were mosfets, because they offer faster switching than IGBTs. The two mosfets will work with the same duty cycle of 50% and will not conduct at the same time in order to avoid shoot-through.

When using induction heating, the circuit is not only formed by two mosfets, but it is necessary to implement the circuit by means of a resonant circuit. See next point for further explanations.

### 2.2. Resonant Circuit

The output of an induction heating circuit is the work coil, which is used to generate the desired EMF. In practice, the work coil is used to form a resonant circuit. This fact offers some benefits, as an example it can be mentioned that it reduces the losses in the switches due to the fact that the zero-current switching strategy is possible to be used. It consists in switching the MOSFETs when the sinusoidal waveform passes through zero (10). This strategy is quite advantageous due to the fact that the size of the converter is reduced. The switches do not need to withstand high currents during the switching and for that reason the switching stress is reduced. As mentioned before, the switching losses are reduced, and as result, the EMI associated with the switch-mode converters is diminished.

There are two main topologies to design a resonant circuit: series resonant tank and parallel resonant tank. The circuit chose was a combination of both topologies in order to have the desirable characteristics of series and parallel resonant inverters.

#### 2.2.1. Series Parallel Resonant Inverter

The picture below shows the final circuit used to simulate the behaviour of the inverter an also implement in the laboratory.

It is formed by two inductances and two capacitors. The resistor simulates the losses of the circuit due to the imperfection of the capacitors and the coils, which have parasitic resistance. That resistance is a combination of the resistance of the tank capacitor and the resistance of the work coil:

$$R = R_w + R_s \quad (2.1)$$

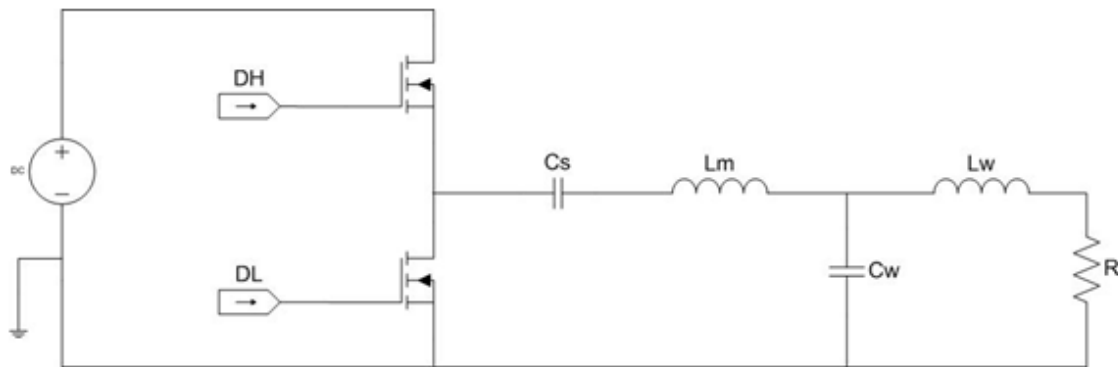


**Figure 2-1 Schematic of the circuit implemented**

In order to be able to produce the induction heating, it is necessary high currents flowing through the work coil. Installing the work coil inside a parallel resonant circuit is possible to magnify (increase) the currents, and as an advantage of this disposition, the mosfets does not have to carry the full circulating current, which flows through the work coil. The capacitance will resonate with the work coil at the intended frequency, and as a result the current will be increased; meanwhile the inverter does not work with such level of current. In the preceding picture,  $L_w$  and  $C_w$  correspond to the work coil and the capacitor in parallel resonating at the desire frequency.

In addition, it should be mention that the inverter operated better with higher voltages and lower currents. For this reason a series resonant circuit was installed before the parallel one. In other words, the series part of the circuit increases the voltage keeping low the currents and the parallel part does the opposite, obtaining the desired high value of the current at the work coil.

Associated with the values for the series circuit an impedance matching was calculated too and added to the final disposition. In the circuit above  $C_m$  corresponds to the value of the capacitance for the impedance matching and  $L_m$  corresponds to the inductance.

#### **2.2.1.1. Impedance matching**

The impedance matching refers to the sub-circuit installed between the output of the half bridge and the work coil. Its function is to transform the relatively large loss resistance across the tank circuit to a lower value that better suits the inverter attempting to drive it (11).

The series inductance placed before the tank capacitor is used to prevent the high currents at the output of the half bridge. The absence of this series inductance along with the squared voltage, which carries all the harmonics, will produce those high currents. The series capacitor or DC-blocking capacitor is used to remove the DC component of the squared waveform. It should be also noticed that the reactance of the tank capacitor decreases when the frequency increases, and that fact produces higher currents in the switching transitions. Put differently, if there is not install the impedance matching, the equivalent input impedance of the resonant tank will be small due to the small impedance of the tank capacitors. This fact will cause that this high current will be also present at the power mosfets, and thus, there will be an excess of power dissipation at the power mosfets, which makes more difficult the thermal management, the converter is less efficient and it is more expensive the implementation.

Previous statement can be explained as follows:

Considering the circuits from the figures 2-2 and 2-3, the first equation represents the output current of the half bridge when the converter has not installed the impedance matching and the second equation represents the same current when the converter has installed the impedance matching. It can be seen that the expression that relates the voltage with the current is as follows in each case:

$$I_{total1} = \frac{V_1}{\frac{Z_{cw}(Z_{Lw} + R)}{Z_{cw} + Z_{Lw} + R}} \quad I_{total2} = \frac{V_1}{(Z_{Lm} + Z_{Cm}) + \frac{Z_{cw}(Z_{Lw} + R)}{Z_{cw} + Z_{Lw} + R}} \quad (2.2)$$

Considering the impedances as follows:

$$Z_L = j\omega L \quad Z_L = \frac{1}{j\omega C} \quad (2.3)$$

As the impedance in the first case is removed, the current demanded by the circuit is bigger than in the second circuit. The addition of the impedance matching makes larger the denominator of the expression 2.2 attempting a larger current value.

Next simulations show the both cases: inverter without the implementation of impedance matching and the inverter with the implementation of the impedance matching. The schematic of the simulated cases is depicted in the next figures. The simulations were run with LTspice.

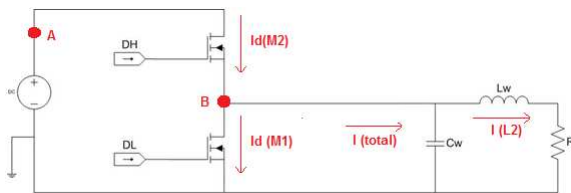


**Figure 2-2 Resonant circuit without impedance matching**

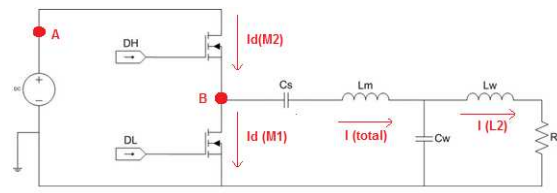


**Figure 2-3 Resonant circuit with impedance matching**

In the forthcoming figures are depicted the results of the simulations. In the figures are represented the values of the voltage V (A,B) and the current at Id (M2). The total current at the impedance matching is given by:  $I(\text{total}) = I_d(M2) - I_d(M1)$ . In the simulation is only represented the current when conducting high side mosfet in order to show clearly the current spikes.

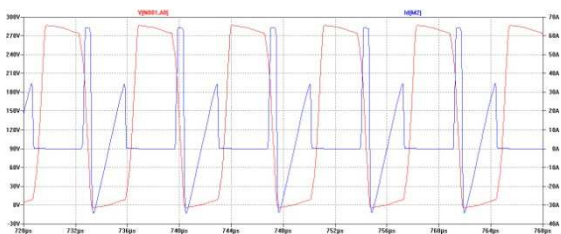


**Figure 2-4 Current and voltage waveforms in the MOSFET without impedance matching**

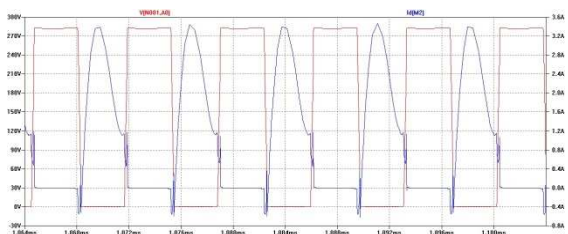


**Figure 2-5 Current and voltage waveforms in the MOSFET with impedance matching**

If there is not impedance matching the inverter will charge and discharge rapidly the tank capacitor producing high current spikes at the switching instants, it can be appreciated in the left picture, where the circuit does not have the matching network and the range of current reaches the 70A (Blue line), meanwhile in the other picture, where the circuit has install the

impedance matching, the value of currents are below 4A. In both cases the currents in the output inductor were close to 300A.

The explanation to that improvement is that adding the matching network, all the harmonics that the voltage waveform is carrying are filtered and the input impedance to resonant circuit has increased its value, reducing the high current spikes.

### 2.2.2. Parameter Calculation

The procedure of each part of the circuit is explained making a separation between the parallel and the series circuit.

#### 2.2.2.1. Parallel Circuit

The value of the work-coil was taken from (12) as a reference. This value was possible to achieve it in the laboratory with an air coil inductor and it was:

$$\begin{aligned} L_w &= 1.4 \mu\text{H} \\ R &= 5 \text{ m}\Omega \end{aligned}$$

As those values should resonate to the intended frequency, the values were obtained with the next formula:

$$\omega_0 = \frac{1}{\sqrt{L_w * C}} \quad (2.4)$$

Where:

$\omega_0$ = radian frequency, which is equals to  $2*\pi*f$

$L_w$ = work coil

$C_w$ = tank capacitance

Finally the capacitance value is given by:

$$C_w = \frac{1}{4 * \pi^2 * f^2 * L_w} \sim 900\text{nF} \quad (2.5)$$

#### 2.2.2.2. Series Circuit

The value chose for the inverter that will represent the matching network was chosen taking as a reference (12):

$$L_m = 33 \mu\text{H}$$

DC-blocking capacitor ( $C_s$ ) is used to remove the DC component at the output of the half bridge. This capacitor should be sized sufficiently large that does not take place in the impedance matching and does not affect the operation of the resonant tank (13). Therefore, the resonant capacitance was calculated by means of preceding equation:

$$C_m = \frac{1}{4 * \pi^2 * f^2 * L_m} = 34 \mu\text{F} \quad (2.6)$$

As was mentioned before, this value should be larger. It was found that a more suitable value was 390 nF.

### 2.2.3. Simulation Results

Applying a voltage level of 282 V the output current in the inductor looked:

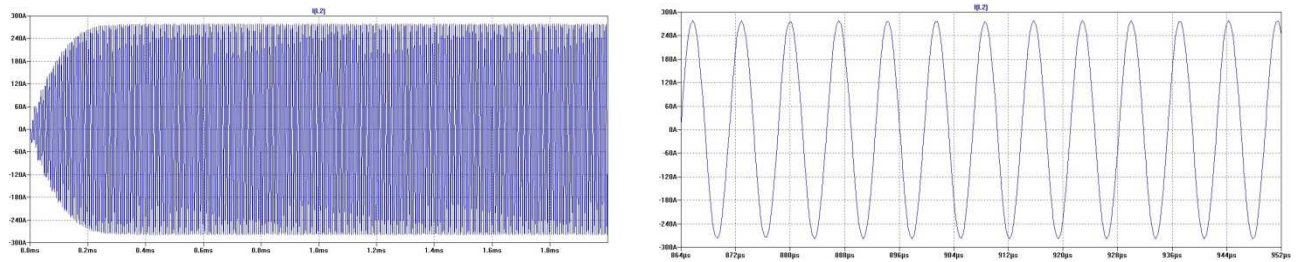


Figure 2-6 Current output in the work coil

The first image is the whole waveform including the transient and the steady state. As it can be appreciated in the second one, where just some periods of the waveform are shown, it has the desire frequency of 140kHz and amplitude close to 300A.

The output of the half-bridge converter is a square wave with the same amplitude as the input voltage:

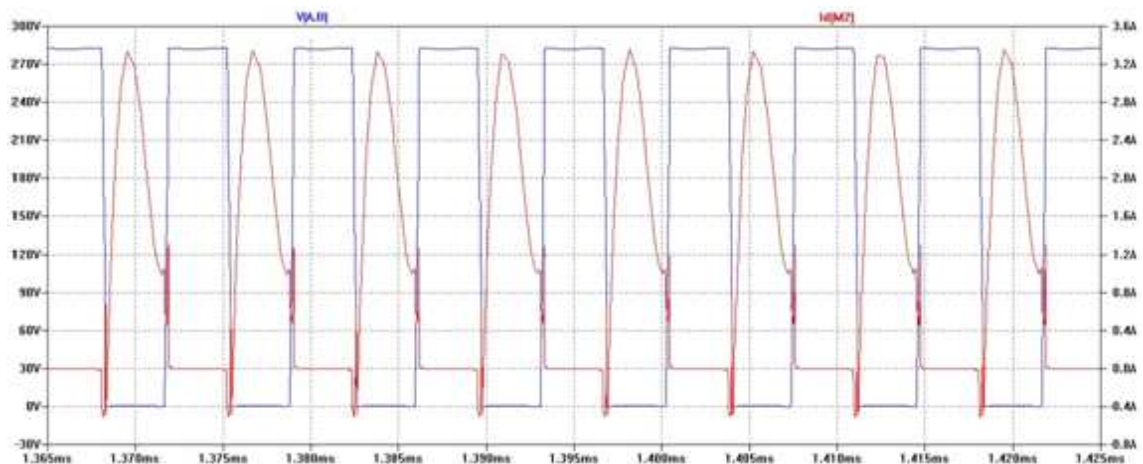


Figure 2-7 Voltage and current output waveforms of the half-bridge converter

The current reaches a maximum of 3,3A becoming negative in the switching transients. The total power dissipated in the power mosfets is 2.3 W. Later it will be studied that this value is just an approximation in the simulation able to show that the soft switching is produced.

### 2.3. Switching mosfet

As it was explained before, switching circuit is mounted in half bridge topology, which is divided in low side mosfet and high side mosfet.

Driving low side mosfet does not present any problem since source leg is connected to ground, and thus, when the mosfet driver generates the driving pulse, the mosfet will switch from not conducting to conducting state due to the gate voltage is higher than the source voltage. By contrast, high side mosfet presents floating source voltage; next figure shows the floating voltage between 0 and 300 volts.

The problem to drive this mosfet lies on driver mosfet due to the signals provided are referenced to ground. So if the high side mosfet gate presents 15 volts and the source presents 300 volts, the mosfet will not conduct. So, it is completely necessary that the gate signal reach

at least 315 volts. Therefore, mosfet driver must present high side pulse isolated from ground and it must be referenced to the floating point.

The mosfet driver chose is a dual output high side and low side. The advantage of the dual output mosfet driver is that the propagation delay is matched for both channels. Latter characteristic is of paramount importance in order to avoid the undesired shoot-through. Besides the proper mosfet driver, it is necessary to implement a supplementary circuit in order to achieve the conditions for driving the high side mosfet.

Different circuits have been developed to give solution to this problem as charge pump driver or bootstrap drive. Bootstrap drive was the solution chosen due to it is the most suitable circuit since it can operate from frequencies in the tens of Hz to hundreds of kHz.

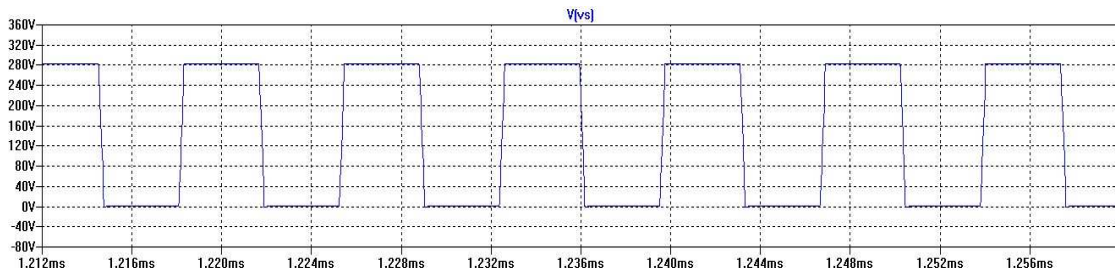


Figure 2-8 Vs\_floating reference for high side mosfet.

### 2.3.1. Bootstrap drive

Next figure shows the bootstrap driver circuit. As can be seen, the bootstrap circuit is formed by one resistor, one diode and one capacitor. The resistor is usually removed in the case of high frequency switching because it can cause a wrong signal.

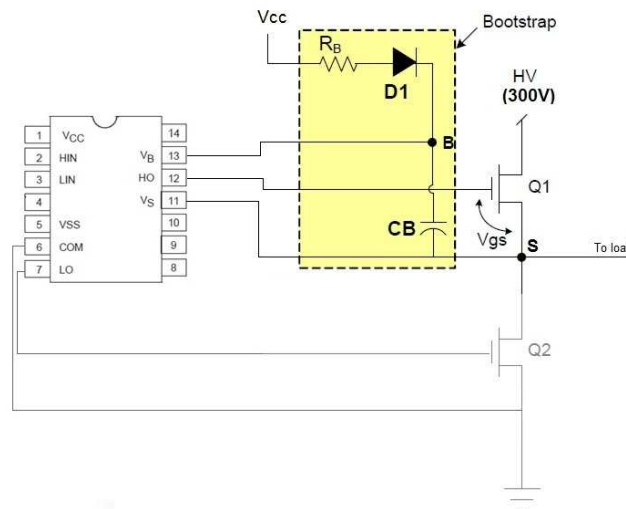


Figure 2-9 Bootstrap circuit implemented with mosfet driver and power mosfets. (14)

The working principle of bootstrap circuit is trivial. When high side mosfet is not conducting, and low side mosfet does, the voltage at the floating point ( $V_s$ ) is 0 volts. Under this condition, the current flows from  $V_{cc}$  to ground. The current flows through the path made by diode, capacitor and low side mosfet. During this transient, the capacitor is charged around 15 volts. After that, mosfet driver turns off the low side mosfet, and after the blanking time, which is 250 ns, it turns on the high side mosfet. At the moment that high side mosfet is conducting,  $V_s$  switches from 0 volts to 300 volts. As a consequence the diode is reversed bias and it cannot

conduct any current. The capacitor, which reference is set at 300 V, is pulling up the voltage at  $V_B$  leg until 315 volts. The voltage drop between  $V_B$  and  $V_S$  is the 15 volts necessary to drive the high side mosfet.

### 2.3.2. Bootstrap elements calculations.

The calculations of the components that form the bootstrap circuit are based on (14):

#### Calculation of capacitor:

The calculation of the capacitor is based on the required voltage between its terminals and the necessary charge to keep the efficient charging and discharging at the switching frequency. The first step is to establish the minimum voltage drop between  $V_B$  and  $V_S$  to guarantee when the high side mosfet is at on state. This condition is given by:

$$\Delta V_{BS} \leq V_{cc} - V_F - V_{GSmin} - V_{CEon} \quad (2.7)$$

Where:

$V_{cc}$  = Mosfet driver voltage supply

$V_F$  = Bootstrap diode forward voltage

$V_{GSmin}$  = Minimum gate voltage to maintain

$V_{DSon}$  = Drain-source voltage of low side mosfet

$$\Delta V_{BS} \leq 18 - 0.9 - 15 - 1.95 = 0.15 \text{ V} \quad (2.8)$$

The previous equation is given under the next condition:  $V_{GSmin} \leq V_{BSUV}$ , where  $V_{BSUV}$  is the high side supply under-voltage negative going threshold. This condition is set since  $15 \leq 9$ .

The minimum capacitance value is given by the total charge in the capacitor and the allowable voltage drop:

$$C_{BOOT \min} = \frac{Q_{TOT}}{\Delta V_{BS}} \quad (2.9)$$

$$Q_{TOT} = Q_G + Q_{LS} + (I_{LK\_GE} + I_{QBS} + I_{LK} + I_{LK\_DIODE} + I_{LK\_CAP})T_{HON} \quad (2.10)$$

Where:

$Q_{TOT}$  = Total required charge in the bootstrap circuit

$Q_G$  = Mosfet turn on required gate charge

$Q_{LS}$  = Level shift charge required per cycle (5nC)

$I_{LK\_GE}$  = Mosfet gate-source leakage current

$I_{QBS}$  = Floating section quiescent current

$I_{LK}$  = Floating section leakage current

$I_{LK\_DIODE}$  = Bootstrap diode leakage current

$I_{LK\_CAP}$  = Bootstrap capacitor leakage current (the value is 0 if the capacitor is not electrolytic)

$T_{HON}$  = High side on time

$$Q_{TOT} = 83\text{nC} + 5\text{nC} + (1\mu\text{A} + 130\mu\text{A} + 50\mu\text{A} + 50\mu\text{A} + 0) * 3.425\mu\text{s} \quad (2.11)$$

$$Q_{TOT} = 88.79 \text{ nC}$$

Finally, the minimum capacitance value is:

$$C_{BOOT \min} = \frac{Q_{TOT}}{\Delta V_{BS}} = \frac{88.79\text{nC}}{0.15} = 591 \text{ nF} \quad (2.12)$$

### Calculation of bootstrap diode:

The diode in the bootstrap circuit must be performed according to the next three points

1. Diode must withstand the power rail voltage, i.e. at least 300 volts.
2. The maximum reverse recovery time is 100 ns, i.e. ultra fast diode.
3. The forward current that the diode must withstand is given by next equation

$$I_F = Q_{TOT} * \text{frequency} \quad (2.13)$$

$$I_F = 88.79\text{nC} * 140\text{Khz} = 13 \text{ mA} \quad (2.14)$$

## **2.4. Mosfet and driver losses**

Power dissipation should be taken into account in the designing process of the circuit in order to match properly the mosfet driver and power mosfets. Moreover, the calculations of the losses are of paramount importance to avoid overheating in the junction of the mosfet.

This overheating related to power dissipation will be controlled by heat sink (see point 2.5).

### **2.4.1. Calculation of mosfet driver losses**

Mosfet driver dissipation is mainly due to the charging and discharging of the mosfet gate capacitance and operating frequency. At lower switching frequencies that dissipation becomes higher. The next equation defines the losses for charging and discharging of the capacitance of the mosfet.

$$P_C = C_G * V_{DD}^2 * F \quad (2.15)$$

Where:

- $C_G$ = mosfet gate capacitance
- $V_{DD}$ = supply voltage of mosfet driver
- $F$  = switching frequency

Mosfet gate capacitance is formed by two kinds of capacitance, the gate to source capacitance and gate to drain capacitance. The value of the gate capacitance is taken indirectly from the next graph, which is given in the datasheet, and it shows the dependency between the voltage applied in gate-source terminals and total gate charge.

For the case of the project the total gate charge is 83 nC. From this value the gate capacitance can be derived as shows next equation.

$$C_G = \frac{Q_G}{V_{DD}} \quad (2.16)$$

So the power loss due to charging and discharging is given by:

$$P_C = Q_G * V_{DD} * F = 83 \text{ nC} * 18 \text{ V} * 140 \text{ kHz} = 0.209 \text{ W} \quad (2.17)$$

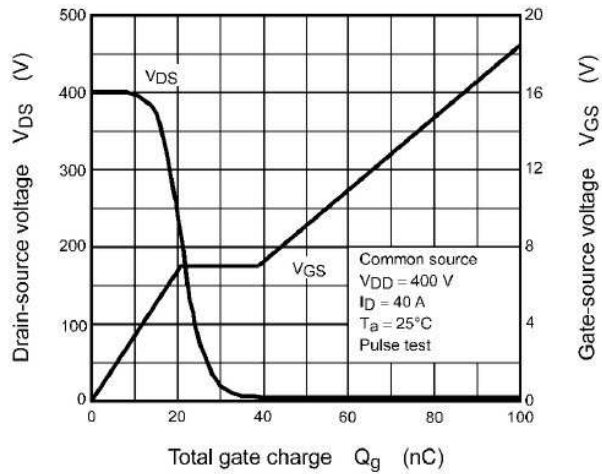


Figure 2-10 Gate-source voltage against total gate charge of the power mosfets (15)

### 2.4.2. Calculation of power mosfet losses

Switching devices offer ideally instant switch, i.e. no time transitions on-off-on, and no losses. The real devices do not behave as ideal ones and they present power dissipation, time transition on-off-on. So, it is of paramount importance to take into account these parameters when designing the converter, thus the converter will work as was expected, avoiding future problems as failure, destruction or no safety conditions.

Power mosfet is a switch device and it presents losses, which mainly are formed by resistive and switching losses. Next figure shows a switching behaviour for general switch device, which is valid for power mosfet, since the power dissipations of power devices are generic (10).

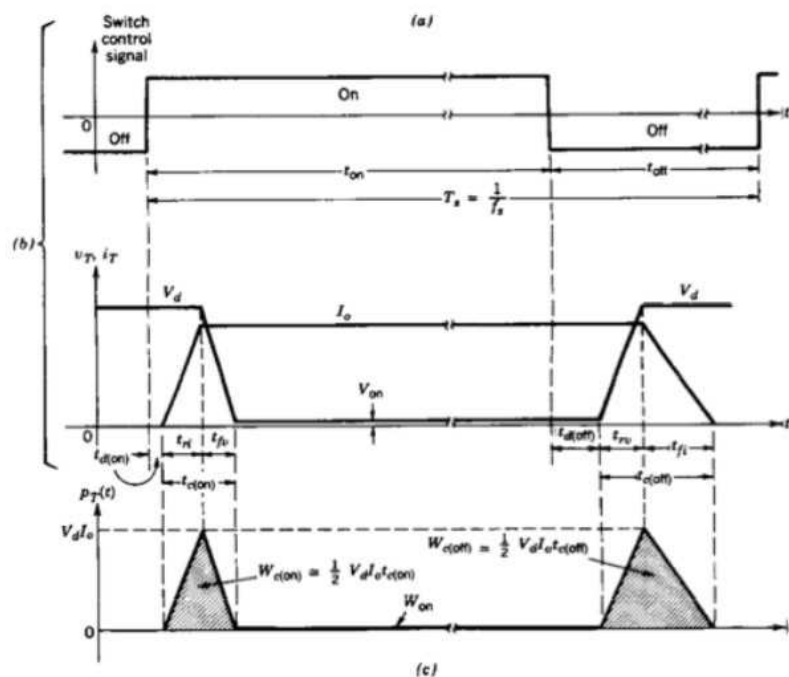


Figure 2-11 Switching characteristics (linearized). A. Switching signal. B. Switch waveforms. C. Instantaneous switch power loss (16)

First graph shows the switch control signal, which is generated by PWM and mosfet driver.

The second graph represents drain-source voltage and current through power mosfet. It should be noticed that the switching waveforms are represented by linear approximation. As can be seen, current is delayed with respect to switch control signal,  $t_{d(on)}$ . After the delay, the current starts to increase its value linearly until it reaches the nominal current  $I_0$ . The time spent during this increment is the current rise time  $t_{ri}$ . When the current reaches its nominal value, the voltage starts to decrease linearly until  $V_{on}$ . This transient time is defined as voltage fall time  $t_{fv}$ . Next changes will occur until the switch control signal modifies its value. When the switch control is off again, the process is inversed as preceding one. The voltage is delayed for a  $t_{d(off)}$  time and after that, it starts to increase until it reaches  $V_d$ . The time consumed for this increment is defined as voltage rise time  $t_{rv}$ . At this moment  $I_0$  starts to decrease until falls to the leakage, which is considered negligible. The time consumed for this transient time is called current fall time  $t_{fi}$ .

Third graph illustrates the instantaneous switch power loss. As can be seen, there are 3 stages in which power mosfet dissipates energy: During the turn on transition, during on state and during turn off transition. It could be taken into account the off state, because power mosfet consumes leakage current, but it is so small energy consumption that it can be neglected.

- [Turn on transition](#)

Turn on transition is formed by two times,  $t_{ri}$  and  $t_{fv}$ , so the complete transition is

$$t_{c(on)} = t_{ri} + t_{fv} \quad (2.18)$$

- [On state](#)

The time for this state is  $t_{on}$ , which is the interval that switch control signal is on. The energy dissipation is approximately:

$$W_{on} = 0.5V_{on}I_0t_{(on)} \quad (2.19)$$

- [Turn off transition](#)

Turn off transition is also formed by two times,  $t_{rv}$  and  $t_{fi}$ , so the complete transition is

$$T_{c(off)} = t_{rv} + t_{fi} \quad (2.20)$$

As an approximation of the energy dissipated the next equation can be used

$$W_{c(on)} = 0.5V_D I_0 t_{c(off)} \quad (2.21)$$

The dissipated energy during turn on and turn off transition can be written as

$$W_{c( switching )} = 0.5V_D I_0 (t_{c(on)} + t_{c(off)}) \quad (2.22)$$

- [Power losses switching](#)

From the dissipated energy the power dissipation can be derived since it is well known the amount of times that turn on and turn off transition will take place, i.e. the frequency of the switch control signal. So the average switching power loss during the on and off transitions is

$$P_{switching} = 0.5V_D I_0 f_s (t_{c(on)} + t_{c(off)}) \quad (2.23)$$

- [Power losses on state](#)

Power losses during on state can be represented by;

$$P_{on} = V_{on} I_0 f_s t_{on} = \frac{V_{on} I_0 t_{on}}{T_s} \quad (2.24)$$

- [On resistance of power mosfets](#)

The on resistance available in the datasheets is made under standard test conditions (STC). This means that the temperature of the resistance is taken at 25 °C. Since the on resistance is temperature dependent, the value of the on resistance at working temperature must be calculated. The forthcoming power losses calculations are done considering a maximum working temperate of 100°C. The calculation of the resistance is given by (10):

$$R_{on}(T) = R_{on}(25^{\circ}\text{C}) * [1 + 0.005 * (T - 25^{\circ}\text{C})] \quad (2.25)$$

Where:

$R_{on}(T)$ = resistance at T temperature.

$R_{on}(25^{\circ}\text{C})$  = resistance of power mosfet given in the datasheet.

T= working temperate

### 2.4.3. Simulation and calculation of power mosfet loss

The simulation to calculate the power mosfet loss was done with LTspice programme. The next assumptions were considered.

The calculations were done for 140 kHz, which is the resonant frequency. Moreover the circuit was simulated taking into account all the series resistance of each component.

These series resistance values were taken in the laboratory by means of the LCR meter; hence the simulation and power losses are more realistic.

Moreover, there were not any mosfet which had the same characteristics as the one used in the real converter, even so, one mosfet was taken from the library and it was used as a reference in order to made the simulation and compare the results with calculated ones.

#### Simulation

Next figure shows the schematic which was made by means of LTspice. The measurements at the simulations were only taken from the high side mosfet. Low side mosfet presents the same power dissipation since it flows through this mosfet practically the same current and it presents the same voltage drop while conducting, and it has the same voltage between its terminals while not conducting. The DC power supply voltage at the simulation was set at 300 volts.

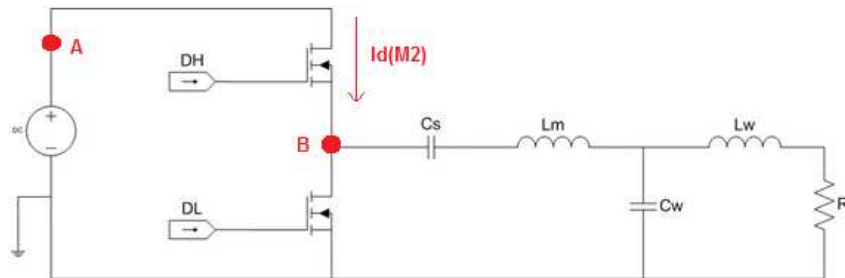


Figure 2-12 Schematic of the circuit simulated in LTspice

In the figure are depicted the measurements points and the used references. The current at high side mosfet is represented as  $I_d(M2)$  and the voltage at the mosfet terminals is represented as  $V(A,B)$ .

Forthcoming figure illustrates the current (blue) and the voltage (red).

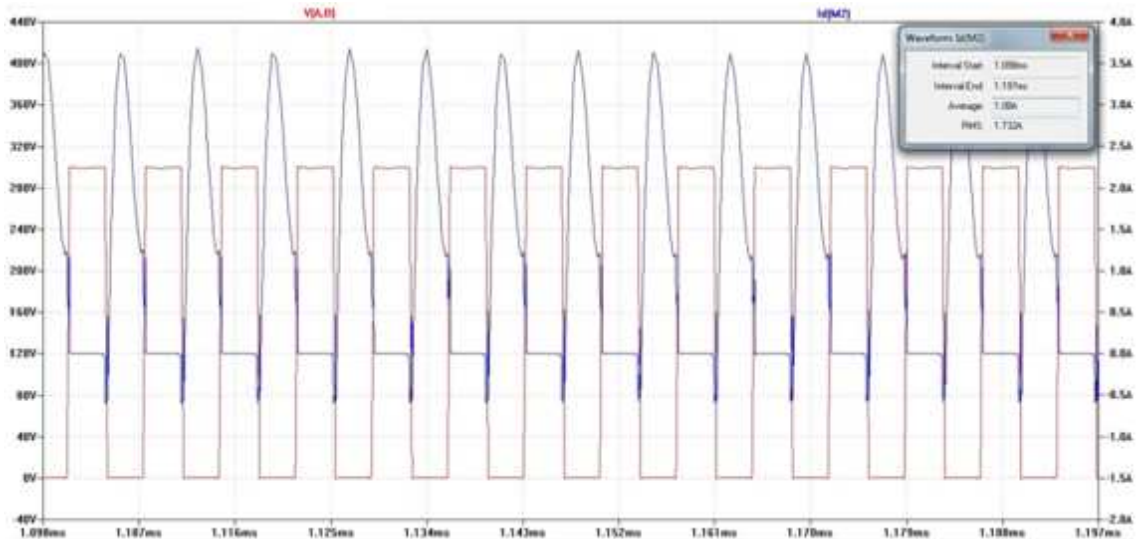


Figure 2-13 Results of the simulations (Voltage-red and current-blue)

Forthcoming figures show the results both average power losses and current through high side mosfet.



Figure 2-14 Result of power loss and current at high side mosfet

The important data from the figures are the average power, which presented 1.93 W and the RMS current, which presented 1.73 A<sub>RMS</sub>.

The calculation, using previous equations, makes necessary to take some values from the mosfet datasheet.

In the simulation an approximated mosfet was chosen, since the programme did not have exactly the same mosfet used in the real setup. So, next calculation was done for the mosfet present in the simulation, which is Infineon SPA11N60C3.

Turn-on delay time	$t_{d(ON)} = 10 \text{ ns}$
Rise time	$t_r = 5 \text{ ns}$
Turn-off delay time	$t_{d(OFF)} = 41 \text{ ns}$
Fall time	$t_f = 5 \text{ ns}$

Table 2.1 Rise and fall times of power mosfet SPA11N60C3

- The time during transitions is

$$t_{c(ON)} = t_{d(ON)} + t_r = 10 \text{ ns} + 5 \text{ ns} = 15 \text{ ns} \quad (2.26)$$

$$t_{c(OFF)} = t_{d(OFF)} + t_f = 41 \text{ ns} + 5 \text{ ns} = 46 \text{ ns}$$

- Power loss during switching is

$$P_{\text{Switch}} = 0.5 V_d I_0 f_s (t_{c(ON)} + t_{c(OFF)}) \quad (2.27)$$

$$P_{\text{Switch}} = 0.5 * 300 * 1.73 * 140 * 10^3 * (15 + 46) * 10^{-9} = 2.2 \text{ W}$$

- Power loss during on state is

$$P_{\text{on-loss}} = V_{\text{ON}} I_0 f_s t_{\text{ON}} \quad (2.28)$$

$$P_{\text{on-loss}} = 0.11 * 1.73 * 140 * 10^3 * 3.425 * 10^{-6} = 91 \text{ mW}$$

- Total power dissipation

$$P_{\text{total}} = P_{\text{Switch}} + P_{\text{on-loss}} = 1.97 \text{ W} + 0.086 \text{ W} \approx 2.3 \text{ W} \quad (2.29)$$

#### Calculation of power losses for chosen power mosfet

Previous paragraph showed the validation data between calculations and simulation. This paragraph shows the calculation for the chosen mosfet.

Turn-on delay time	$t_{d(\text{ON})} = 120 \text{ ns}$
Rise time	$t_r = 60 \text{ ns}$
Turn-off delay time	$t_{d(\text{OFF})} = 160 \text{ ns}$
Fall time	$t_f = 13 \text{ ns}$

**Table 2.2 Rise and fall times of power mosfet TK40J60U**

- The time during transitions:

$$t_{c(\text{ON})} = t_{d(\text{ON})} + t_r = 120 \text{ ns} + 60 \text{ ns} = 180 \text{ ns} \quad (2.30)$$

$$t_{c(\text{OFF})} = t_{d(\text{OFF})} + t_f = 160 \text{ ns} + 13 \text{ ns} = 173 \text{ ns}$$

- Power loss during switching:

$$P_{\text{Switch}} = 0.5 V_d I_0 f_s (t_{c(\text{ON})} + t_{c(\text{OFF})}) = 0.5 * 300 * 1.73 * 140 * 10^3 * (353) * 10^{-9} = 12.82 \text{ W} \quad (2.31)$$

- Power loss during on state:

$$P_{\text{on-loss}} = V_{\text{ON}} I_0 f_s t_{\text{ON}} = 0.11 * 1.73 * 140 * 10^3 * 3.425 * 10^{-6} = 91 \text{ mW} \quad (2.32)$$

- Total power dissipation:

$$P_{\text{total}} = P_{\text{Switch}} + P_{\text{on-loss}} = 12.82 \text{ W} + 0.091 \text{ W} \approx 13 \text{ W} \quad (2.33)$$

#### **2.4.4. Maximum operating point at working conditions**

The absolute maximum ratings of the mosfet datasheet are:

Drain-source voltage	600V
Drain current	40 A
Power dissipation	320 w

**Table 2.3 Electrical characteristics of power mosfet TK40J60U**

The maximum voltage that can be applied at the converter is 300 V, because of is the maximum voltage that the power supply can supply. The maximum allowable voltage at the mosfets terminals is 600 volts, so the voltage is not a limitation.

By contrast, the maximum current may present some problems since the datasheets values are calculated for working within determined operating conditions. So, next equations will verify the maximum allowable current in the converter when the maximum allowable voltage is supplied.

- Power loss during switching:

$$P_{\text{Switch}} = 0.5 V_d I_0 f_s (t_{c(\text{ON})} + t_{c(\text{OFF})}) \quad (2.34)$$

$$P_{\text{Switch}} = 0.5 * 300 * 40 * 140 * 10^3 * (353) * 10^{-9} = 296.52 \text{ W}$$

- Power loss during on state:

$$P_{\text{on-loss}} = V_{\text{ON}} I_0 f_s t_{\text{ON}} \quad (2.35)$$

$$P_{\text{on-loss}} = 2.6 * 40 * 140 * 10^3 * 3.425 * 10^{-6} = 49.86 \text{ W}$$

- Total power dissipation:

$$P_{\text{total}} = P_{\text{Switch}} + P_{\text{on-loss}} = 296.52 \text{ W} + 49.86 \text{ W} \approx 346 \text{ W} \quad (2.36)$$

As can be seen  $346.38 \text{ W} > 320 \text{ W}$ , so in the case that the circuit will demand  $40 \text{ A}_{\text{RMS}}$  the switches will operate above the maximum power they can withstand. The maximum current to be inside the working range, must be lower than  $37 \text{ A}$ , as it is demonstrated in the next paragraph.

- Power loss during switching:

$$P_{\text{Switch}} = 0.5 V_d I_0 f_s (t_{\text{C(ON)}} + t_{\text{C(OFF)}}) \quad (2.37)$$

$$P_{\text{Switch}} = 0.5 * 300 * 37 * 140 * 10^3 * (353) * 10^{-9} \approx 274 \text{ W}$$

- Power loss during on state:

$$P_{\text{on-loss}} = V_{\text{ON}} I_0 f_s t_{\text{ON}} \quad (2.38)$$

$$P_{\text{on-loss}} = 2.405 * 40 * 140 * 10^3 * 3.425 * 10^{-6} \approx 46 \text{ W}$$

- Total power dissipation:

$$P_{\text{total}} = P_{\text{Switch}} + P_{\text{on-loss}} = 274.28 \text{ W} + 46.13 \text{ W} \approx 320 \text{ W} \quad (2.39)$$

Even the limit was  $37 \text{ A}$ , the chosen value as a maximum operating current is  $35 \text{ A}_{\text{peak}}$  due to the PCB design was based on (17), and this standard only covers up to  $35 \text{ A}_{\text{peak}}$ . For  $35 \text{ A}_{\text{peak}}$ , which is approximately  $25 \text{ A}_{\text{RMS}}$ , the total power loss is  $205 \text{ W}$ .

In order to prevent any damage in the circuit, this value will be considered as the maximum allowable current in the converter; being as a reference for the crowbar circuit protection design.

#### 2.4.5. Simulation and calculation of power mosfet loss with low quality factor at the work coil

The final work coil made at the laboratory has the values calculated at chapter 5. However, first work coil made at the laboratory presented a resistance of approximately  $200 \text{ m}\Omega$ . The reason of this higher resistance than expected one was due to the poor junction between the cable, which was made the work coil, and the connection terminals. The cable used to make the work coil is HF Litz wire. This type of cable is formed by few hundreds of wire strands, which are electrically insulated between them by means of enamel film. When the work coil was made it was not available any soldering machine, which would have provided high temperature and would have allowed by means of tin to join the wire strands at the ends of the cable and the most important, it would have been vaporized the enamel at those points. Even so, the work coil was made and it was mechanically joined to the connector terminals and the result was a poor quality factor of the work coil. This work coil was not applied in the laboratory setup; however, the next paragraphs show how this work coil can affect the power loss at the mosfets.

#### Simulation

Next figure illustrates the current (blue) and the voltage (red) in the high power mosfet.

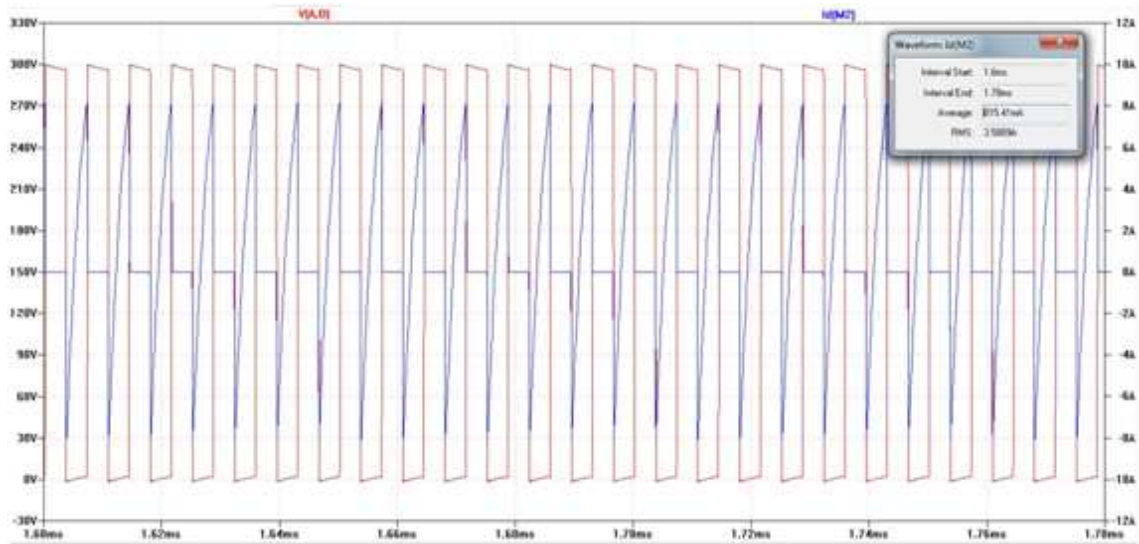


Figure 2-15 Results of the simulations (Voltage-red and current-blue)

Forthcoming figures show the results both average power losses and current through high side mosfet.



Figure 2-16 Result of power loss and current at high side mosfet

The important data from the figures are the average power, which presented 6.41W and the RMS current, which presented  $3.6A_{RMS}$ .

Calculation of power losses for chosen power mosfet

- Power loss during switching:  

$$P_{Switch} = 0.5 V_d I_o f_s (t_{C(ON)} + t_{C(OFF)}) = 0.5 * 300 * 3.595 * 140 * 10^3 * (353) * 10^{(-9)} = 26.7 \text{ W} \quad (2.40)$$
- Power loss during on state:  

$$P_{On-loss} = V_{ON} I_o f_s t_{ON} = 0.2337 * 3.595 * 140 * 10^3 * 3.425 * 10^{(-6)} = 0.411 \text{ W} \quad (2.41)$$
- Total power dissipation:  

$$P_{total} = P_{Switch} + P_{On-loss} = 26.6497 \text{ W} + 2.15 \text{ W} \approx 27 \text{ W} \quad (2.42)$$

As can be seen, the increment of the parasitic resistance at the resonant tank circuit will affect the power dissipation at the power mosfet. An increment of 175 mΩ causes a power dissipation increment of 14 W.

## 2.5. Heat sink design

Power losses calculated previously are dissipated in form of heat. This heat and its evacuation must be controlled in order to prevent an excess of temperature at the mosfet junction.

The average allowable temperature at the junction for power semiconductor devices is commonly 100°C, and the mosfet used in the converter can withstand until 150 °C.

Normally, these power semiconductor devices can operate above this temperature, even so, it is not recommended to do it because the more temperature, the more increment of power dissipation. Also the reliability of the device decreases and the operation would be inefficient.

To control the temperature at the junction, one heat sink is added in each switch of the converter.

In order to choose a proper heat sink for the application, it is necessary to understand how the heat is evacuated from the junction of the semi-conductor:

The heat generated at the junction is transferred from it to the ambient by conduction mechanism. The conduction principle is trivial, if there is gradient of temperature in a determined section of material; there is a net flow of energy from the higher to the lower side (10). This heat exchange that takes place between different areas is defined by the concept of thermal resistance.

The model of the thermal resistance is analogous with electrical resistance. Therefore, the transfer of the heat can be modelled as an electrical circuit, in which the power dissipation is represented as current source. The different areas of the device, which formed the path from the junction to the open air, can be modelled as different thermal resistance. See next figure.

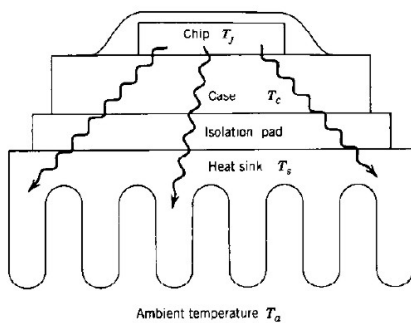


Figure 2-17 Cross section profile of semiconductor device (10)

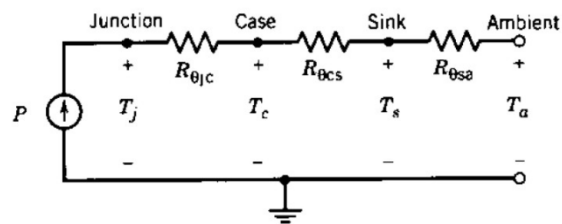


Figure 2-18 Equivalent circuit based on thermal resistance (10)

Where:

- $P_d$  is the power dissipation at the mosfet
- $R_{\theta jc}$ =thermal resistance between junction-case
- $R_{\theta cs}$ =thermal resistance between case-heat sink
- $R_{\theta sa}$ =thermal resistance between heat sink-air

The total thermal resistance from junction to open air is given by:

$$R_{\theta ja} = R_{\theta jc} + R_{\theta cs} + R_{\theta sa} \quad (2.43)$$

The equation that defines the circuit is as follows:

$$T_j - T_a = P * (R_{\theta jc} + R_{\theta cs} + R_{\theta sa}) \quad (2.44)$$

And from previous equation, the thermal resistance value of the heat sink can be derived as:

$$R_{\theta sa} = \frac{(T_j - T_a)}{P_t} - (R_{\theta jc} + R_{\theta cs}) \quad (2.45)$$

As it derives from the previous equations, it is necessary to know the values of the total dissipation power (it was previously calculated), the maximum allowable temperature at the junction (mosfet datasheet), the ambient temperature where the converter will operate (it will be considered 30 °C), the thermal resistance between junction-case (mosfet datasheet) and the thermal resistance between case-sink.

The latter variable can be reduced by the use of thermal greases. This material fills the micro gaps which are presented at the junction of the case and heat sink and it improves the heat transfer, further reducing the heat thermal resistance; otherwise the device may be overheated because of the increment of the resistance and as a consequence of the reduction of the heat flow between surfaces, see next figure.

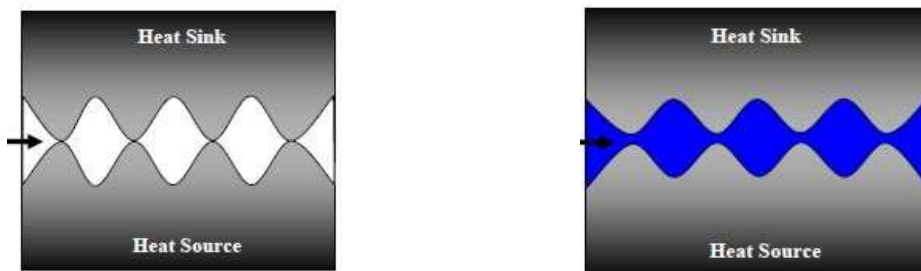


Figure 2-19 Heat sink with and without thermal grease (18)

The thermal grease used between the surfaces is Dow Corning 340 heat sink compound and it has a thermal resistance of 0.162 °C/W.

Finally, in order to compute the equation, the ambient temperature was considered 30°C, the maximum allowable junction temperature is 100°C, and junction-case thermal resistance is 0.39 °C/W; so the equation gives as result:

$$R_{\theta sa} = \frac{(100 - 30)}{13} - (0.39 + 0.162) \leq 4.8 \quad (2.46)$$

It should be noticed that previous calculations were made in order to provide an idea about the temperature behaviour of the mosfets and also an approximation about the needed heat sink. Even though, more parameters must be taken into account in order to offer an accurate solution. Since heat sink release its heat to open air by convection mechanism, the behaviour may vary depending on the surrounding air flow and also if the converter is located inside a cabinet. In consideration of previous statement, one fan was added to provide a continuous air flow. Using fan offers the possibility of choosing much smaller and lighter heat sinks because it reduces considerably the thermal resistance (10).



# 3. Control Designing

A description about the designed control system in the converter is explained in this chapter.

## 3.1. Frequency analysis

There are different methods to represent the frequency analysis of a system, however, only Bode diagram was chosen. This method results in a plot of magnitude versus frequency and phase versus frequency. The frequency scale and the magnitude are plotted on a logarithmic scale. The main advantage of the Bode plot over other types of plots for frequency response is that the effects of adding a real pole or a real zero to transfer function can be seen rather easily (19). Moreover is really intuitive and easy to understand the behavior of the system about magnitude versus frequency.

In order to show the behavior of the converter, an analysis of the current output at the work coil respect to the current output at the half bridge was made.

The transfer function of the system is:

$$\frac{I(s)}{I_{total}(s)} = \frac{1}{1 + RC_w * s + L_w C_w * s^2} \tag{3.1}$$

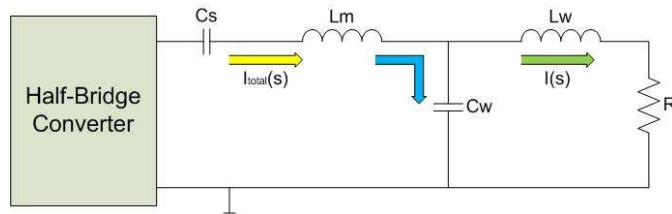


Figure 3-1 Current paths in the resonant circuit

This transfer function relates the total current provides by the converter and the output current in the work coil.

It is possible see the resonant frequency range of the system.

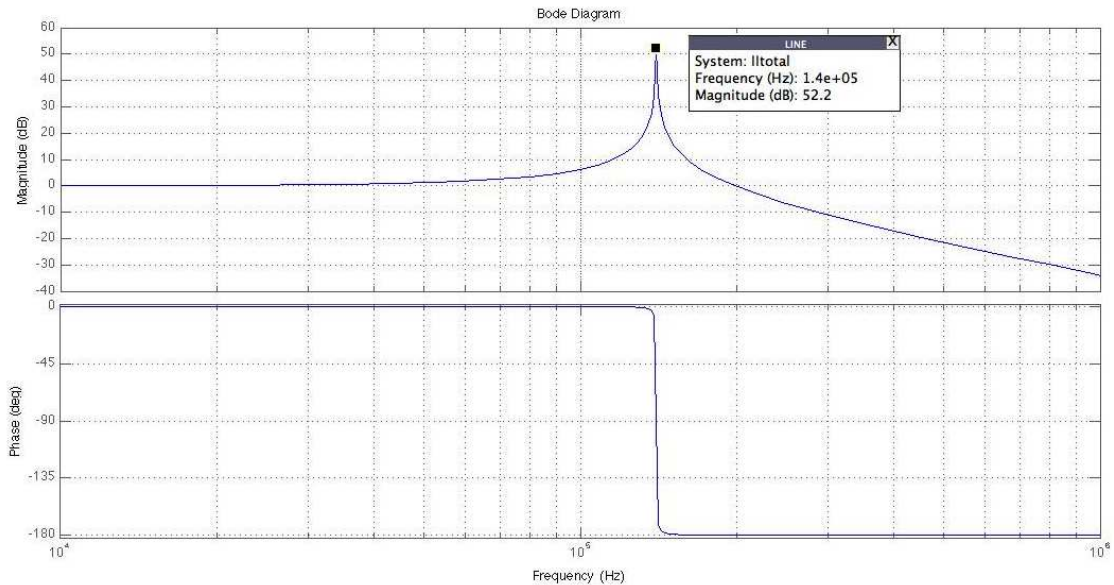


Figure 3-2 Bode Diagram of the resonant current

The resonant peak is placed at 140kHz as it was expected; decreasing rapidly once that frequency is exceeded.

For low frequencies the system has null gain, meaning that the ratio between currents is keeping constant until the frequency of 30kHz, where the amplitude trace is starting to increase.

This analysis enables a comparison with the previous calculated values and an approximation of how the converter will respond, depending on the quality factor values of the work coil. In order to study this behaviour of the converter another analysis was made for different quality factors inductors.

The results can be appreciated in the picture below:

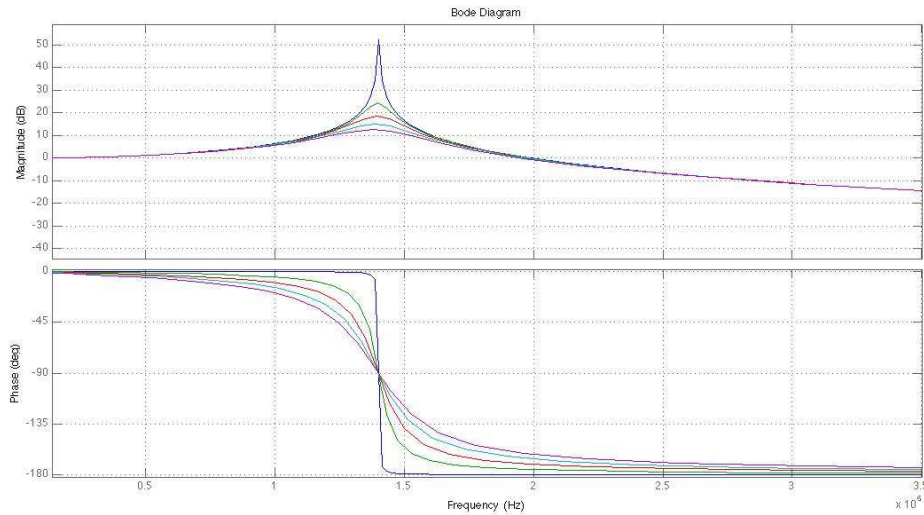


**Figure 3-3 Bode Diagram of the resonant current for different values of Q**

The values for the different resistances were:

$$R = [0.0030 \ 0.0772 \ 0.1514 \ 0.2256 \ 0.2998]$$

It should be noticed that the lowest resistance value at the work coil, the highest the resonance and thus, the highest the current.

The final value obtained in the laboratory for the work coil was inside the resistance range previously simulated, being approximately  $0.005 \ \Omega$ , expecting an approximated gain value of 50dB with a Q factor of 255.

## 3.2. Control Design

Once the frequency analysis was implemented it was necessary to design a proper control for the converter, in order to control the switching frequency of the semiconductors and with that, the output current in the work coil.

With this strategy the highest current will be set at 140kHz, but it makes possible to get different current ranges depending on the desired specifications.

The control has to be accurate, due to the fact that the frequency range of the resonant peak is narrow and few changes will produce big changes in the currents.

The frequency range considered on this project to make the converter work under normal operation was from 120kHz to 150kHz. Working at resonant frequency the maximum current will be obtained in the work coil.

If the value of 150kHz is over passed, the gain in dB decays fast, making the current in the output almost zero.

To make the design the main reference used was (20). This paper presents a methodology to design a control for a system that presents an inverse response, which means that the initial response of the plant is in the opposite direction with respect to the ultimate steady-state value of it.

The idea of this method consists in match the three first terms of a Maclaurin expansion with the coefficients of a PID controller.

From the generic transfer function below:

$$T(s) = \frac{y(s)}{u(s)} = \frac{R(s)G(s)}{1 + R(s)G(s)} \quad (3.2)$$

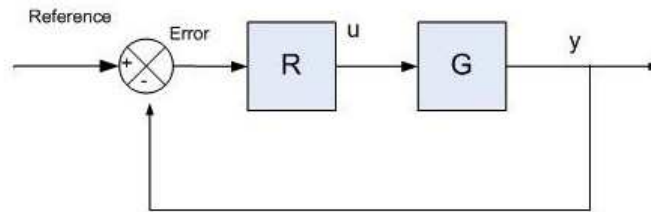


Figure 3-4 Block diagrams of the controller and the plant

Being R the final controller and G the plant of the system. The value of the controller is achieved by selecting a transfer function T(s) physically possible that ensures the closed loop of the system achieves good control performance and robust stability.

T(s) is constructed following the same procedure explained in (20), having the follow structure:

$$T(s) = \frac{1}{G(s)} = \frac{1}{(K * s + 1)^2} e^{-(H+2\tau_z)*s} \quad (3.3)$$

Considering  $H + 2 \cdot \tau_z$  the overall dead time of the plan and K is a closed-loop response adjustable parameter. When this latter parameter tends to be zero, the setpoint response tends to be optimal.

Depending on the value chosen for K, the response will be faster and less robust or more accuracy to the desire control value but slower. Therefore a compromise between these specifications has to be found.

Joining both equations 3.2 and 3.3 the result will be:

$$R(s) = \frac{1}{G(s)} \frac{T(s)}{1 - T(s)} \quad (3.4)$$

Now the controller equation of R(s) can be derived analytically. However the resulting equation cannot be transformed directly into a PID controller. At this point is when the Maclaurin expansion formula should be employed, in order to reproduce the desired PID controller in a simple way.

Assuming,  $R(s) = \frac{M(s)}{s}$ , it is obtained:

$$R(s) = \frac{1}{s} \left[ M(0) + M'(0) * s + \frac{M''(0)}{2!} + \dots \right] \quad (3.5)$$

The result of the expansion will give the desired coefficients:

$$K_f = M(0) \quad T_i = \frac{1}{M(0)} \quad T_D = \frac{M'(0)}{2!} \quad (3.6)$$

In order to follow this procedure one MATLAB script was implemented, where the values for the parameters were calculated with the MATLAB function *diff*.

The values for the rest of the parameters need were taken from the same reference (20), were some examples has been implemented. The value for the dynamic of the sensor was:  $H=0.8$  and  $\tau=0.5$ . For the parameter  $K$  of the controller different values were implemented, choosing the one that fits better with the requirements of the system:  $K=2$ .

The final controller for the converter was:

$$R(s) = 7994.6 - \frac{3998.5}{s} - 0.00025 * s \quad (3.6)$$

Although the three components of the PID controller were calculated, just the proportional and the integral were used in the real control programmed in the microcontroller, due to the fact the addition of the derivative part was introducing perturbations in the simulation.

### 3.3. Control Implementation and Simulation

In order to check dynamically the control implemented, a Simulink model was designed and checked the parameters of the PID on it.

A cascade control was implemented, using PLECs library for designing of the power electronics components (Half-bridge inverter and resonant tank) and SIMULINK tools to design the control loop.

The system was looking as the picture below:

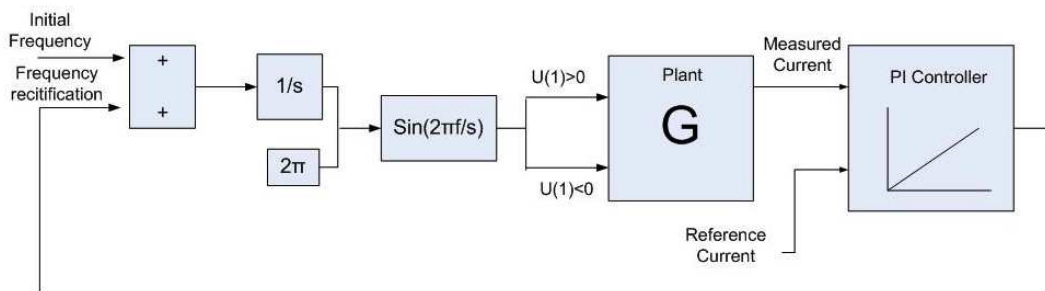
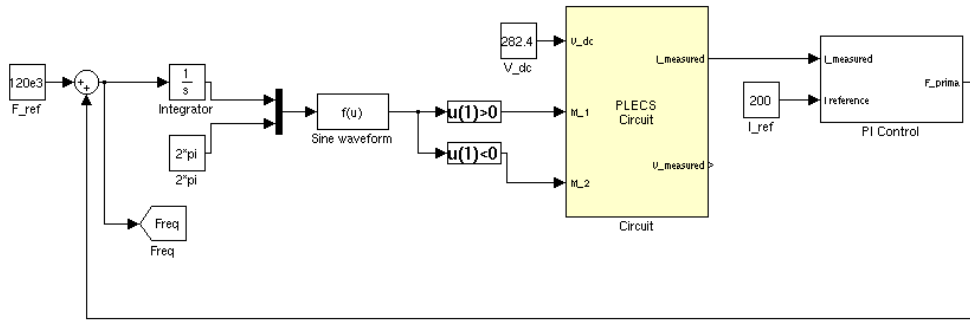


Figure 3-5 Schematic of the system implemented



**Figure 3-6 SIMULINK implementation of the system**

As it can be seen from the picture, the first side of the block diagram is the responsible to provide the square waveform to the converter, with the required frequency. The initial frequency is 120kHz in order to provide a first reference for the system. Once the transformation is made and the waveform is sinusoidal with the frequency specified, two filters are set responsible of provide the signals to the switches inside the plant. The upper filter puts a one in the output when the signal is positive and zero when is negative, the second one does the opposite. In this way it is possible to obtain the switching frequency.

Inside the plant, the current in the inductor is measured to provide the feedback for the current loop. In the picture below, it is shown the converter circuit implemented with PLECS library, as it can be appreciated is the same implementation as the one made with LTSpice:

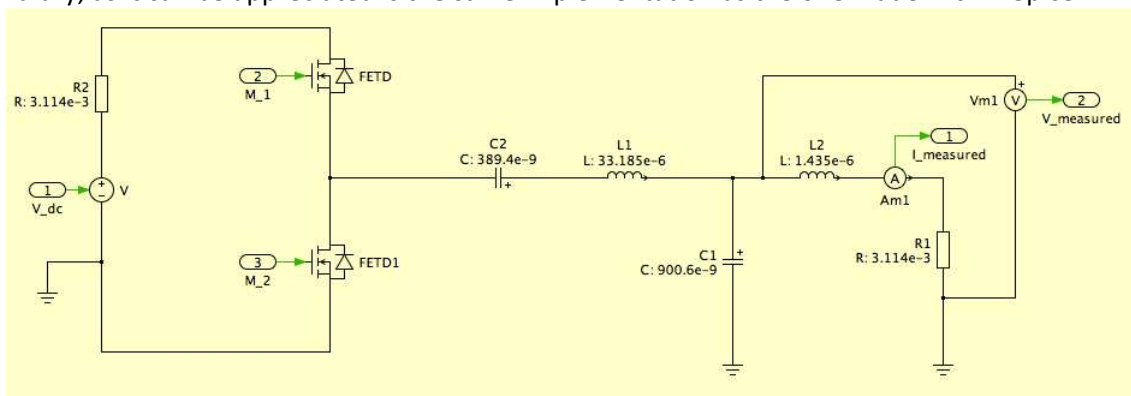


**Figure 3-7 PLECS model of the converter**

Current and voltage reference were taken to see the behavior of the plant, but in practice just the current will be used for the controller.

The next step in the loop is to get the reference current. The user sets the value for the reference current, which will be the obtained at the output of the converter.

An image of the controller is shown to make easier the explanation:

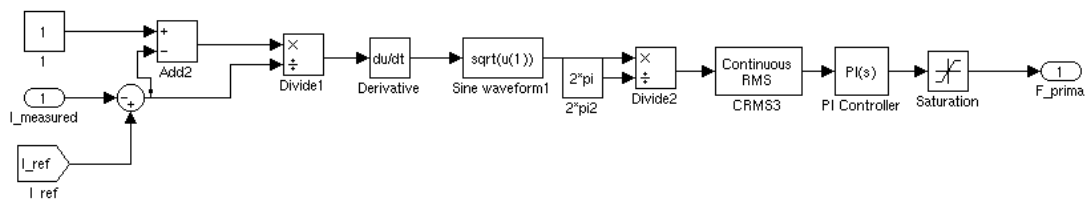


**Figure 3-8 SIMULINK model of the Controller**

The control makes a comparison between the current output in the inductor and the reference current, calculating the error. The current waveform calculated has already the desired

amplitude and it is just necessary to know its frequency, in order to feed the converter with the same value to get the desired current waveform in the output of the inductor.

To find that frequency, a Laplace transformation of the error current calculated is made, considering the instantaneous value of a sinusoidal waveform (21):

$$I_e = \hat{I}_e \cos(\omega t) \qquad I_e(s) = \frac{s}{s + \omega_e^2} \qquad (3.7)$$

The instantaneous current can be expressed in terms of the sinus or the co sinus, just affecting the angle phase of the waveform. The Laplace transformation provides a value independent of the frequency.

That value of frequency would be the error frequency that the initial frequency value needs to reach the reference current. The unit values of  $\omega$  are rad/sec and it is transformed into Hz before passes through the PI SIMULINK block, which is set with the values already calculated in the previous explanation and it is added into the initial frequency value to close the loop.

To check the behavior of the control some simulations were run. In order to show that the control is following the reference a general view of the current waveform is shown. The second trace corresponds to the frequency value applied to the switches.

Different values of reference current were set:

<b>Instant value [Seconds]</b>	<b>Value set [Amperes]</b>
From the begin to 1.60	200 A
1.60 – 2.35	300 A
2.35 – 2.48	150 A
2.48 – 2.60	250 A
2.60 – 2.75	100 A
2.75 – 2.90	300 A
2.90 – 3.10	150 A
3.10 – To the End	280 A

**Figure 3-9 Values of reference and measured current of the controller**

The response as it can be appreciated is quite fast and the final value quite accurate to the reference. In the figure 3-10 it can be appreciated the reference current (red) and the measured current (green). The measured is following the reference working inside the specified frequency margins, as it can be checked in the trace below.

It could be possible make the response more accurate changing the parameter K explained before in the Control Design paragraph to get the values for the PID, but the response will be much slower.

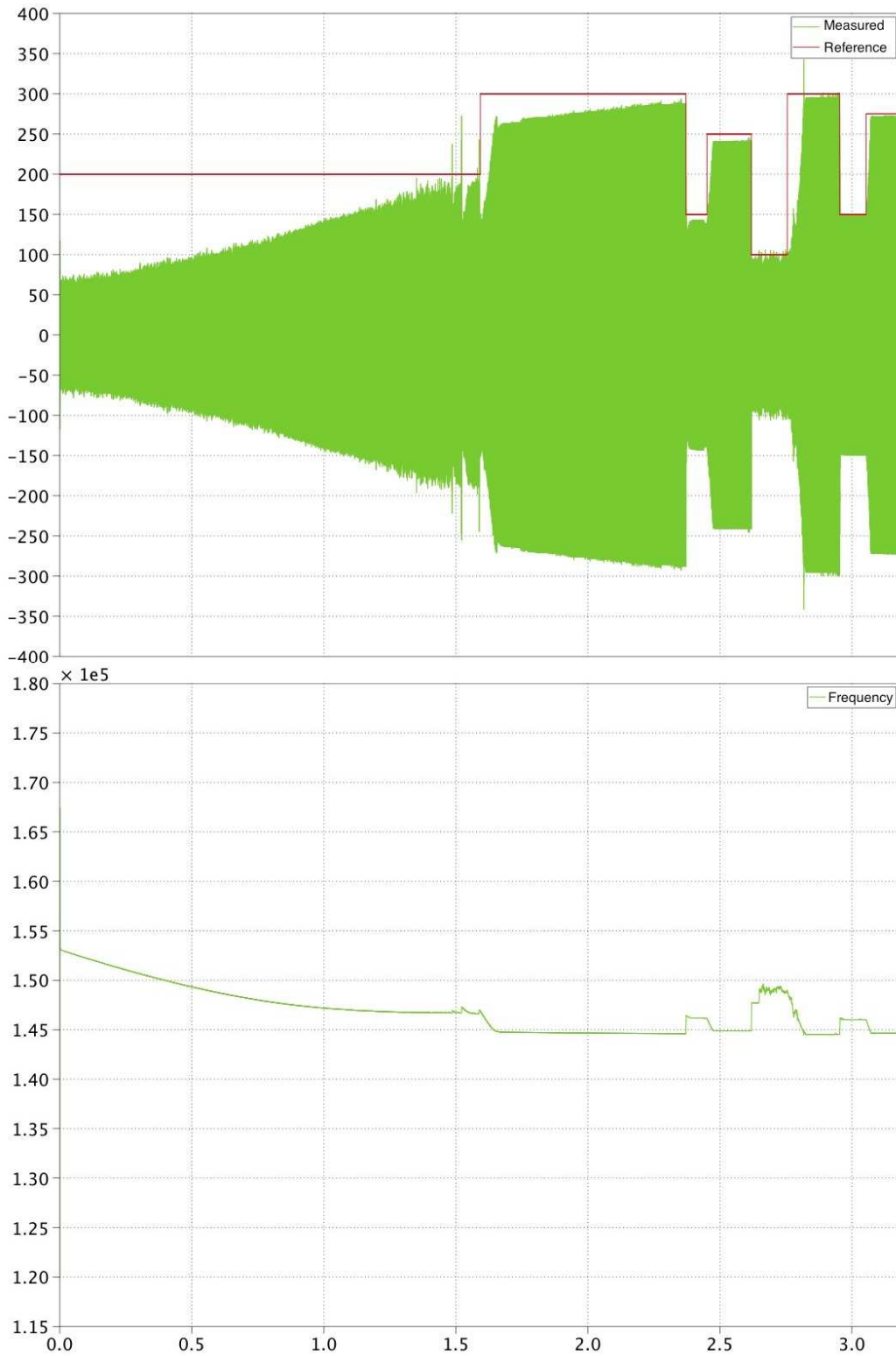


**Figure 3-10** Traces of the output current and frequency range

If a small value of current is set in the input reference, the frequency over passes the 150 kHz and the slope of the gain traces in the Bode diagram becomes negative, making the value of the current output very small. It can be appreciated in the next capture:

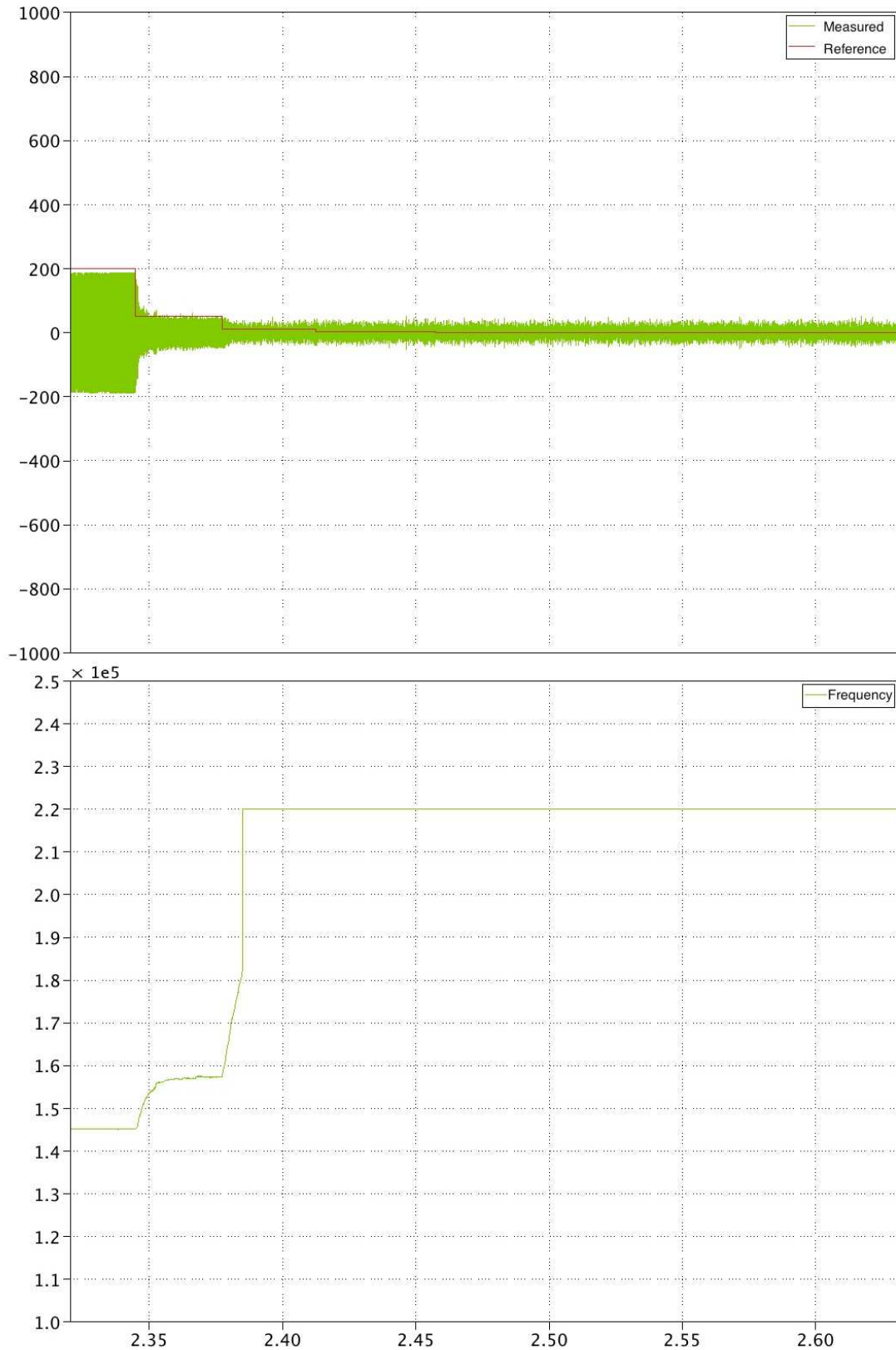


**Figure 3-11 Current Waveform and frequency for a zero current reference**

The frequency reaches 220kHz and the current waveform becomes irregular and unsmooth, as it was expected from the frequency analysis.

After developed all this frequency analysis and control design, the procedure to implement it inside the microcontroller was considered and explained in the next chapter.

### 3.3.1. Discrete Correlation

However, as it was observed, the control simulations were made for a continuous model, but the control implemented in the microcontroller was discrete.

This procedure was made in purpose following paper (22). The first step of this method is to design the control loop in the s-domain, as it would be a continuous-time system and then, the controller is converted into discrete-time by some approximate techniques to yield a discrete-time compensator.

This technique presents the advantage of working inside the s-domain, but with the required discrete transformation some poles are distorted making the system losing observability and controllability (23), making necessary a trial and error process after the design.

Taking the value of the controller previously calculated without the derivate parameter (eq 3.6), the bilinear transformation was applied:

$$s = \frac{2}{T_s} \left( \frac{z - 1}{z + 1} \right) \quad (3.8)$$

To be able to apply this transformation a time sampling has to be calculated. In order to choose a proper sampling time some considerations were made, following (24).

In order to choose a proper sampling time it is necessary to consider that if this value is too large, the dynamics of the process will not be captured and the accuracy of the system will be poor. On the other side if a short value is chosen, too much data will be collected that will involve inconsequential information.

Considering all this, the criteria used to chose the proper sampling time was to calculate a sampling time 15 times bigger than the frequency of the signal that it wants to be obtained. In this case and as the resonant frequency is 140kHz the sampling time was:

$$T_s = \frac{1}{10 * 140\text{KHz}} \quad (3.9)$$

Applying the Tustin equation (eq. 3.8), the result of the converter was:

$$R = \frac{7995z - 1}{z - 1} \quad (3.9)$$

This value was the one implemented in the control programmed in the microcontroller.



## 4. Microcontroller Programming

An explanation of the structure of the program implemented in the microcontroller is developed in this chapter. The microcontroller used for this application was a dsPIC30F1010 from Microchip. All the data and previous considerations were consulted from (25).

### 4.1. Control Loop Considerations

The structure for the control implemented with the microcontroller is shown in the figure below:

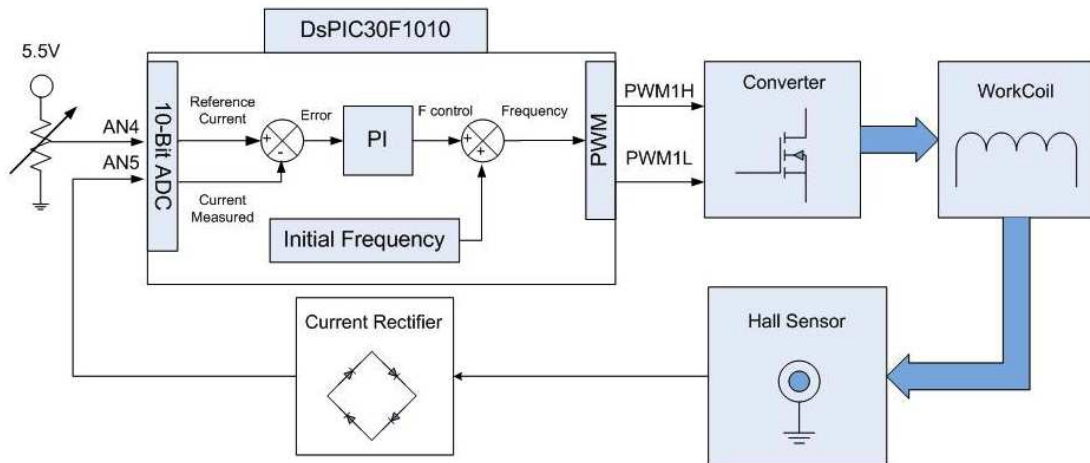


Figure 4-1 Schematic of the microcontroller functions inside the system

The explanation for the system shown in the picture is as follows:

There are two analog inputs plugged to the microcontroller: one is the current reference and the second one is the current measured by means of a hall sensor. Both signals are connected to the microcontroller through the analog-digital converter. The reference is set through one potentiometer.

Inside the microcontroller a PI controller is implemented. The output of the controller is added to the reference frequency value of 120kHz. Enabling an easier and faster control, due to the device implement fewer calculations.

Once the final value of the frequency is obtained, is loaded in the PWM register. The programming of this function will be explained later.

In the output of the work-coil a hall sensor is set to measure the value of currents obtained for that frequency. As the output current is sinusoidal, a bridge rectifier is rectifying the current and feeding again the analog input closing the loop.

### 4.2. Main structure

The whole code was implemented using C language due to the fact is faster and easier to programming.

It has, in total, six main functions and two interrupts. The flow chart of the program looks like:

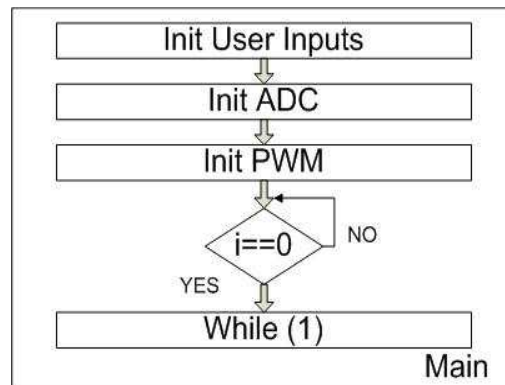


**Figure 4-2 Flow-chart of function Main**

The function main involves the initialization of the ports and the peripherals: PWM and analog-digital converter. The microcontroller starts to produce the signals of the PWM at a frequency of 140 kHz and stays on that point until the user pulses the switch. In that moment  $i \neq 0$  and the control implemented through the ADC starts to work, staying inside an infinite loop until the user stops the program.

To make it understandable there is one explanation of each function.

#### 4.2.1. Init User Inputs

In this function all the ports used are declared and initialized:

- The analog-digital converter inputs. The inputs are connected to Port B.
- The switch that produces the state changes of the variable  $i$  is connected at pin 6 of the *PORTF*.

This disposition for the inputs was chosen in that way in order to take advantage of the Development Board employed in the setup. It already includes a switch and a potentiometer connected to the referred ports.

#### 4.2.2. Init ADC

The analog-digital converter configuration is developed in this section. This converter provides 10-bit number depending on the voltage that receives in the input pin. The converter has ten channels, corresponding each one of them with one input pin, making conversions by pair of channels. Once the conversion is done, the ADC module has some specific register where those conversions are stored. This register is *ADCBUFx*, depending on the inputs channels chosen.

The pair of channels chose in this case was the pair number three, corresponding with the channels four and five. The input pins are *RA4* and *RA5*. The conversion will be stored in *ADCBUF4* and *ADCBUF5*.

The peripheral is configured in order to produce an interruption after every pair of conversion. As just the conversion pair number three is configured, the device will not make any reading or conversion from the other channels.

The converter needs a signal to trigger and start the reading and conversion process. In this case the PWM module provides this triggering signal. It was chosen in that way because the PWM module is already configured and working; saving memory of the microcontroller and time.

The working mode would be as follows: The peripheral reads the specified register, makes the conversion and charges the value of it in the corresponding module: *ADCBUF4* and *ADCBUF5*.

The converted value is in fractional format, in order to enable more accurate calculations in the control function.

### 4.2.3. Init PWM

This function initializes the registers need to produce the switching signals and the triggering signals for the A/D Converter.

The PWM module has different operation modes, depending on the application. For this case, the mode chose was Complementary PWM. This mode presents a PWM signal in the *PWMH* pin and another complementary signal, with the same specifications of the previous one, in the *PWML* pin. This working mode is selected through the register *IOCONx: PWM I/O Control Register*.

The duty cycle is set constant at 50% and keeping a dead time of 240ns. Both are specifications need for the proper work of the converter. The configuration of the register were made, taking into account the following equation:

$$PTPER = \frac{\text{ReferenceClock} \cdot PLL \cdot 2}{PWM_{\text{switchingfrequency}}} = \frac{14.55\text{MHz} \cdot 32 \cdot 2}{PWM_{\text{switchingfrequency}}} \quad (4.1)$$

Where *PTPER* is the register that provides the frequency specifications of the PWM signal.

To specify the duty cycle of the signal, the *MDC* register is configured as follows:

$$MDC = \frac{PTPER}{2} \quad (4.2)$$

Finally to specify the dead time of the signal, there are two registers, one for each signal. In this case, the value of both registers is the same:

$$DTRx = ALTRx = \text{Dead\_Time} \cdot \frac{T_{PLL}}{2} \quad (4.3)$$

The PWM module is configured to enable immediate updates, in order to not accumulate delays after the controller is providing the appropriated signal.

For this configuration, the module generates a signal of 140 kHz and keeps constant on that frequency until the user pulses the *SWITCH S2*. In that moment, the control will start working and the frequency will be tuned by the PID Controller depending on the specifications that the user will set through the potentiometer in the input.

## 4.3. Interrupts

There are two interrupts designed in the microcontroller, working independently one from the other: The first is produced when a conversion from the A/D Converter is done and the second is produced when the user pulses the *SWITCH S2*.

### 4.3.1. A/D Interrupt

The A/D Converter, triggered by the PWM signal, reads the data from the input pins: *RA4* and *RA5*. Makes the conversion and loads it in the *ADCBUF4* and *ADCBUF5* registers.

Before load the values in the respect *ADCBUFx*, the module produces an interrupt. The values calculated are stored in two variables called: *Ref\_Current* and *Meas\_Current*. Corresponding with the values from the reference input and the hall sensor.

These values have to be processed by the microcontroller in order to adapt them inside the margins of their correspondent variables. The microcontroller implements the conversion but does not understand the values. For that reason, the following equations are implemented:

$$Re f\_Current = \frac{ADCBUF5 \cdot 150kHz}{3.3V} \quad Meas\_Current = \frac{ADCBUF4 \cdot Max\_Current}{3.3V} \quad (4.4)$$

The highest voltage value of the ADC is 3.3 V. The reference current is the value of current obtained for a frequency of 140 kHz and the current measured will be tuned to produce a feedback corresponding the highest current produced in the work coil for an input in the ADC of 3.3V. In this way the controller will work inside the frequency margins mentioned in the previous chapter, being the highest value of current at 140kHz.

After the calculations of the inputs, the PID Control function is called, in order to perform the changes and load them inside the registers of the PWM module.

In this interrupt the two main functions responsible of the control takes place: PI Control and PWM signal. As these functions are more extents there is one independent section for them.

### 4.3.2. Switch Interrupt

This interrupt is produced when the user pulses the *SWITCH S2* of the Development Board of the microcontroller. The Structure is as follow:

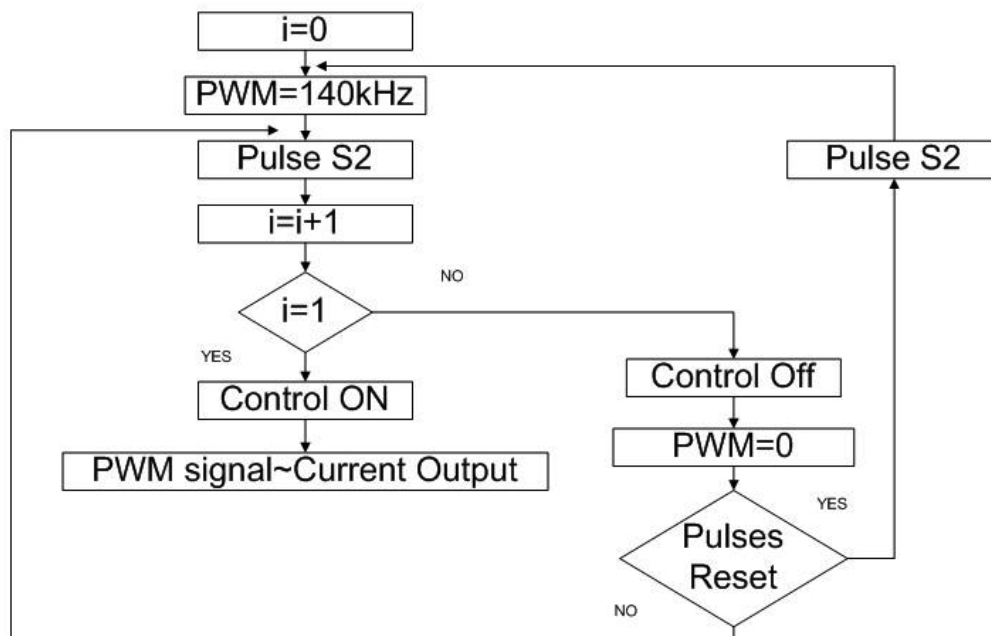


Figure 4-3 Flow-chart of the operation mode

When the microcontroller is turn on the converter starts to produce a signal of 140kHz. If the user pulses *SWITCH S2*, the variable *i*, used to analyze the states of the *SWITCH S2*, is set to 1. The control is activated and the loop is closed, allowing changes in the frequency inputs and due to this fact, changes in the current value of the inductor. Put differently, until the switch is not pulse the first time, the control is deactivated, generating a constant PWM signal of 140kHz.

When the switch is pulsed by the second time, the converter switches off, generating a zero signal. If the reset is pulsed, all the variables are reset. When the user pulses *SWITCH S2* again the PWM will generate again the frequency of 140kHz.

If the reset is not pulsed, the converter starts to work again with the control.

This interrupt has higher priority than the one of the A/D Converter. It was programmed in purpose to allow the microcontroller stops irrespective of the conversion state.

This operating mode of the microcontroller was designed considering that once the converter is fed at the maximum voltage (300V), the converter will start providing the maximum current in the work coil at the resonant frequency. Keeping constant the voltage, the control of the current will be achieved just by changing the switching frequency, inside the frequency ranges exposed before.

## 4.4. PID Control and PWM signal Generator

These two functions are the responsible to provide the converter the desired value of switching frequency. Both are called inside the interrupt of the A/D Converter.

### 4.4.1. PID Control

This subroutine uses the previous calculated variables *Ref\_Current* and *Meas\_Current* in fractional format. *Meas\_Current* is subtracted from *Ref\_Current* in order to calculate the error. The error value is parsed into proportional, integral and derivative components to produce a *ControlOutput* used to compensate the current error (26). The expression that defines the control output:

$$\begin{aligned} \text{ControlOutput} = \text{ControlOutput} + \\ + \text{ControlDifference}[0] * \text{PIDCoefficient}[0] \\ + \text{ControlDifference}[1] * \text{PIDCoefficient}[1] \\ + \text{ControlDifference}[2] * \text{PIDCoefficient}[2] \end{aligned}$$

The PID controller implementation takes advantage of the MAC instruction of the dsPIC DSC for fast execution.

The digital control implemented is based on the following formulas:

<i>ControlOutput</i>	The output of the controller
<i>ControlDifference[0]</i>	Most Recent Error
<i>ControlDifference[1]</i>	Previous Calculated Error
<i>ControlDifference[2]</i>	Current Error before <i>ControlDifference[1]</i>
<i>PIDCoefficients[0]</i>	$K_p + K_i = K_d$
<i>PIDCoefficients[1]</i>	$-K_p - 2K_d$
<i>PIDCoefficients[2]</i>	$K_d$

The format of the calculations produced by the PID control is in Fract16 and it uses the MAC instructions.

The Fract16 format is useful for this kind of implementation due to the fact that is free of overflow on multiplication. The variable *ControlOutput* represents the output of the controller from -1.0 to 0.99997. The use of this format presents a high advantage: the multiplication of two 16-bit numbers will require 32 bits for the result, but according to this format is possible to round it into a 16-bit number committing an error of  $2^{-16}$  (27), (28).

The MAC instructions are useful to implement the calculations rapidly enough for the controller output (29)

It uses two table vectors where are accumulating the values of the calculations and prefetching the next ones. One of the table vectors is for X Memory and the other is for Y memory. These are the two registers that the microcontroller uses to implement the calculations with the MAC instructions.

For the case of the controller implemented, the vector table X stores the ControlDifference vector and the table vector Y stores the PIDCoefficients vector. In order to make the explanation easily to understand an example is presented, taking one of the instructions from the program:

```
_builtin_mac(x_prefetch,y_prefetch,  
            &ControlDifferencePtr, &x_prefetch,2,  
            &PIDCoefficientsPtr,&y_prefetch,2,0);
```

In this case, x\_prefetch and y\_prefetch are two back-up variables used just to implement the calculations. ControlDifferencePtr and PIDCoefficientsPtr are the pointers that store the actual value of the X or Y table vectors.

1. The first elements from the vector ControlDifference and PIDCoefficients are multiplied and the result is stored in the accumulator, in this case: ControlOutput register.
2. From the address in the X space pointed by the register ControlDifferencePtr, loads the value of the next element to the register x\_prefetch.
3. After reading the array element in the X space, increments the value of the register ControlDifferencePtr, storing the next value of the array.
4. From the address in the Y space pointed by the register PIDCoefficientsPtr loads the value of the next element to the register y\_prefetch.
5. After reading the array element in the Y space, increments the value of the register PIDCoefficientsPtr to point at the location of the next element of the Y array.

The final value of all the calculations is stored in the ControlOutput register, following the equation previously shown.

The hardware specialized for DSP instructions, allows that all these instructions are executed in one instruction cycle, performing all the calculations very fast.

When the calculations are made the error values are stored for next calculations and the PWM function is called.

The flow chart for this routine is shown below:

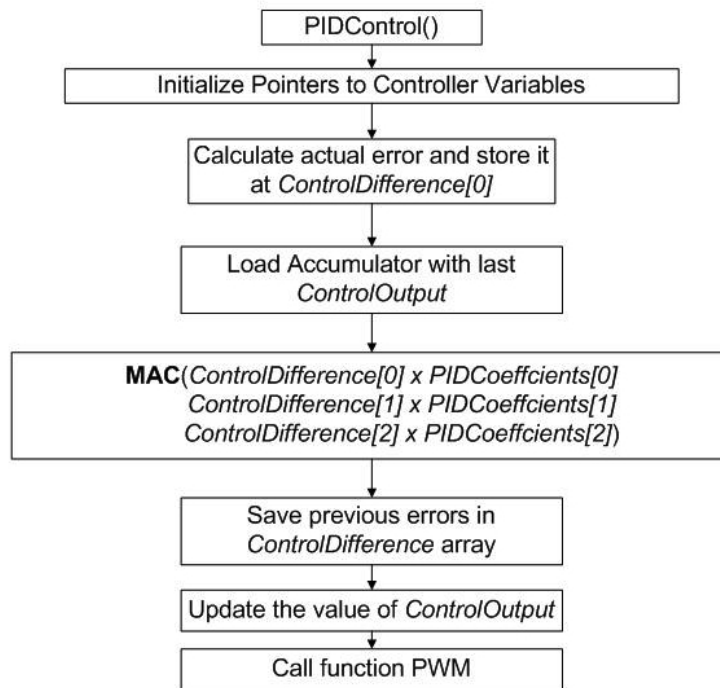


Figure 4-4 Flow-chart of the PID function

In order to prove that the controller was working proper some simulations were made using the PWM module.

The input reference was a frequency value instead of a current value and in the Measured\_Current variable the output from the PWM module (*PTPER*) was charged. On this way the reference was set with the potentiometer and it was possible to see the changes in the output of the PWM.

The system was fast enough, having small differences in the output respect with the reference. This was fixed increasing the value of the integer parameter of the controller. The results of the simulations are exposed below:

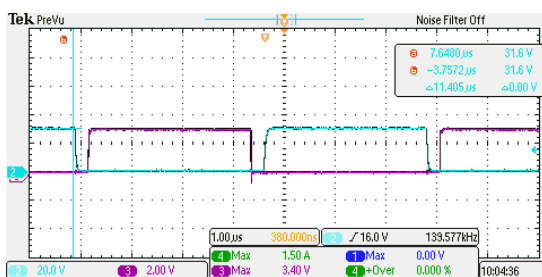


Figure 4-5 Scope waveform with 140kHz

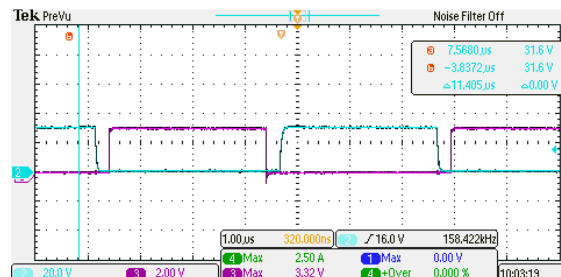


Figure 4-6 Scope waveform with 160kHz

From these simulations just it is just possible to see that the frequency has changed, in the first picture the frequency was set at the resonance value and in the second picture a value of 3.3V was set in the potentiometer of the reference obtaining almost the value of 160 kHz desired.

#### 4.4.2. PWM function

This function is based on the previous one explained before. In this case is just need to update the latest value of the register and due to the fact that the immediate update bit is set to one, the output of the PWM is automatically update to the new value.

The two only registers that are affected by the changes from the controller are:

$$PTPER = ControlOutput$$

$$MDC = PTPER/2$$

The first register corresponds with the frequency of the PWM and the second one with the duty cycle of it. As the duty cycle remains constant and is the 50%, no more calculations are needed.

## 4.5. Simulation results

Some simulation results are shown below:

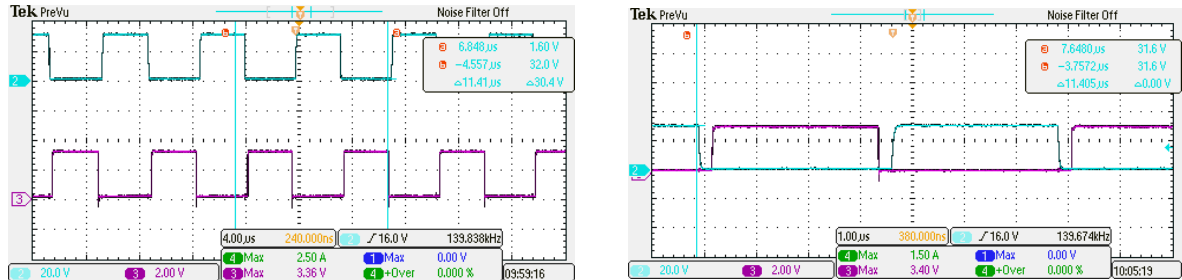


Figure 4-7 Scope signals of the PWM waveforms

As it can be seen the frequency of the waveform is 140kHz, being complementary waveforms and with a duty cycle of 50% and a dead time to enable the soft switching of the switches of 240ns approximately.

## 4.6. Conclusions

To perform an accurate and precise control the implementation of the MAC instructions is helpful and performing the equations through the Fract16 format enables rounding value for the operations instead of truncation, enabling more accurate results, without missing information due to the overflow on the multiplication.

The use of interrupts enables to program an easier code. The program is inside an infinite loop where the ADC interrupt is produced. It reads the inputs for the conversion and inside of it, calls the PID Control and after provides the controlled signal the PWM is updated. This procedure enables a fast control.

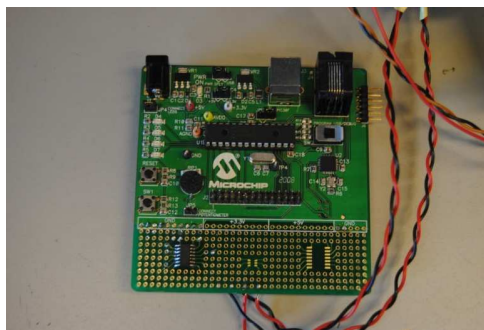


Figure 4-8 Image of the microcontroller programmed

# 5. Inductor Designing

The Inductor designing process developed to obtain the desired values for the inductances is explained in this chapter.

There are two main parts inside this chapter five: The first part is the explanation of the procedure to build the regular inductance, with a magnetic core. The second one has to be with the explanation to design the inductor responsible to produce the magnetic field. That inductor is an air-coil inductor and has different procedure.

## 5.1. Core Inductor Procedure

There are several ways to design one inductor. The procedure chosen was the one explained inside the (30) used in parallel with the specification from the manufacturer. A brief explanation will be presented in this report.

The material of the magnetic core for this inductor is Kool Mμ. This core has a distributed air gap made from 85% Iron, 9% Silicon and 6% Aluminium alloy powder for low losses at elevated frequencies (31).

Before starting with the calculation, all the parameters are presented below:

*L: Inductance value: 33,185μH*

*N: Inductor Number of turns.*

*AL: Value from the manufacturer. Relates the inductances of the core with the square of number of turns.*

*ΔB: Value of the flux density.*

*Ac: Cross section of the core: 1.444cm<sup>2</sup>.*

*ρ: Value of the resistivity of the copper: 1,724e-6 Ωcm.*

*MLT: Mean Length Turn. It is a value provided by the manufacturer: 6,995cm.*

*WA: Core Window Area: 9,48 cm<sup>2</sup>.*

*AW: Section of the wire.*

*R: Resistance of the wire.*

The number of turns is calculated from the manufacturer through the parameter AL:

$$A_L = \frac{L}{n^2} 10^9 \quad (5.1)$$

This equation relates the inductance and the air gap. The core used has a distributed air gap. In the case that it does not have that distribution the air gap length may be calculated.

From the datasheet AL=156 nH/turns<sup>2</sup>; the value for the inductance is a parameter known. The number of turns obtained was 15.

With the number of turns, the section and the voltage it is possible to calculate the flux in the core with the next expression:

$$\Delta B = \frac{\lambda}{2 * n * A_t} 10^9 \quad (5.2)$$

The λ parameter is calculated through the integral of the positive part of the applied voltage waveform. In this picture below is easier to understand it:

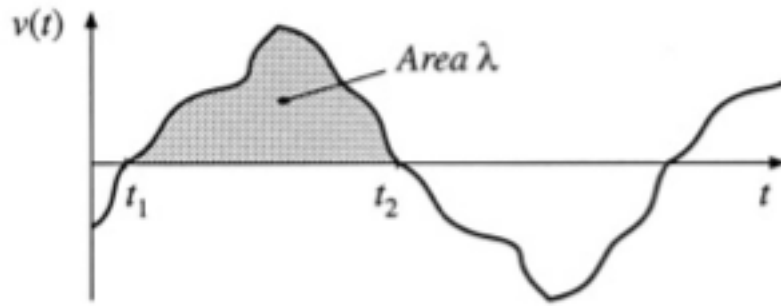


Figure 5-1 Arbitrary terminal waveforms (30)

This value is related with the voltage frequency, the duty cycle of the waveform and its amplitude through the formula:

$$\lambda = D * T_s V_{amp} \quad (5.3)$$

### 5.1.1. Power Losses

With the previous values is possible to calculate the power losses of the inductor.

The core losses are strong dependent on the frequency and the flux, but each material has different behaviour. To calculate this value, the manufacturer provides an equation that relates those parameters:

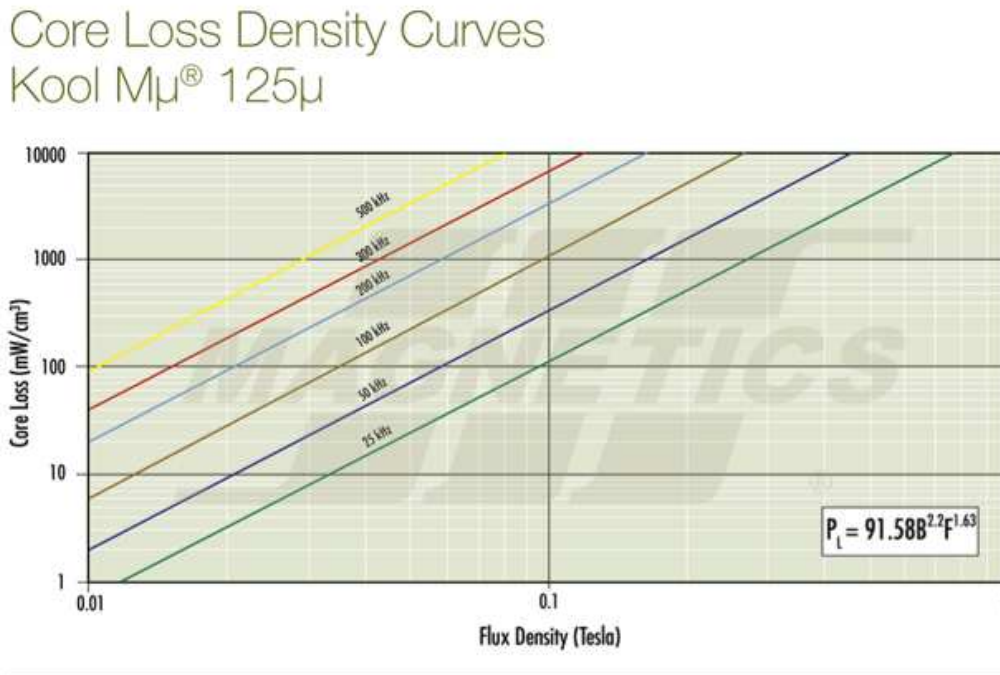


Figure 5-2 Core Loss Density Curves of the Core Material (31)

With the value of the flux previously calculated and a frequency of 140kHz, the value obtained was: 11,867 W/cm<sup>3</sup>.

The copper losses can be calculated with the expression:

$$P_{Cu} = \frac{\rho * n * MLT * I^2}{W_A} \quad (5.4)$$

It is strongly dependent on the amount of wire used. The value obtained is: 4,84 mW.

The total amount of losses is the summity of the losses in the core and the copper. The final result is: 11,87 W.

As the total power losses were too high, it was considered a reduction of the flux. This is possible by increasing the size of the cross section and maintaining constant the turns.

This is not strictly possible due to the fact that if a new core is added to the previous one, the air gap changes and the inductance obtained for the same number of turns is bigger.

In the laboratory a comparison with different cores and different turns was made to see if the ratio between the air gap and the inductance was changing. The results were:

With two cores and 15 turns, the inductance obtained was 89,9μH; almost three times bigger that the one expected. That means that the air gap has changed increasing the parameter  $A_L$ :

$$A_{L2} = \frac{L}{15^2} \sim 400 \text{ nH/turns}^2 \quad (5.5)$$

Considering the equation to obtain the air gap length (30):

$$l_g = \frac{\mu_0 * A_c * n^2}{L} \quad (5.6)$$

Considering that the air gap is distributed in the same ratio in both cores, it is possible to obtain a comparison between the sections  $A_c$  and the inductance coefficient  $AL$ :

$$\frac{A_{L1}}{A_{L2}} = \frac{A_{c1}}{A_{c2}} \quad (5.7)$$

The inductance coefficient is directly proportional to the section. Therefore increasing the size the double;  $AL$  increases the double too.

With the new value of  $AL=399,55 \text{ nH/turns}^2$  to obtain the same inductance it is just need 9 turns.

Making again the previous calculations the results are exposed below:

$$\begin{aligned} \Delta B &= 0,195 \text{ T} \\ P_{Cu} &= 0,968 \text{ W} \\ P_{Fe} &= 7,946 \text{ W} \\ P_{tot} &= 8,914 \text{ W} \\ N &= 9 \text{ turns} \end{aligned}$$

The new power losses are few smaller in comparison with the previous ones but still it is a reduction.

The wire's calculations were taken into consideration too. Calculating the minimum cross section needed and the final resistance of the wire:

$$A_w \leq \frac{K_u * W_A}{n} \quad (5.8)$$

For this section the resistance obtained is:

$$R = \frac{\rho * n * MLT}{A_w} = 1.14 \text{ m}\Omega \quad (5.8)$$

## 5.2. Air Coil Inductor Procedure

This was the topology chose for the inductor responsible to provide the magnetic field. This topology presents certain advantages in comparison with the previous one:

- The problem with the saturation is avoided because there is no magnetic core.
- It is free of iron losses, which affect ferromagnetic cores.
- Increasing frequency the Q-factor of the inductor becomes more efficient due to the same fact as the previous point, no ferromagnetic losses.

As the inductor has no ferromagnetic core, more wire turns are needed to achieve the same inductance value. This means: larger coils, lower self-resonance and higher copper losses. To avoid these two last drawbacks, the inductor is installed inside a resonant tank and the cable used to build the inductor is a low resistance conductor, where each strand of the cable is independent from the whole structure, achieving smaller resistance.

The two main topologies inside the air-coil inductor are: Single layer coil and multi layer coil:

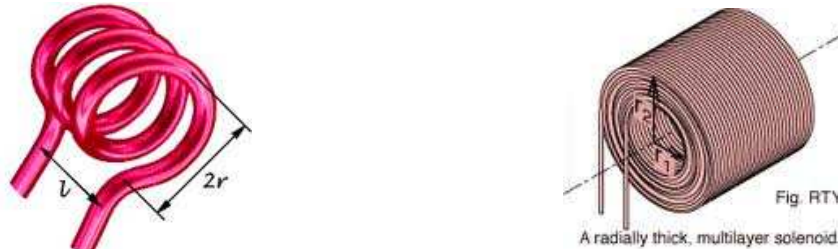


Figure 5-3 Different configurations of air coil inductors (32)

The first type presents some advantages to the second one: lower self-capacitance and higher self-resonant. It is a topology easier to build and appropriate for the project.

### 5.2.1. Core Inductor Procedure

To calculate all the parameters of the inductor, the Wheeler's formula was used (32):

$$L = \frac{0.001 * N^2 * r^2}{(228 * r + 254 * l)} \quad (5.8)$$

The physical parameters are shown in the picture above.

L: Value of the inductance [H]

r: Coil radius [m]

l: Coil width [m]

N: Number of turns

To minimize the length of the cable as much as possible and with it decrease the iron losses, a MATLAB script was programmed, where all these parameters were taken into account.

To be able to apply that equation some constraints have to be considered:

- The coil length in meters has to be shorter than 0,8 the value of the radius.
- The number of turns multiplied by the thickness of the cable cannot be smaller than the total wide of the inductor.

The final result was inside a matrix 100 x 100 where all the parameters that fulfil the constraints were inside.

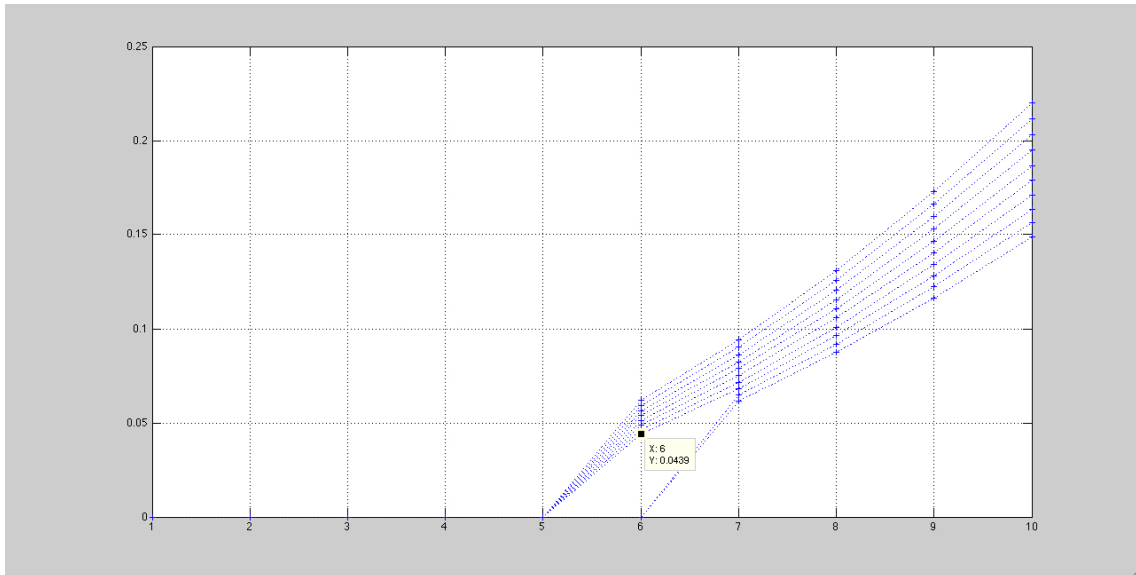


**Figure 5-4 Plot of all the possible values of the inductor**

The selection criterion was that value of width, which would fit the inductance value with the shortest length of wire possible.

An approximation for the power losses was considered, applying the equation [Same equation as before]

The final results are include in the table below:

Final Inductance value [ $\mu\text{H}$ ]	1.432
Coil Width [cm]	4.39
Coil Radius [cm]	5.22
Number Of Turns	6
Minimum Length of wire need [m]	0.984
Thickness of the wire [mm]	7.1
Power Losses [W]	4.286

**Table 5.1 Obtained values of the work coil**

The final disposition of the inductor was



**Figure 5-5 Picture of the work coil**

Due to the final layout of the converter, it was decided to remove one of the turns of the inductor, in order to have more wire distance and make easier the connection of the hall sensor.

As it can be appreciated in the picture above, the final number of turns is five and it remains more length wire to connect the inductor to the PCB. The MATLAB script is added in the appendixes.

## 6. Protection system

This chapter presents the designed strategy for protecting the circuit and keeping safe the user. It contains a study about main possible malfunction events, general description about working principle of the protection. Further details are explained after general description and finally the protection-timing chart is depicted.

### 6.1. Study of malfunction events

The CL-LCR resonant converter was designed to operate in a safe mode both the circuits and user. Ageing, wrong production of components, wrong use or configuration between other reasons may cause malfunction behaviour of the system, and the probably destruction or human damage. Designing the protections must be based upon these different possibilities of malfunction events. The system was simulated by means of PLECs to recreate all the possible cases and observe the response of the rest of the system. Next list shows the simulated cases.

- Short-circuit high side mosfet
- Short-circuit low side mosfet
- Short-circuit both mosfets

The simulations have been done considering that the power supply provides 300 V and, the switching frequency set at 140 KHz. It should be taken into account that the power supply is ideal, so it will provide infinite current. Also the copper losses were not taken into account. So the main reason of the simulation is to offer behaviour of the circuit in the ideal scenario. Next figure shows the implemented system in PLECs.

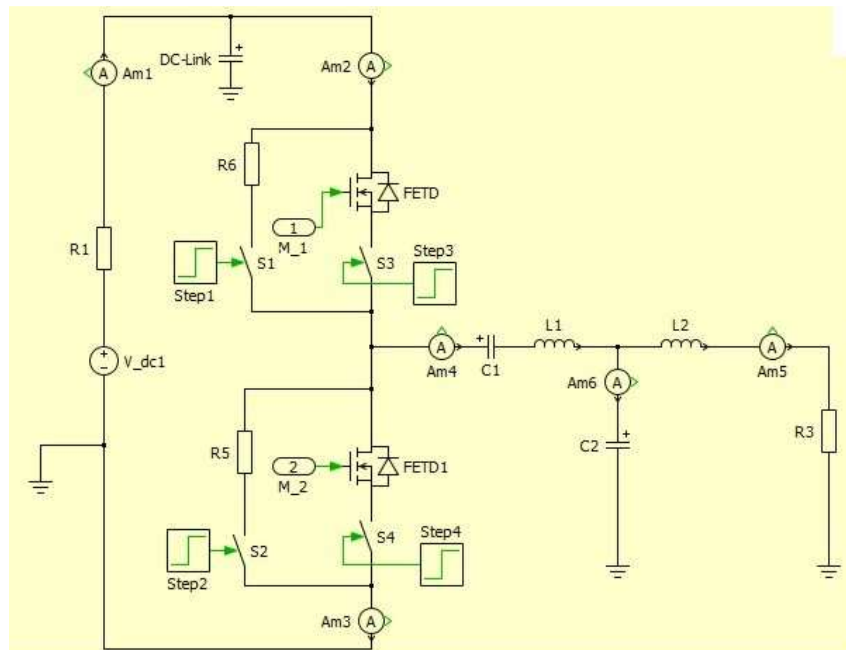
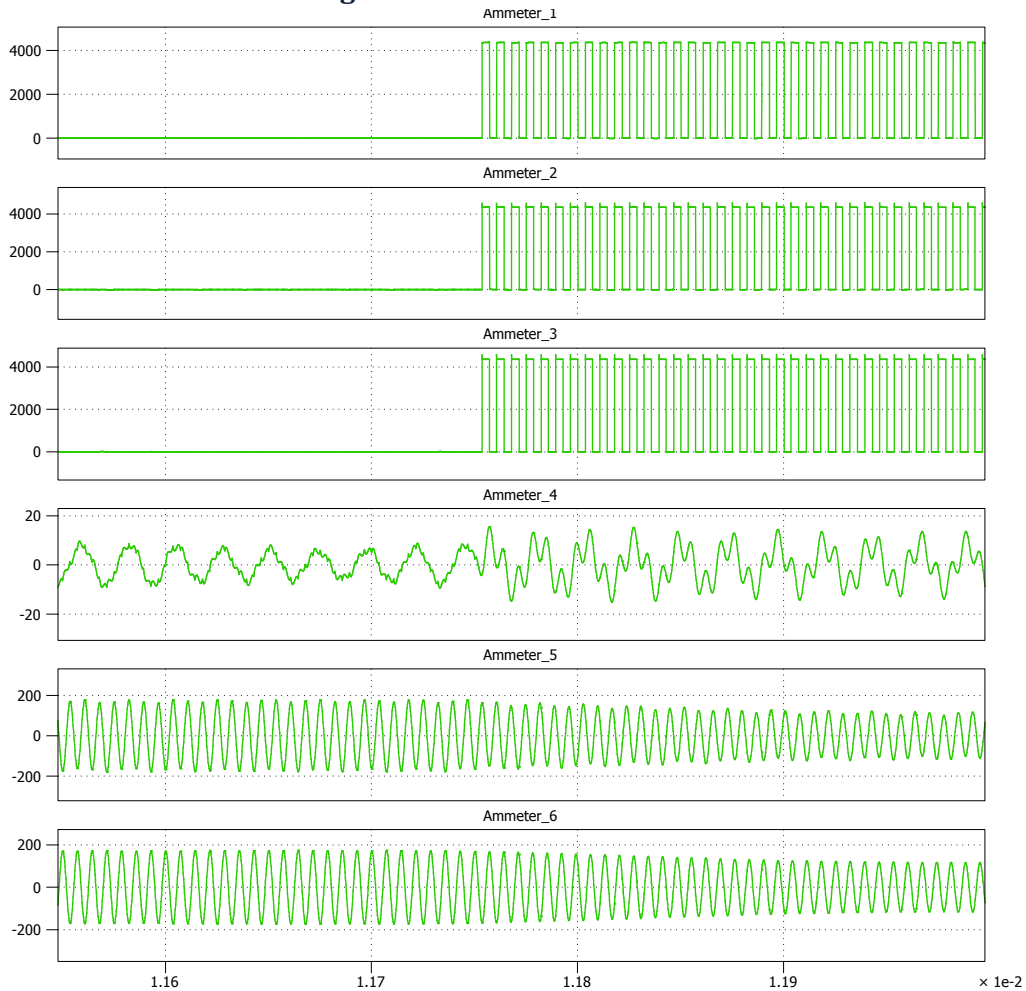


Figure 6-1 Implemented circuit for short-circuit simulation

As can be seen in the figure 6-1, there are some switches; the aim of the switches is to simulate a short circuit event. In case of short circuit, one switch, which is normally opened, is connected in parallel respect to the mosfet. A small resistance was added in series with the switch due to PLECs does not allow to simulate short circuit event; however the small value of resistance represents accurately the short circuits events. The current was visualized by means of the ammeters and one scope. The ammeters were placed in specific points (see figure 6-1)

to study the behaviour of the circuit at those points. Ammeter\_1 is the current provided by power supply, ammeter\_2 is the current at high side mosfet, ammeter\_3 corresponds to the current at low side mosfet, ammeter\_4 measured the current flowing to the CL- resonant tank circuit, ammeter\_5 and 6 are current in the inductor tank and capacitor tank respectively.

### 6.1.1. Short-circuit high side mosfet



**Figure 6-2 Current when occurring short circuit at high side mosfet**

Before short circuit event 8  $A_{RMS}$  were flowing through the ammeters 1, 2 and 3. After short circuit, the current waveform became squared wave and the value increased until 4000  $A_{peak}$ . This is due to the input of resonant circuit is oscillating between the voltage that provide the voltage supply and ground. The resonant circuit suffered harmonic injection at the moment of the short circuit. At the resonant tank the current suffered a reduction from 200  $A_{peak}$  to 100  $A_{peak}$ .

### 6.1.2. Short-circuit low side mosfet

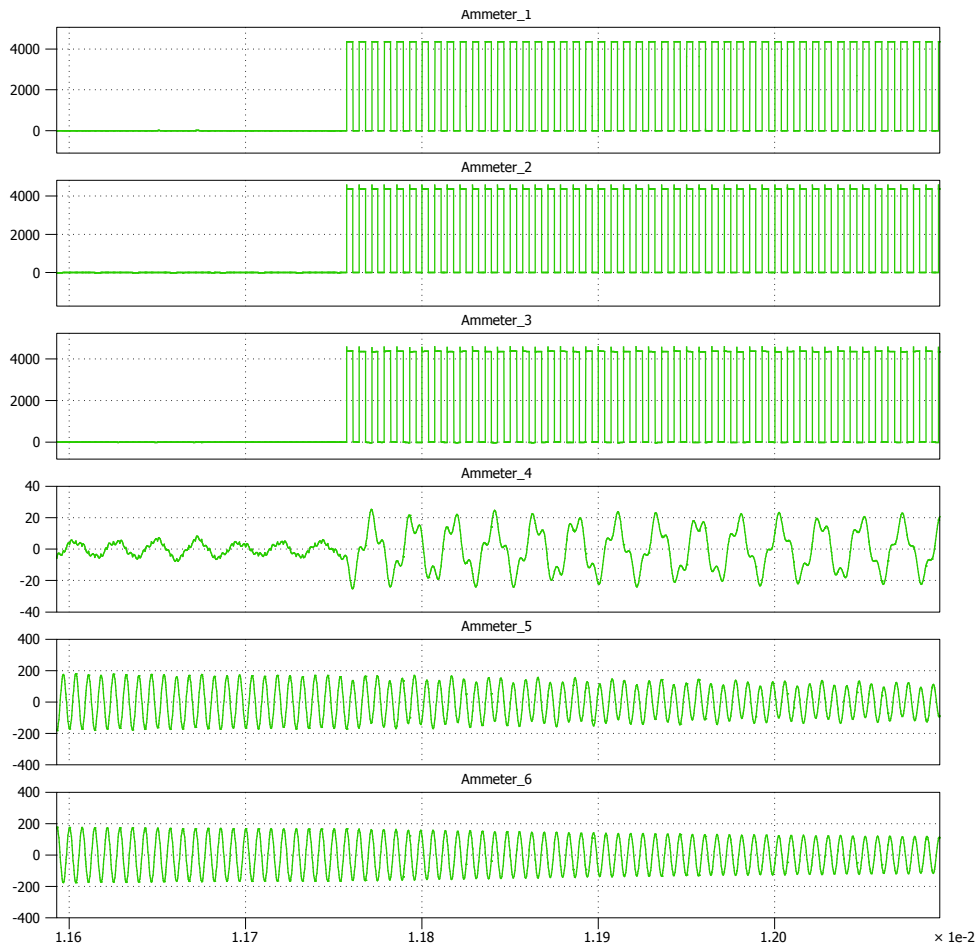


**Figure 6-3 Current when occurring short circuit at low side mosfet**

This case shows the same results as previous simulation. High current flows through the mosfets. There are presence of harmonics (see ammeter 4) and 100 A of decrement appeared at the resonant tank.

### 6.1.3. Short-circuit both mosfets

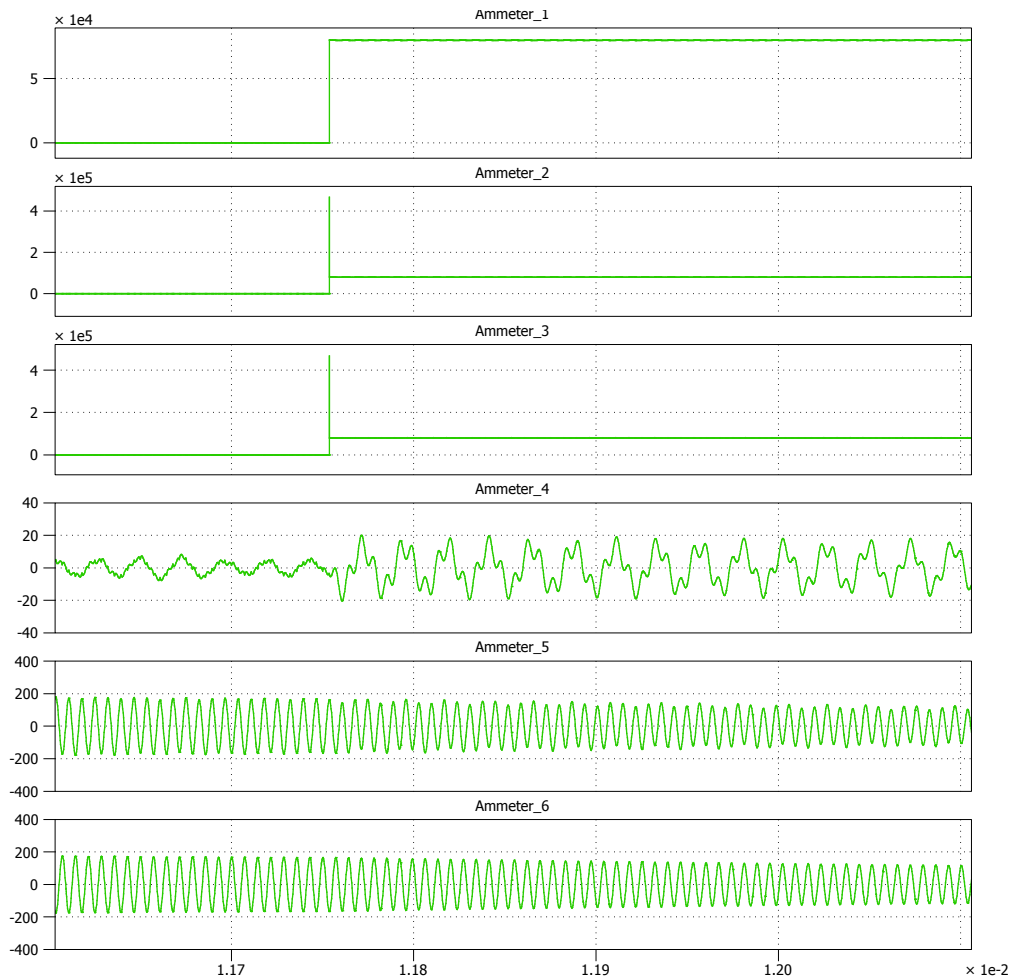


Figure 6-4 Current when occurring short circuit at both mosfets

The short circuit on this case presented a step waveform at the output of the ideal voltage supply. The value of the current changed from 11.38 A<sub>peak</sub> to greater than 5 kA. This step waveform leads to a Dirac current waveform at both mosfets. As can be seen, the current drops until 1 kA juts when the step waveform reached the maximum value. The three last graphs show the same behaviour as previous cases.

### 6.1.4. Conclusion from simulations

High current will flow through the mosfet in the case of short circuit. It should be noticed that this high current will not flow through resonant circuit, since power supply is short-circuited and injects almost all the current to ground. It should be remarked that this is only an ideal scenario, therefore real case will not reach 5kA because the short circuit current is affected by the applied voltage and also by parasitic resistance (PCB tracks, cables, equivalent series resistance ESR from capacitor). Calculations of the available short circuit current can be seen at point 6.4. Although it will not reach 5 kA, it will reach high current and as a consequence the destruction of the mosfets will take place since they can only withstand a pulse current of 80 A. The resonant tank may withstand this short circuit conditions since the current did not increase too much but it was reduced. So some prevention and protection of malfunction must be designed to avoid human and circuit damage. Some of the reasons that may cause these events are ageing, defective component, shoot through due to wrong configuration of switching, malfunction of the code in the dspic or latch in the trigger signal.

## 6.2. General system protection

The mosfets are the critical components in the converter. They are the most vulnerable component, while the other components can withstand greater current. The protection was designed to avoid the previous events taking as a designing reference next parameters: Overcurrent and prevention of latching up due to the code or other electrical/electromagnetic reasons.

### 6.2.1. Overcurrent

The importance of tracking and avoiding overcurrent was clearly shown in the preceding simulations. The overcurrent is sensed by means of hall sensors. They are placed in strategic points of the circuits to track instantaneously the current at certain points in the converter. In the next figure current sensors are depicted by red circle.

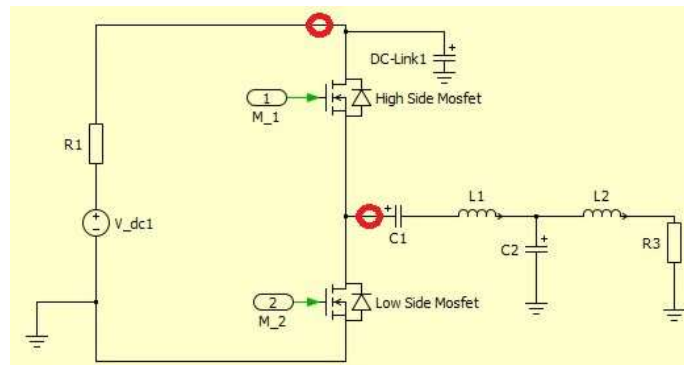


Figure 6-5 Hall sensors in the circuit

When the sensors track one value that is above the one was set as 35 A, a crowbar protection circuit is triggered to take the entire current in and blow the fuse. (See 6.6 crowbar circuit).

### 6.2.2. Watchdog

Watchdog is a feature of some microcontrollers and consists in an internal timer that should be declared at the beginning of the code. The aim of the watchdog is to avoid possible malfunction of the software which may caused problems in the switching signal. Sometimes the microcontrollers get inside of infinite code loop due to EMI, high temperature, input signal that exceeds the operation limits between other reasons. This loop may generate an undesired behaviour of the signal and the mosfets may be turned on/off improperly (33).

Watchdog was programmed for each segment of code because each segment has a predetermined duration. In case that the watchdog timer exceeds the programmed time for one segment of the code, the microcontroller will reinitialize and will start from the beginning the programme.

Last but not least, logical circuit was designed to avoid possible latch-up of the mosfets. See point 6.5.1 for further information.

## 6.3. Crowbar protection design

The crowbar protection is made by means of two capacitors (crowbar capacitors), one fuse, two thyristors or Silicon Controlled Rectifier (SCR), one inductor. When designing crowbar protection circuit, the use of relays was taking into account instead of using one fuse. Electromechanical relays were refused because the time response is into the range of some ms and also will not be able to disconnect until the current pass through zero. High current

produced by short circuit or malfunction must be clear from the circuit faster than some ms, otherwise the mosfet/s or even more components may blow up, so electromechanical relays are not suitable for this purpose.

The disposition of the crowbar protection circuit is depicted in the next figure.

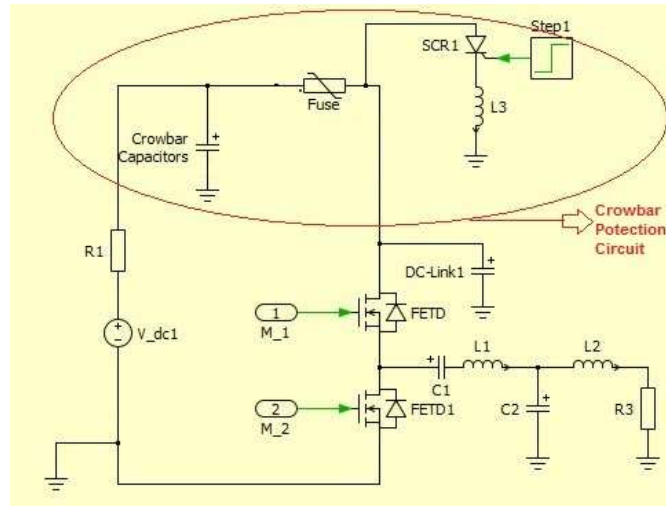


**Figure 6-6 Crowbar protection circuit**

All the components, which formed the crowbar circuit, were positioned at strategic place in the converter in order to disconnect the power supply when abnormal operation takes place. The operating principle is trivial, when some of the hall sensors measure an overcurrent event; the digital control (see point 6.5 for further explanations) generates one signal to trigger the SCR. At the moment that the SCR is latched, the current will flow directly to ground because the SCR will bypass directly the crowbar capacitors to ground. This trigger will produce a high current, which will flow through the fuse and SCR, and thus, it will blow up the fuse, and the converter will be disconnected from power supply.

### 6.3.1. SCR

SCR are well known for withstanding high current during normal operation. Nevertheless the most important parameter when designing crowbar protection circuit is called fusing energy ( $I^2t$ ) and is defined as the maximum forward non-repetitive overcurrent capability that the device is able to handle without any damage (34). This parameter must be matched with the fusing energy of the fuse in order to blow the fuse before SCR may be damaged.

#### *a. Driving SCR*

SCR will not work as a normal switch, i.e. SCR as part of crowbar protection circuit will switch once to cause a short circuit between crowbar capacitors and ground, so the drawn current will be high. This current may destroy the SCR in case of the  $di/dt$  exceeds the maximum value. The  $di/dt$  is also affected by how the gate is driven on, i.e when the gate is driven on, conduction across the junction starts in a small region and progressively propagates across the total junction. Anode current will initially be concentrated in this small conducting area, causing high current densities, which can degrade and ultimately destroy the device. To minimize this  $di/dt$  effect, the gate should be turned on hard and fast such that area turned on is initially maximized. (34)

In order to turn on the SCR hard and fast the drive signal should be greater than the needed one for normal operation. Next figure shows the gate trigger characteristics and power ratings of the SCR.

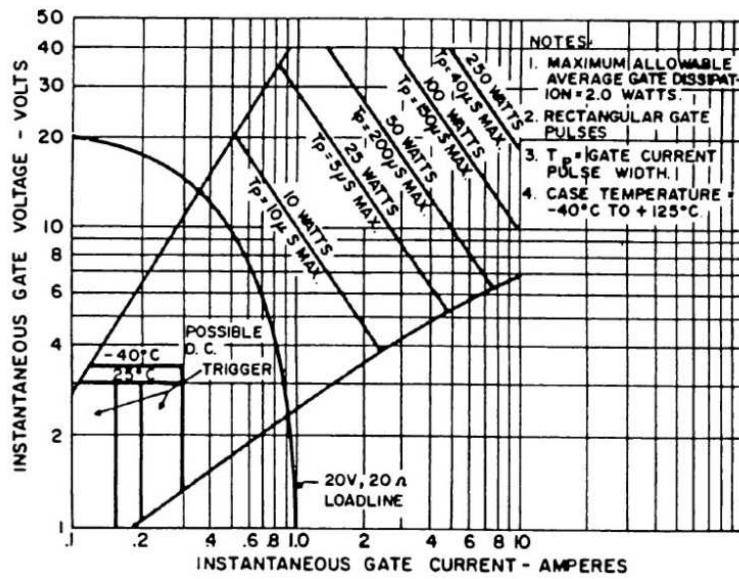


Figure 6-7 SCR triggering characteristics (35)

As can be seen the gate can withstand more power dissipation than the average one, which is 2 watts, this condition can be only applied when providing shorter pulse at the gate. The SCR driver can ideally provide 20 volts and 2.3 amps, this values produce a dissipation of 41.1 watts. AS can be seen in the laboratory work, the maximum limits were set at 20 volts / 1 amp which give 20 watts. Hence, 25 watts was taken as a reference in order to set the adequate width of the pulse signal, which corresponds to 5  $\mu$ s as maximum width.

In the first design, the pulse signal was set at 70 ns (see point 7.1.1). According to laboratory work was found out that the width of this pulse was not long enough to trigger the SCR1 properly. In order to avoid any problem when triggering SCR, 4.5  $\mu$ s was set as pulse width, which it is closed to the maximum value 5  $\mu$ s. See chapter 7 for further information about laboratory work.

### 6.3.2. Fuse

The fuse was chosen according to the converter requirements. Standard fuses were not suitable for the crowbar protection, so high speed fuse or semiconductor fuse has been selected in order to offer adequate protection. One of the main differences is the nominal melting times; this value is presented in the datasheet as a graph plotted against RMS short circuit current. See figure next figure.

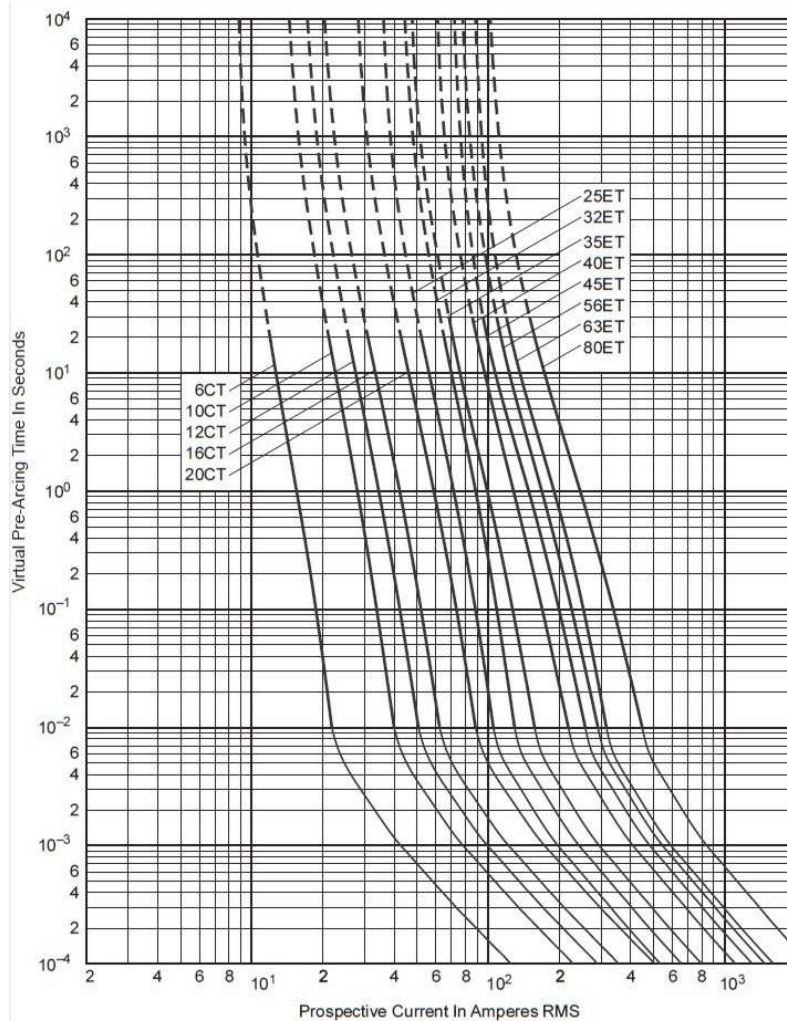


**Figure 6-8 Prospective current against pre-arcing time of fuse (36)**

Once the type of fuse was chosen other parameters must be taken into account, like  $I^2t$ .  $I^2t$  value of the fuse must be always lower than the SCR one in order to blow the fuse before the SCR is destroyed. So  $(I^2t)_{fuse} < (I^2t)_{SCR}$  (34). According to datasheets of the components the  $(I^2t)_{fuse}$  is 1635 ( $A^2t$ ) at 660V, at different voltage the value must be derated as follows  $K \cdot (I^2t)_{fuse}$  at 660V, where  $K=0.5$  at 300V. SCR presents also different values for  $I^2t$ , which depends on the exposure time. However, the minimum value is 2850 ( $A^2t$ ), which is greater than the fuse value 817.5 ( $A^2t$ ).

After running some test in the laboratory was found out that high speed fuses were not suitable for the initial design of the crowbar protection. These types of fuses were designed to operate under longer short circuit events. The initial crowbar design presented a rise time of 13.4 ns, which is really far from the minimum value presented in the datasheets (100  $\mu s$ ). Therefore, in order to overcome this problem the initial crowbar circuit protection was redesigned. As the main problem was the width of the short circuit current, the strategy was focused at this point. The width was made longer by means of one inductor connected in series with the SCR. Usually this strategy is used in order to protect the SCR when the increment of amperes/second (A/s) ratio of the circuit is greater than the SCR one, although this was not the case; it was still the best solution.

### 6.3.3. Inductor

The calculation of the value of inductor was based upon the time constant of the crowbar circuit when SCR is latched. This time constant is given by the value of resistance along the current path and the value of the inductor. The resistance was calculated in the report at point 6.4.4 in order to obtain the short circuit current, and has a value of approximately 250 mΩ. It should be noticed that the time constant of R-L circuit defines the rise time that will take the current to reach the 63.2 % of its final value. The minimum needed time is 100 μs, so it will be used this value to calculate the value of the inductor, which is given by:

$$L = R * \tau = 250 * 10^{-3} * 150 * 10^{-6} = 25\mu\text{H} \quad (6.1)$$

### 6.3.4. Discharging path

In case of overcurrent, the digital control circuit and crowbar protection circuit will disconnect the converter from power supply. Also the mosfets will switch off by means of the digital control circuit, see point 6.5.1. Therefore, the DC-link (at high side mosfet) and the blocking capacitor (at the input of resonant circuit) will be charge even there is no power in the circuit. So if the operator needs to change the fuse, or other actions related to the maintenance theses capacitor must be discharged. Thus, one resistor was placed in parallel with the DC-Link and another resistor was placed in parallel with DC-blocking capacitor. The drawback of this strategy is the extra power loss added to the circuit. In order to avoid these losses, high resistance must be chosen. In this way, the current consumption will be minimized, but it should be noticed that if the value of the resistance is too high the time constant will be high, and thus, the discharging time will be also high, so the value of the resistance must be a trade-off between power losses and time constant. Figure 6-9 shows the present case. The open circuits simulates the blown fuse and the mosfets in off state, so there would not be any path in order to discharge the energy stored at the capacitors if there were not be the resistors R4 and R2.

The energy at tank capacitor will be discharged at the resonant tank circuit even there were not be any resistance in parallel with the blocking capacitor, because the intrinsic resistance of the resonant circuit will damp the resonance.

The crowbar capacitors will be discharged at the moment that the user switches off the power supply.

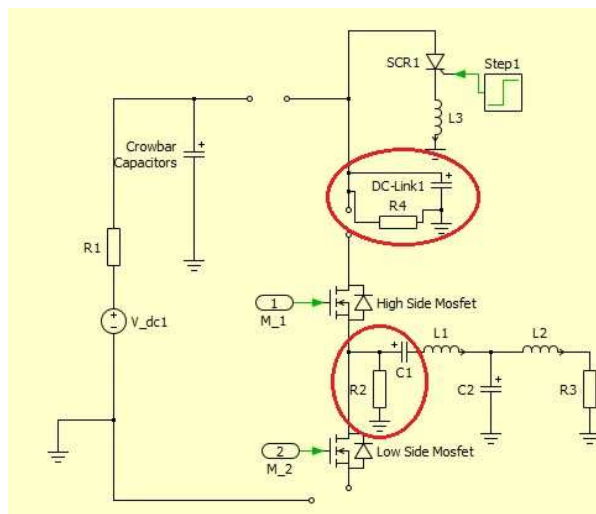


Figure 6-9 Discharging path (red)

## 6.4. Short circuit current

The short circuit current must be calculated in order to design the proper protection. Mainly, the short circuit current at the crowbar point will be influenced by the impedance of the circuit. Assuming that the circuit is working at the resonance frequency, the impedance will be given by total equivalent resistance through the next path: equivalent series resistance of crowbar capacitors (ESR), resistance of the tracks of PCB, the initial resistance value of fuse, cable resistance and dynamic impedance of SCR. Next points will show how to calculate all these parameters.

### 6.4.1. Calculation of resistance of the track of PCB

The resistance of the track depends upon dimensions of the track and the resistance of the material, which is made the PCB and it is given by (37):

$$\text{PCB track resistance} = \frac{R \times L}{W \times T} \quad (6.2)$$

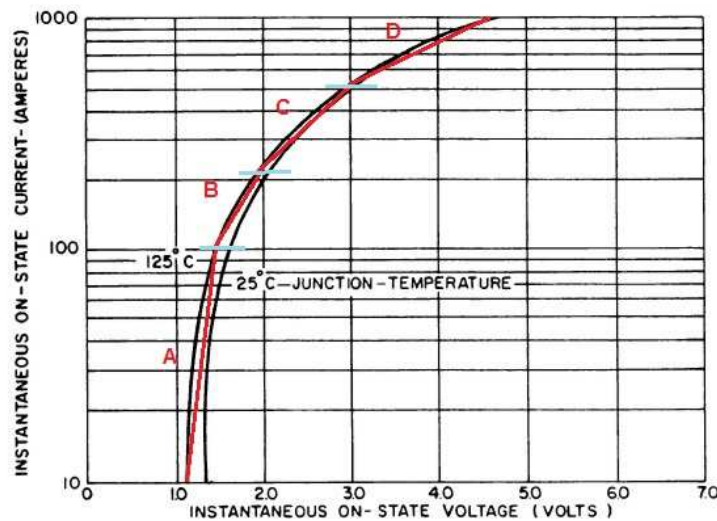
Where:

- R=Resistance (temp. coeff.)[uΩ] =  $[1,7241 \times 10^{-6} \times [1 + 0,0039 \times (T - 20)]] = 1.757$
- L=Length[cm]=11
- W=Width[cm]=1.5
- T=Thickness[cm]=0.0105

The resistance of the track of PCB is approximately: 1 mΩ

### 6.4.2. Dynamic impedance of SCR

The dynamic impedance of SCR must be derived from the figure given in the datasheet which shows on state voltage against on state current, see next figure.



1. MAXIMUM ON-STATE CHARACTERISTICS

Figure 6-10 SCR on state electrical characteristics (35)

The figure shows the dynamic behavior of the SCR at different temperatures (black). It should be noticed that the figure was also divided in 4 sections (red-A, B, C and D) which approximately represents the different slopes of the curve per each section. The slope is the resistance of the SCR at each segment. Assuming that the short circuit current will be into the range of 1 kA, only the resistance of segment D was calculated.

$$R_d = \frac{\Delta V_F}{\Delta I_F} = \frac{4.5 - 3.0}{1000 - 500} = 3 \text{ m}\Omega \quad (6.3)$$

The resistance of the SCR is: 3 mΩ

#### 6.4.3. ESR, fuse and cable resistance

The ESR value of the crowbar capacitor was taken from the datasheet and tested during the laboratory work. The next value represents the maximum value.

$$R_{\text{crowbar capacitor}} = \text{ESR} = 600 \text{ m}\Omega$$

The crowbar capacitor link was formed by 2 capacitors connected in parallel, so the equivalent ESR is 300 mΩ. From the laboratory test was derived that the real equivalent resistance is approximately 240 mΩ.

Next values were measured in the laboratory with a LCR meter and the result was as follows

$$\begin{aligned} R_{\text{fuse}} &= 450 \text{ }\mu\Omega \\ R_{\text{cable+bananas}} &= 35.7 \text{ m}\Omega \end{aligned}$$

#### 6.4.4. Short circuit current

Short circuit current is given by the Ohm law, which is the applied voltage divided by impedance, and the impedance is the addition of all the resistance which formed the path of the short circuit current. Short circuit current is given by:

$$I_{\text{pk}} = \frac{V_{\text{dc-link}}}{\Sigma R_i} = \frac{300}{1.2 * 10^{-3} + 3 * 10^{-3} + 35.7 * 10^{-3} + 240 * 10^{-3} + 450 * 10^{-6}} \quad (6.4)$$

$$I_{\text{pk}} \cong 1.2 \text{ kA}$$

It should be noticed that previous current is the prospective peak value, which is asymmetrical, and the fuse datasheet gives the prospective RMS current, which is symmetrical current. In order to transform the peak current to RMS current the next reference (38) was taking into account and it shows that the RMS value will lie between

$$\frac{I_{\text{pk}}}{\sqrt{2}} < I_{\text{RMS}} < \frac{I_{\text{pk}}}{2.3} \quad (6.5)$$

So the prospective RMS short circuit current will be between 521 and 850 A<sub>RMS</sub>.

## 6.5. Logic circuit-Trigger signal

The logic circuit tracks the current from the converter by means of the hall sensors, and when the overcurrent takes place, this circuit generates the trigger signal. This process must be extremely fast in order to offer fast and safe disconnection of the converter. For this reason, most of the IC's, which formed the logic circuit, belongs to AHCT family. At point 6.5.2 the timing chart of the circuit is shown.

The logic circuit works as follows, the hall sensors are tracking continuously the current of the converter, either positive or negative values. Meanwhile the watchdog controls the right behavior of the code.

Hall sensors generate from the input current a proportional output current. The relation between input and output current for the hall sensors used in the converter is 1/1000, i.e. if

the input current is  $35 A_{peak}$ , which is the maximum allowable current, the output current will be  $35 mA_{peak}$ . This output current will transform into voltage by means of the measuring resistance. This transformation is given by Ohm's law,  $V=R*I$ . The value of this resistance must be into the range that the manufacturer set in the datasheet; otherwise the sensor will consume more power or will provide wrong output current. The measuring resistance must be between 100 and 315  $\Omega$ . Since the resistance used is 133  $\Omega$ , the previous requirement is accomplished.

Next figure shows the digital control for one input of the hall sensor and next paragraph explains how it works the entire circuit.

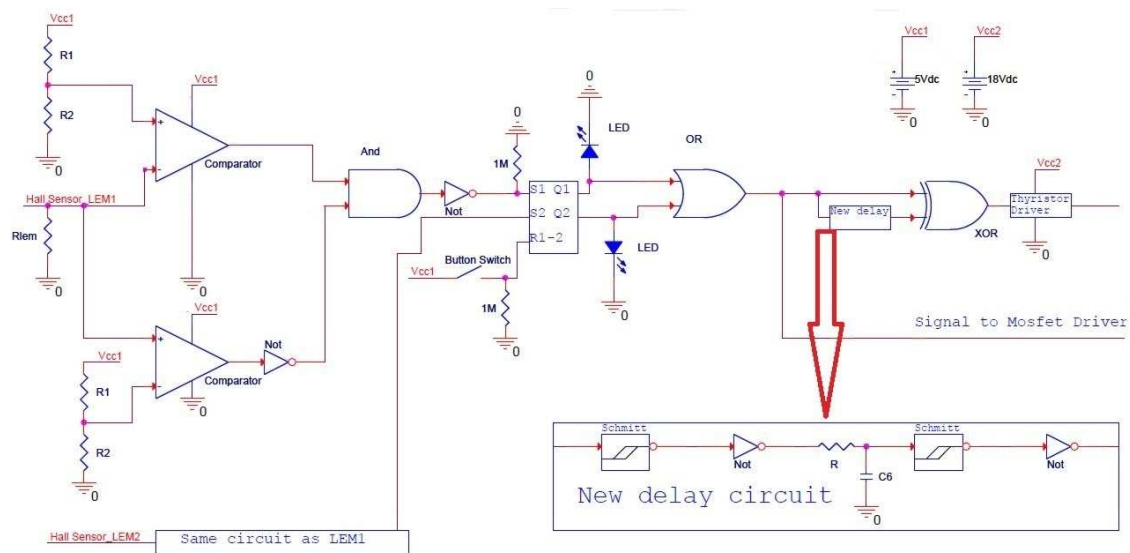


Figure 6-11 Schematic of digital control

The inputs of the logic circuit are the voltage across the measuring resistances from both hall sensors. Since the voltage is predictable the control can be easily implemented. The strategy lies on the comparison of two voltage levels, one is the generated by the sensor, which is 4.6 volts at the maximum allowable current, and the other one is generated by two resistances which form a voltage divider.

The voltage at the midpoint of voltage divider was designed to obtain 4.5 volts, being  $R1=100\Omega$  and  $R2=1K\Omega$ . Therefore, if the voltage level of the measuring resistance is greater than the voltage divider, the comparator will change its logic state and it will trigger all the circuit. The circuit is formed by two comparators with 4 inputs, and the inputs are connected such the comparator device can compare either positive or negative current. The output will be high whenever the current at the converter is not greater than  $35 A_{peak}$ .

After the comparators the both signals are processed by one AND gate, which during normal operation of the converter will provide as an output high logic voltage. The next logic gate is inverter gate, which inverts the signal from high to low logic voltage.

Next the inverter gate, one RS-latch process the signal which output state is low when the converter operates into the current range, but it becomes high when an overcurrent event takes place, and it will remain as high state until the device is not reset by means of one button switch.

After the latch device, one OR gate centralizes the processed signals that come originally from the both hall sensors. Until this point, the signal can be described as step trigger signal, but this step is not useful for the crowbar application since it is necessary to limit the time of the

triggering, otherwise the power dissipation at the gate of SCR will be too high and the device will be destroyed.

So the implementation in order to provide the adequate width is as follows. The RS-latch output signal is divided in two tracks, one is connected directly to one input of the XOR gate, and the other is connected to the sub-circuit called delay time. This sub-circuit is made by means of Schmitt trigger- RC – Schmitt trigger.

XOR gate provides at the output high logic voltage only when both inputs are equal, either “1” or “0”, and the output is low when the one input is low and the other is high or vice versa. Therefore, if an overcurrent event takes place, RS-latch will be high, XOR gate will be also high, and after 4  $\mu$ s approximately, the delay circuit will charge the RC components. The other input of the XOR gate will be high as well, and as a result, the output becomes low. The trigger pulse ends. After the XOR gate, one thyristor driver adapts the signal to the SCR gate.

### 6.5.1. Turning off mosfet

In addition to the trigger circuit, another signal is also generated in order to turn off the mosfets and avoid that high current can flow through them. This signal is generated at the same logical circuit that processes the hall sensor signal. As can be seen in the circuit depicted in previous figure, one of the OR gate output is used to generate this signal. It should be noticed that whenever one sensor measures more than 35  $A_{peak}$ , the RS-latch will be in high logic state until the user press the button switch or reset, therefore, this signal can be used for this purpose.

The signal is conducted until the converter PCB, where is located the mosfet driver. At this PCB the signal is processes at first point by means of one Schmitt- trigger inverter, which will invert the input signal. After that, the output is divided in two tracks that are connected to two AND gates. These two AND gates have as an input the dspic signal, i.e. the PWM signal, and the generated signal by Schmitt-trigger inverter.

On this way, if there is no overcurrent, the Schmitt-trigger inverter will be always high logic level, and the AND gates will not affect the PWM signal; but in case that overcurrent would occur, the Schmitt-trigger inverter will have low logic level, therefore the AND gates will present low logic level, and the PWM signal will not reach any more the mosfet driver. In the next figure is depicted the implemented circuit.

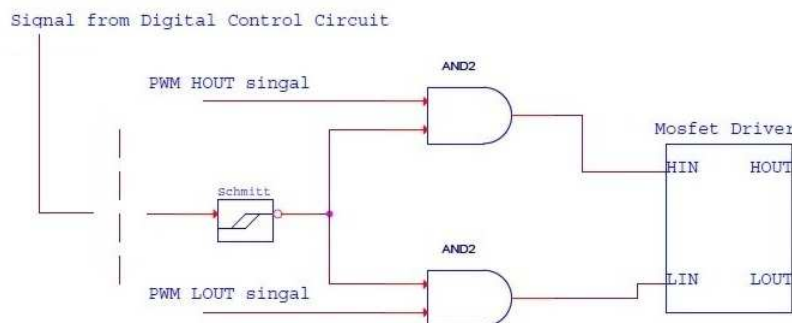


Figure 6-12 Logic control- turn off mosfets

### 6.5.2. Timing chart

Next figure shows the timing chart of the logic circuit when any hall sensor senses an overcurrent. The delay time was taken from the datasheets of the ICs. It should be remarked that only the highest values were taken in order to show the worst case scenario, and also the delay time from datasheets is made by means of an output capacitor which value is 15pF,

meanwhile the input of the logic gates have an input capacitance of 10 pF. So it is expected that the delay time will be lower than the indicated by the timing chart.

The slopes represent the delay time of each logic gate, and the value of each slope is depicted at the bottom of the figure in nanoseconds. Only delay circuit has its value represented at the end of the rising time. The slopes were drawn proportional to each time, but some of them were drawn with dashed lines in order to show that the length of the segment is not proportional; otherwise it would be impossible to represent the graph.

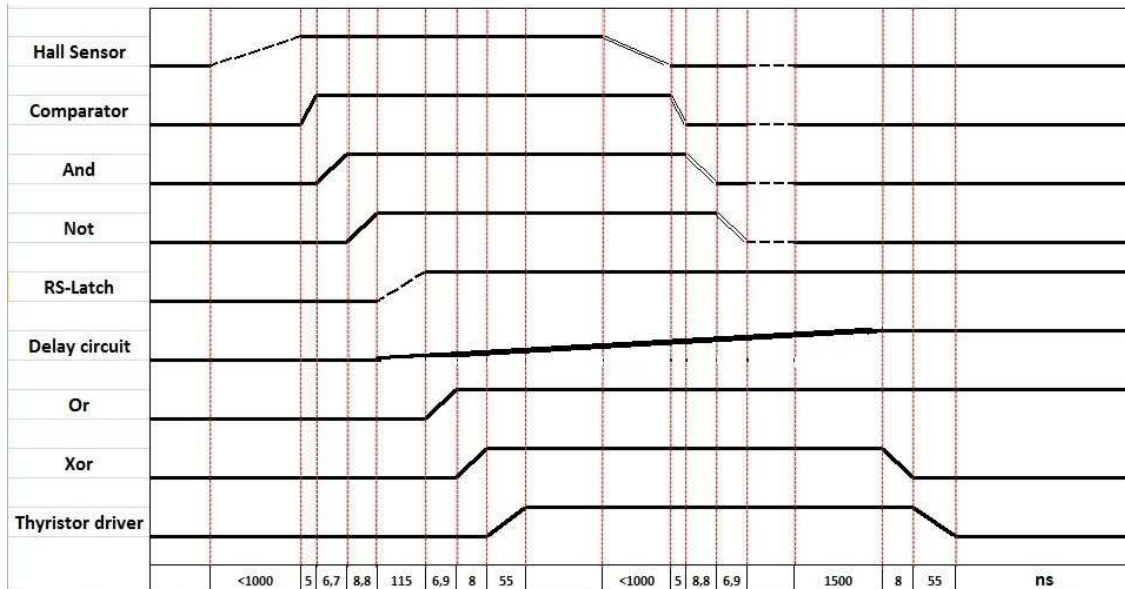


Figure 6-13 Timing chart

According to the timing chart, the trigger signal will be on state 1.14  $\mu\text{s}$  after the overcurrent took place at the converter. The delay circuit provides the proper width to the trigger signal and will become off after 1.213  $\mu\text{s}$ . The total process from sensing the overcurrent to end of the pulse trigger signal takes 2.353  $\mu\text{s}$ .

# 7. Laboratory work- Digital control circuit and crowbar protection circuit

This chapter shows the different experiments that were run in the laboratory related to digital control and crowbar circuit protection. The first part of the chapter is compounded by the results associated to the generation of the trigger signal, after that behavior of SCR is showed and finally the conditions that the fuse blew up.

## 7.1. Digital control-First design

This section is based on the generated signal in the digital control and the response of SCR when this signal was applied. As was explained in chapter 6, the digital control tracks continuously the current at the converter, if the current exceeds  $35A_{peak}$ , the digital circuit triggers and generates the pulse signal to trigger the SCR in order to disconnect safely the power supply from the circuit by means of the fuse. The results obtained in the laboratory experiments show only the signal of interest for SCR, i.e. RS-latch, delay circuit, XOR gate and thyristor gate are the signals of interest, since this ICs compound the last part of the digital control and the most important point, they are the responsible of triggering the SCR properly.

The first design of the digital control was not successful. As it will be showed in the next section 7.1.1, the pulse width of the trigger signal was not enough to latch the SCR and create the adequate short circuit for the crowbar protection. These tests were made with similar circuit as initial one, i.e. some changes were done in order to be able to develop the test. Hall sensors were not able in the lab, so potentiometer was placed instead of the sensors to simulate the overcurrent input in the circuit. Moreover, only one input was tested, since it was not necessary to build 3 three times the same circuit. Next figure depicts the schematic of the circuit of the initial digital control. The main difference of this circuit in comparison with the one depicted in the figure 6-11 is the implementation of the delay circuit. The delay for this digital control was implemented by means of inverter gates, i.e 6 inverter gates were connected in series to create the delay signal. This delay was based on the delay of the component itself, so when the preceding signal (RS-latch) became high, every inverter gate added a small delay.

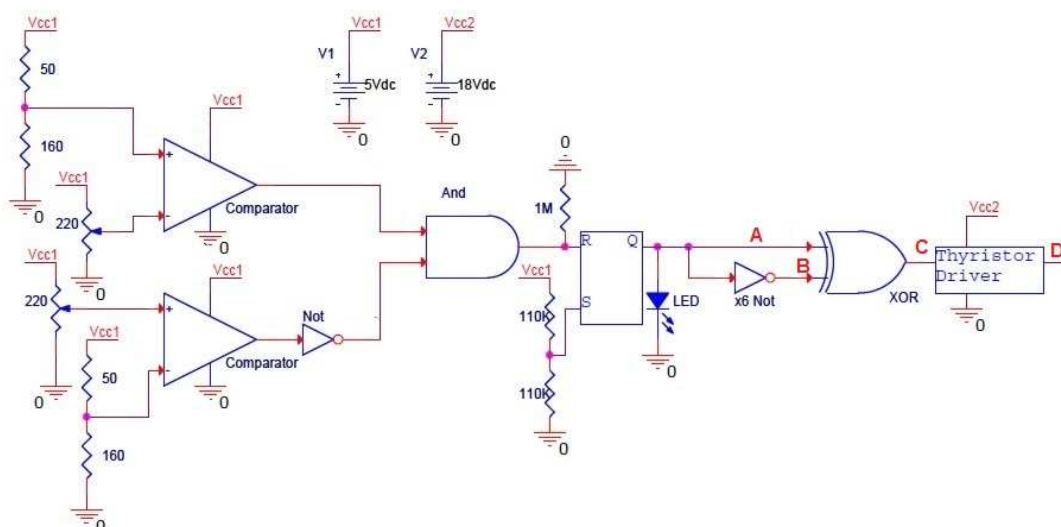


Figure 7-1 First digital control

### 7.1.1. Results of first digital control

Next figure shows the obtained results about digital control circuit, it should be remarked that during this test the circuit was not connected to the SCR, next section will show the behavior of SCR when these signals were applied.

Channel 1(blue) represents the SR-latch output (it is represented as point A in the schematic of the circuit, channel 2 (cyan) represents output of the delay signal (point B), channel 3 (magenta) represents the output of the XOR gate (point C) and channel 4 (green) represented the output at thyristor driver (point D).

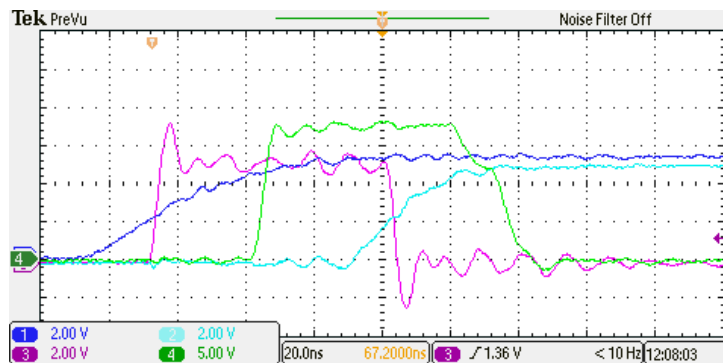


Figure 7-2 Digital control signals

Potentiometer was moved to generate the trigger signal. SR-latch (channel1) was triggered and 20 ns later XOR gate (channel3) generated 4.5 volts. Approximately 30 ns later the XOR output signal activated the thyristor driver (channel4), which reached the expected value of 18 volts. Delay sub-circuit was triggered 80ns later than SR-latch. At the moment that the delay sub-circuit reached 2 volts, XOR gate dropped to 0 volts. 30 ns later SCR driver also dropped to zero.

The figure confirmed that the circuit worked as it was expected, since the goal was to generate approximately 80 ns signal to trigger the SCR faster and during a short period of time in order to avoid its destruction.

The SR-latch generates the on state of the SCR driver and the delay sub-circuit controlled the “on” time adequately.

From the figure can be derived also the different ways of working of the different logic families. The chosen logic families were CMOS and AHCT. CMOS, which are channel 1 and 2, presented a rise time approximately of 30 ns. By contrast AHCT, which are channel 3 and 4, presented rise time of 5 ns.

Besides rise/fall time, it can be seen the difference of the required minimum voltage to activate IC's. CMOS IC's were activated when the inputs signals reached 5 volts and AHCT IC's were activated when the inputs signals reached 2 volts.

### 7.1.2. Triggering SCR

After testing that the trigger worked correctly, these tests show how SCR worked when the trigger signal was applied. Different voltage levels were applied through SCR. Next figure shows the setup implemented at the laboratory to run these tests.

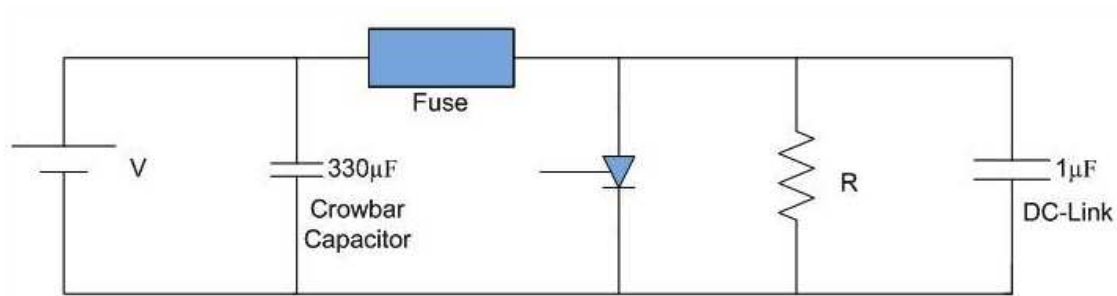


Figure 7-3 Schematic of the setup build in the laboratory

- *Anode-Cathode voltage: 5 volts*

Forthcoming figure shows the results when 5 volts were applied through SCR. Channel 1 is the voltage at SCR, channel 2 is the voltage generated by thyristor driver i.e. gate voltage, channel 3 is the current through gate lead and channel 4 is the current through the SCR.

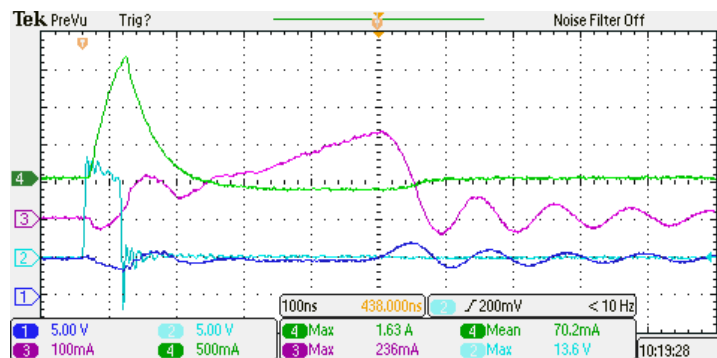


Figure 7-4 Trigger and SCR signals (5V)

The current through SCR reached only  $1.63 A_{peak}$ , when the expected value was approximately  $8.3 A_{peak}$ , which is the prospective short circuit current at these operating conditions. Besides the current, most important factor is the voltage through SCR, as can be seen when the digital circuit triggers SCR, the voltage oscillated but it did not drop its value to 0 volts, which is the desire value because it means that SCR would have been triggered properly. So this test shows that SCR was not trigger and therefore there is no protection for these operating conditions.

Even the result was not expected, some more test with different voltage level were run in order to test if applying higher voltage the SCR could trigger.

- *Anode-Cathode voltage: 10 volts*

Next figure shows the results for 10 volts. Channels are the same as before, channel 1 is the voltage at SCR, channel 2 is the voltage generated by thyristor driver i.e. gate voltage, channel 3 is the current through gate lead and channel 4 is the current through the SCR.

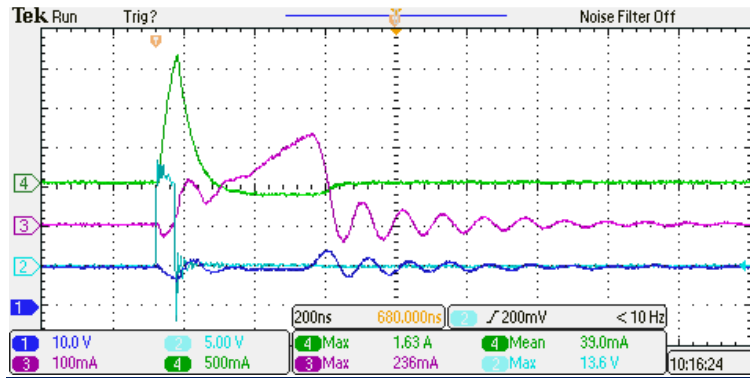


Figure 7-5 Trigger and SCR signals (10V)

The result achieved for this experiment was exactly the same as previous one, the current through SCR was  $1.63^{a_{peak}}$  and the voltage at the SCR terminals did not drop to 0 volts.

- **Anode-Cathode voltage: 30 volts**

Next figure shows the results for 30 volts. Channels are the same as previous tests, channel 1 is the voltage at SCR, channel 2 is the voltage generated by thyristor driver i.e. gate voltage, channel 3 is the current through gate lead and channel 4 is the current through the SCR.

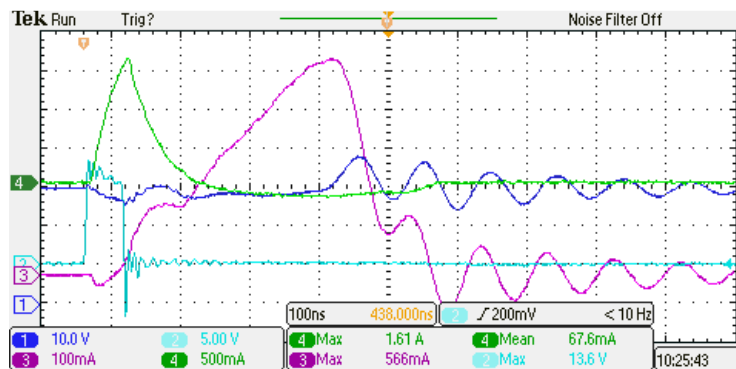


Figure 7-6 Trigger and SCR signals (30V)

The result was not successful; the short circuit current did not vary comparing to precedents tests, neither the voltage at SCR terminal dropped to 0 volts.

### 7.1.3. Conclusions

The protection circuit did not work as it was expected. The peak short circuit current reached the same value for the different tests although they should increase when the applied voltage through SCR increases. Besides the short circuit current, SCR could not latch in on state, therefore the voltage at the anode of SCR remained at power supply voltage, i.e. the converter would not be disconnected from the power supply which was the aim goal of the protection circuit.

Last but not least, the current through the SCR was increasing exponentially until the thyristor driver was on, once the gate voltage dropped to 0 volts the current stopped of increasing its value, by contrast it also dropped to 0 amps. This observation gives as conclusion that trigger width was not longer enough in order to trigger the SCR.

## 7.2. Digital control-SCR

Preceding test showed that digital control was not successfully designed, SCR did not trigger adequately and therefore the converter would not be protected and disconnected from power supply in case of malfunction event. The results gave as conclusion that the width of trigger signal was too small, i.e. SCR could not latch in on state and therefore disconnect the power supply. This section shows the results for the new design and the results about triggering SCR. The voltage applied in the power circuit is up to 50 volts for this section, since it is maximum value that students can reach in the lab without the presence of supervisors.

### 7.2.1. Digital control-longer pulse width

The new delay circuit consists of a Schmitt trigger-RC circuit- Schmitt trigger. As was explained in chapter 4, this configuration permits longer pulse width with fewer components in comparison to previous strategy. The width is controlled by charging time of RC circuit, which is defined by the time constant of RC. The new time delay was set at 4.5  $\mu$ s. See next figure.

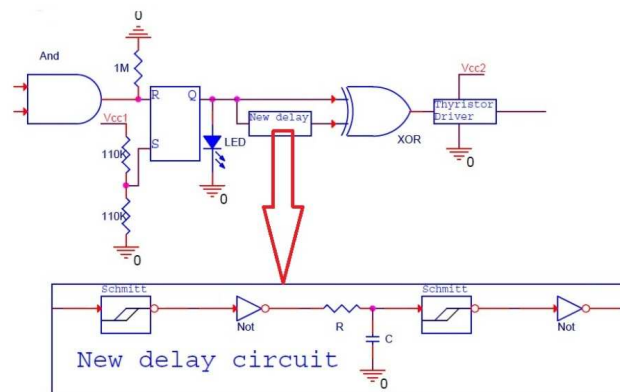


Figure 7-7 Schematic of new delay circuit

Forthcoming figure shows the new delay time that defines the pulse width of the thyristor driver. Channel 1 is RS-latch, channel 2 is the RC charging and channel 3 is the output of the new delay circuit.

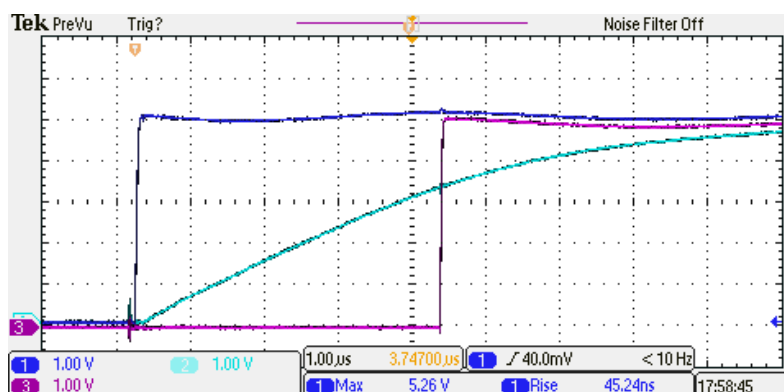


Figure 7-8 New pulse width

### 7.2.2. Triggering SCR.

These sets of tests show the response of the crowbar protection applying different voltage levels through SCR terminals. For the entire next tests channel represents the anode-cathode voltage, channel 2 represents the gate voltage, channel 3 represents current through SCR and channel 4 represents gate current.

- [Anode-Cathode voltage: 5 volts](#)

This test was developed with a gate resistance of  $1\Omega$ . The aim of this small value is to check the amount of current that thyristor driver can supply and the behaviour of the circuit.

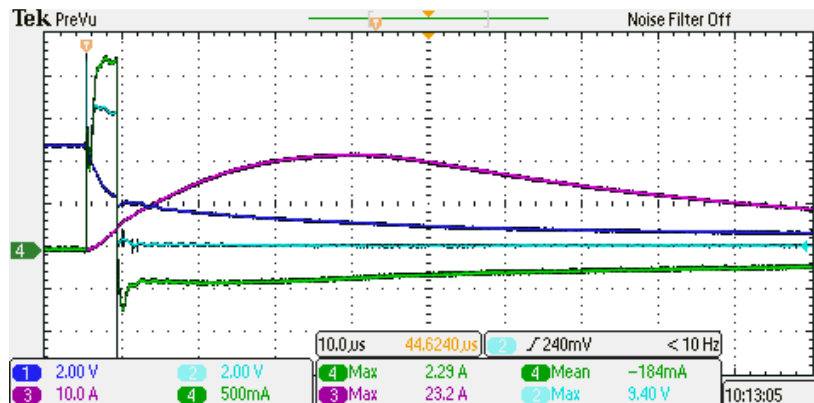


Figure 7-9 Trigger and SCR signals (5V)

Previous figure shows the response of the SCR according to the new pulse applied to its gate. As can be seen the aim was accomplished, the current through SCR did not stop rising when the thyristor driver switched off, by contrast the current kept rising until it reached  $23,2 A_{peak}$ . Also the voltage across SCR dropped to almost 0 volts, so as a conclusion can be said that the new digital circuit triggered adequately the SCR.

Despite the success related to new circuit, it should be noticed that thyristor driver presented voltage/current dropped immediately after their on state. See next figure.

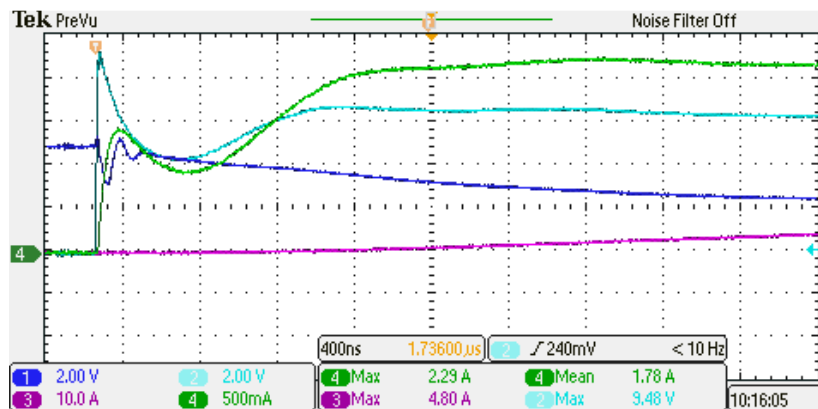


Figure 7-10 Trigger and SCR detailed signals (5V)

Previous figure shows the effect of a low value resistance at the SCR gate. The maximum voltage and current values for thyristor driver were 9.48 volts and 2.29 amps respectively. It should be noticed that after the first voltage peak there was a voltage drop of approximately 5.4 volts. After this transient the voltage was established at 8.2 volts. The current also presented transient behavior. Initially it reached a local maximum of 1.54 amps, then it dropped until 1 amp and finally it reached 2.29 amps. Even this transient cannot be removed it must be diminished.

- Anode-Cathode voltage: 5 volts

This test was applied with the same conditions as previous one but the gate resistance was change from  $1\Omega$  to  $20\Omega$ . This value was chosen according to SCR datasheet, since all values that datasheets provides are based on this gate resistance value.

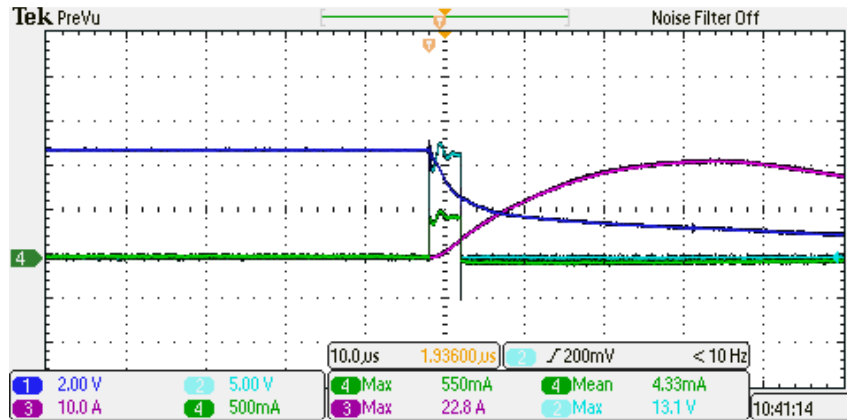


Figure 7-11 Trigger and SCR signals\_new R\_gate (5V)

The figure shows the same behavior according to SCR but the thyristor driver presented less current oscillations, so the signal was more stable. Other difference is the current value; previous case reached  $2.3A_{peak}$  and this case reached  $550mA_{peak}$ , it means that gate dissipates less energy.

This factor is really important when applying pulse signal due to power dissipation, which is related to the pulse width. Previous case presented as maximum power dissipation 21.7 watts and presented case dissipated 7.2 watts. See next figure.

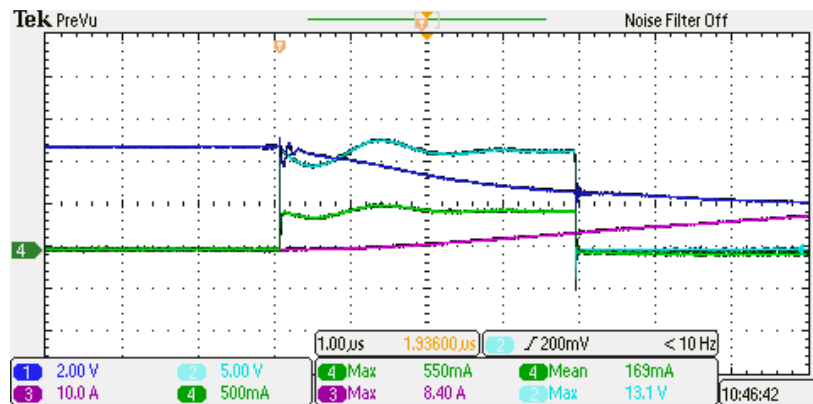


Figure 7-12 Pulse width with R-gate=20

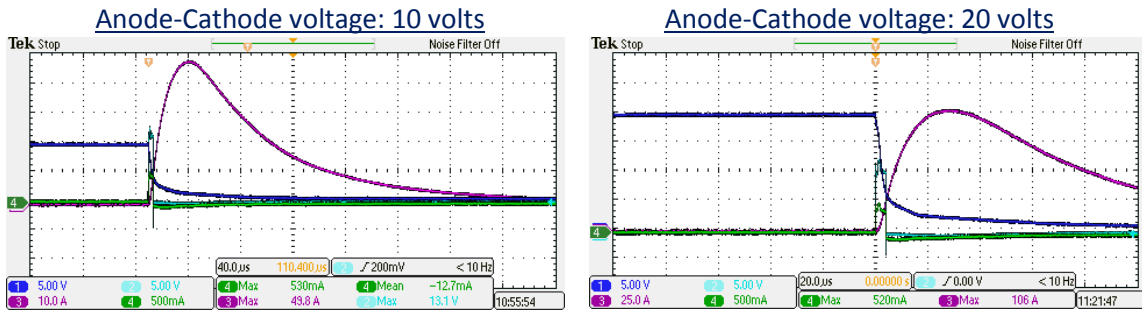


Figure 7-13 Current and voltage across SCR applying 10 and 20 V

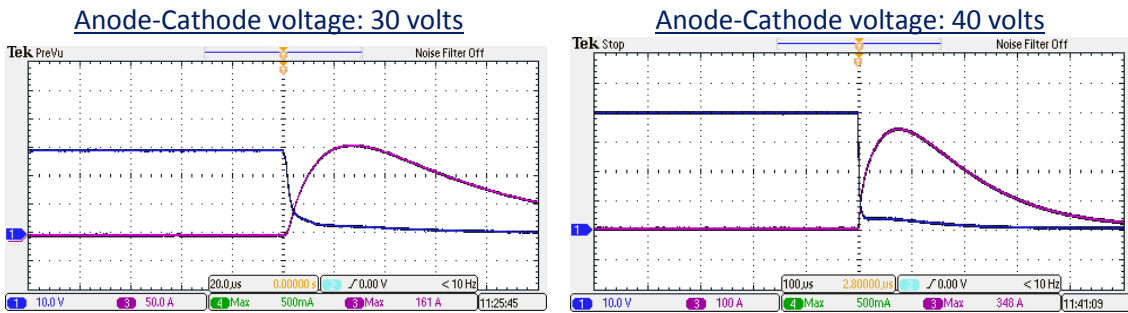


Figure 7-14 Current and voltage across SCR applying 30 and 40 V

Preceding four figures show the response of the circuit under different voltage level, 10, 20, 30 and 40 volts. The behavior was the same for both of them, SCR was triggered properly and thus, high current flowed through SCR and voltage across SCR dropped to 0,09 volts. The peak current values were  $49,8A_{peak}$ ,  $106A_{peak}$ ,  $161A_{peak}$  and  $348A_{peak}$  respectively.

- **Anode-Cathode voltage: 50 volts**

Next figure shows test when applying 50 volts between SCR terminals. It should be noticed that each increment of voltage causes an increment in the prospective short circuit current. This test the short circuit current reached  $436A_{peak}$ .

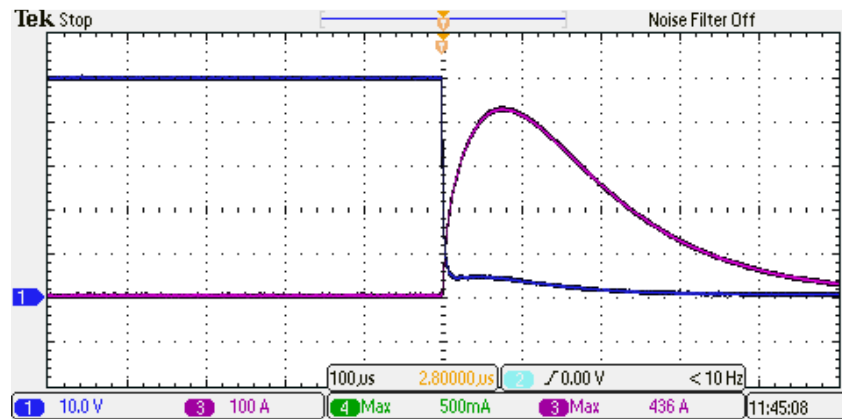


Figure 7-15 Current and voltage across SCR applying 50 V

### 7.2.3. Conclusions

The new triggering circuit worked as was expected and SCR latched in the on state when digital control was triggered. Despite the success of the laboratory work, it should be noticed that the results showed an unexpected behavior. As can be seen the peak current was increasing linearly when the applied voltage was in the range of 5 to 30 volts. After 30 volts the current expected according to previous results would be  $200 A_{peak}$  and  $250 A_{peak}$  approximately when applying 40 and 50 volts respectively. The explanation is as follows, the results for applied

voltage between 5 to 30 volts was done with INSTEK GPS-33303 which it can supply voltage up to 30 volts and 3 amperes. When greater voltage was applied, the power supply was changed for another model which could reach 50 volts, DELTA ELECTRONICA SM 50-S. So as can be easily derived, the power supplies were also providing part of the short circuit current. The reason is that the DC power supplies usually are provided at the output with a capacitor to keep more stable the output voltage, and therefore this capacitor acted as it was connected in parallel with the crowbar capacitor, and as it was explained in chapter 6, it provides to the circuit more available short circuit current.

### 7.3. Test above 50 volts

*This appendix is focused in the behavior of the crowbar circuit when triggering SCR and the applied voltage is in the range of 50 volts to 300 volts.*

#### 7.3.1. Triggering SCR

New DC power supply was set for running new tests. DELTA ELECTRONICA SM 300-S. The tests were run at different voltage levels to study the behavior of the circuit and the power supply, since previous tests with different power supplies showed different behavior at the same conditions. This new power supply has an internal circuit that even during short circuit events tries to keep the voltage between its terminals. It was experimented that when applying voltage from 0 to 30 volts, the voltage dropped to zero and after some milliseconds it recovers again the initial value of the voltage. As the short circuit test may damage this internal control, one power resistance of  $10\Omega$  was placed at the input of the converter, to avoid electrical stress when the provoked short circuit takes place. Moreover other capacitor was placed in parallel to crowbar capacitor. This new capacitor is the same model as the crowbar capacitor one and it was placed in order to provide more current when SCR is triggered. Next figure shows the implemented setup in order to run these forthcoming tests.

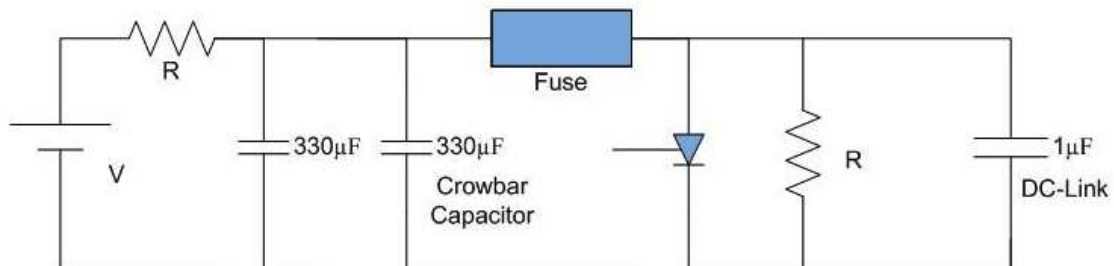


**Figure 7-16 Schematic of the setup build in the laboratory**

Next figures show the different experiments run in the laboratory. Channel 1 (blue) represents the voltage across SCR and channel 2 (green) represents the short circuit current that flowed through SCR.

- Anode-Cathode voltage: 25 volts

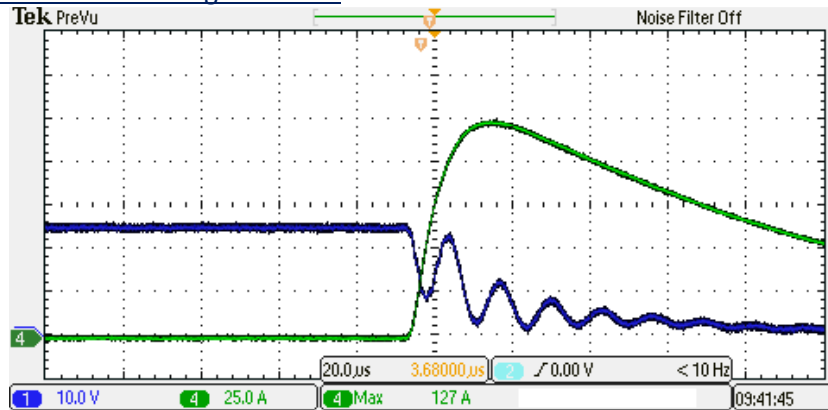


**Figure 7-17 Current and voltage across SCR applying 50 V**

The voltage between the crowbar capacitors was 25 volts due to the power resistance provoked a voltage dropped. The oscillations at the voltage signal are caused by the internal control of the power supply.

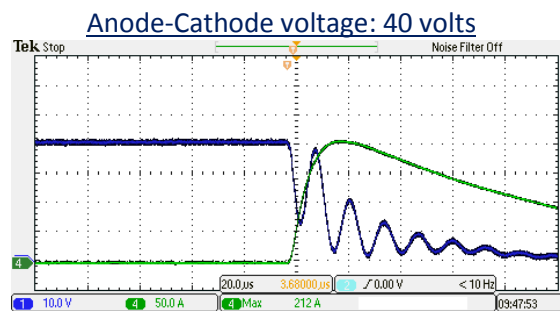
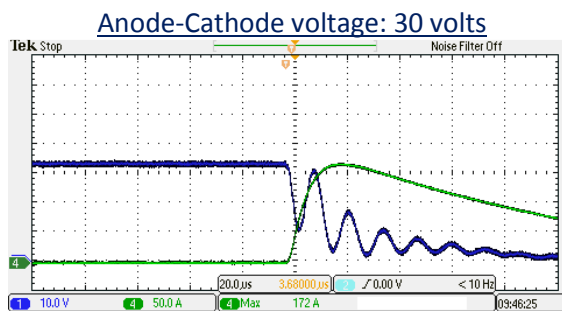


**Figure 7-18 Figure 7-19 Current and voltage across SCR applying 30 and 40 V**

Previous figures show the same behavior at different voltage levels, 30 and 40 volts respectively. The current increased linear to voltage increment. Moreover the power supply tried to keep the voltage between its terminals, it can be seen in the oscillations at voltage graph.

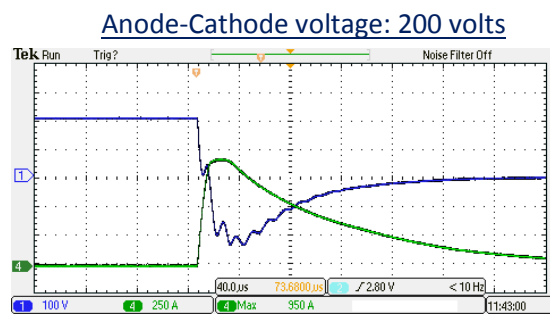
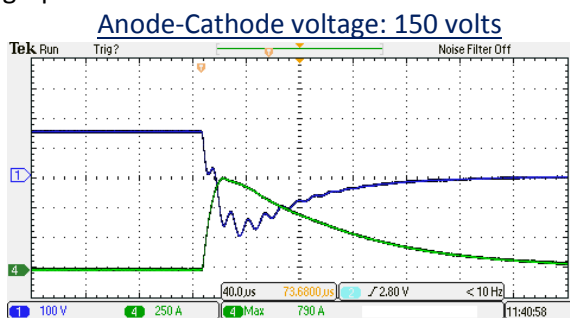


**Figure 7-20 Figure 7-21 Current and voltage across SCR applying 150 and 200 V**

Higher voltage was applied for these tests, 150 and 200 volts respectively. Also the current reached important peak values, 790 and more than 950 A<sub>peak</sub>. It should be remarked that during these experiments the fuse did not blow up even at 950 A<sub>peak</sub>, so other families of fuses were also tested in the setup. The tested fuses were 56ET, 35 ET and 16 CT and no one of them blew up. The problem was not related to the current value, even if it had applied more current, it would not have blown up any of these fuse. The reason and the important parameter was the time exposure, i.e. the time that the current flows through the fuse.

These fuses can withstand high current above their rated value as long as the current pulse lasts some tens of ns. An effort was made to find faster fuses in the market but it was not found any faster fuses than semiconductor ones. Since these were the available fuses, the strategy was focused on creating a wider short circuit current. The best method that was more effective it was the implementation of an inductor in series with SCR.

## 7.4. Test- SCR+inductor

These tests were made with the inductor connected in series to SCR. The first test was done in order to confirm the expected behavior of the current. The second one is when the fuse blew up due to the increment of the short circuit time.

### 7.4.1. SCR-inductor test

As it can be seen in the next figure, the width of the short circuit current has increased in comparison to previous experiments. The maximum current is reached at 150  $\mu\text{s}$  approximately. According to the calculations, the fuse should blow up.

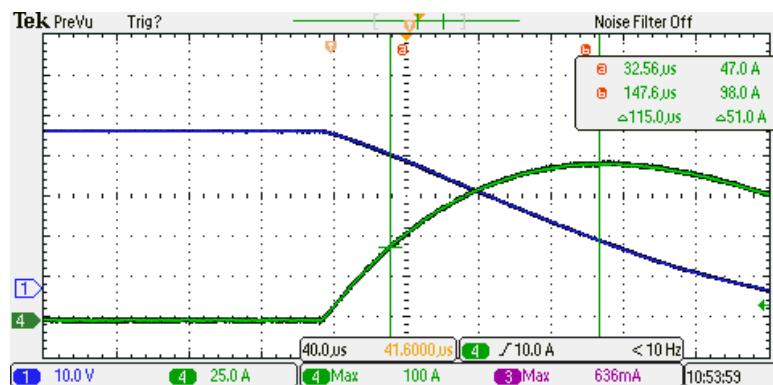


Figure 7-22 Width of short circuit current

### 7.4.2. Fuse

The next figure shows the succeed implementation of the crowbar protection. The fuse blew up at approximately 240  $\mu\text{s}$ , and it took less than 100  $\mu\text{s}$  to clear the arc inside the fuse. It should be noticed that the applied voltage was 120 volts, and it was not applied the operating voltage of the converter. Therefore, the fuse will blow up faster because the stored energy at crowbar capacitor will be also higher.

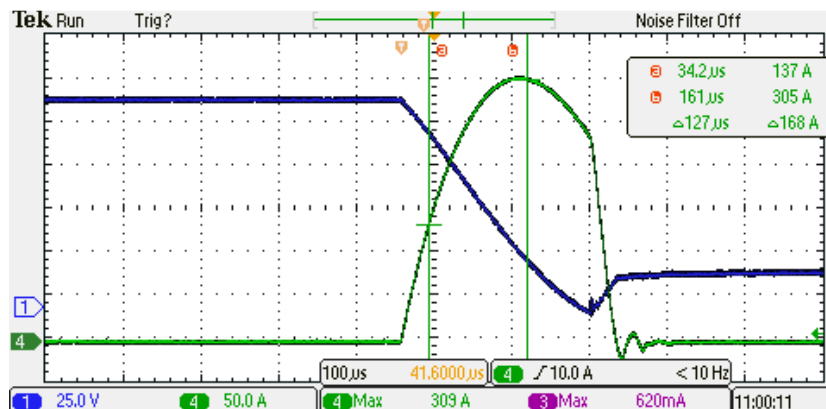


Figure 7-23 Fuse blown up



# 8.Laboratory work: Converter

This chapter begins with some figures which show the designed setup under test in the laboratory. After the setup figures, some tests about the work coil behaviour at different frequencies is presented. Furthermore, explanation and validation about why the resonant tank did not resonate at the expected frequency is exposed.

## 8.1. Setup

The next two figures show the converter with details.

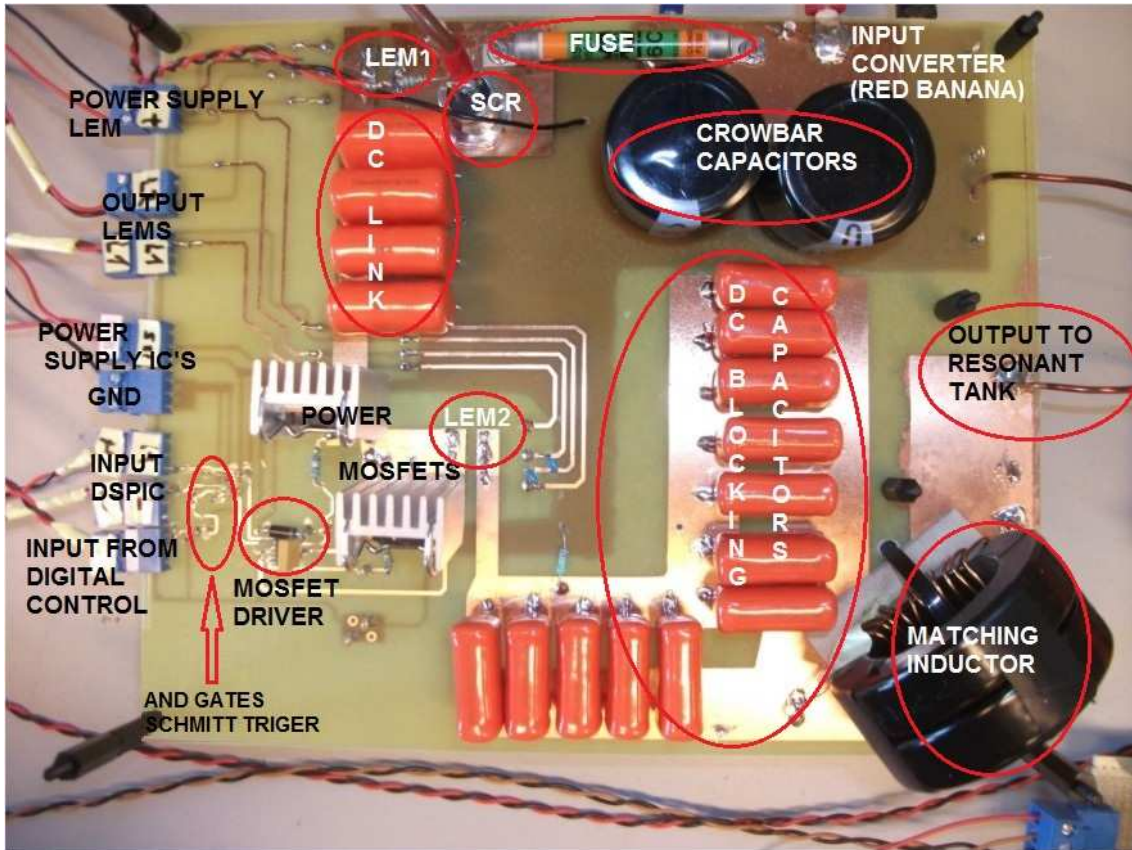


Figure 8-1 Setup buildt in the laboratory

Preceding figure shows where is placed each component in the converter.

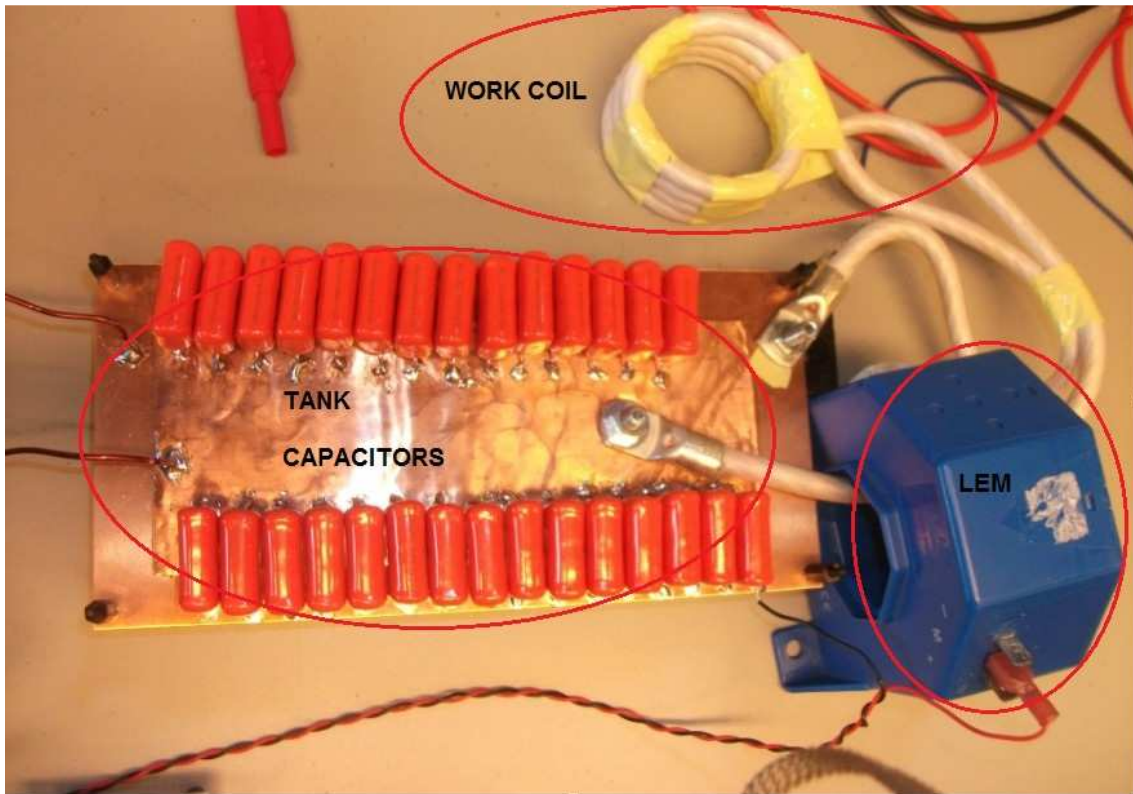


Figure 8-2 Setup built in the laboratory II

Previous figure shows the resonant tank circuit.

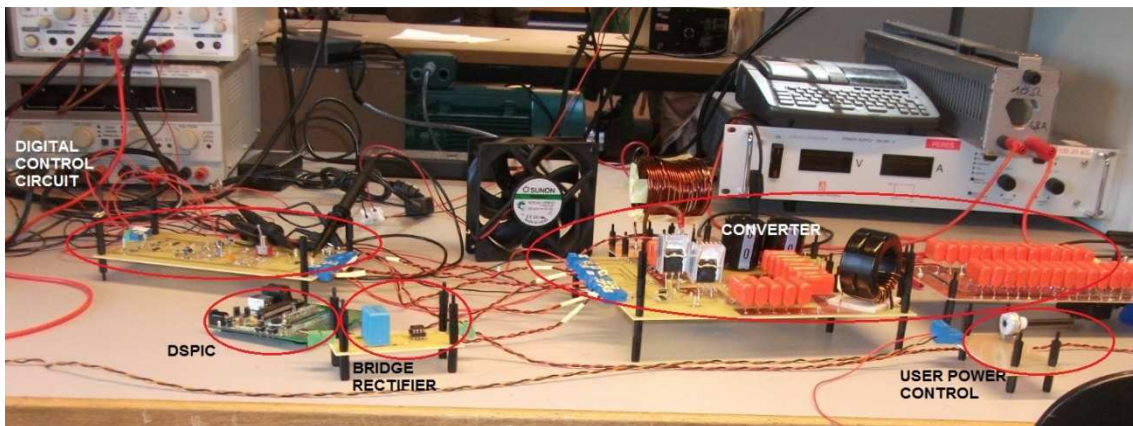


Figure 8-3 General setup

Previous figure shows the general setup implemented in the laboratory.

## 8.2. Testing work coil

This point of the chapter presents the behaviour of the work coil at different frequencies. It should be remarked that the resonant tank was designed to resonate at 140 KHz. As can be seen in the results obtained in the laboratory the resonant frequency was not 140 KHz. At the end of this point is explained why it did not work at this frequency. Moreover is presented the simulation that validates the explanation.

Test 1:

Next figure shows the work coil current applying next conditions:

- Switching frequency: 140.7 KHz.
- Voltage supplied to converter: 42 V.

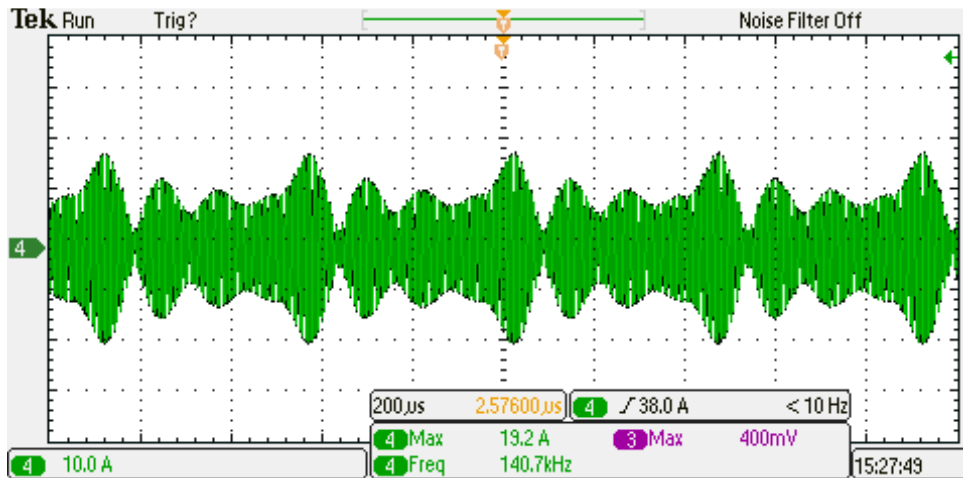


Figure 8-4 Current at work coil (140.7kHz)

The current presented unexpected oscillations at this frequency. Moreover the current at the work coil was only 19.2 amps. Latter current shows that the resonant tank does not resonate at 140 KHz, since the current value was lower in comparison to the expected value.

Test 2:

Next figure shows the work coil current applying next conditions:

- Switching frequency: 138.3 KHz.
- Voltage supplied to converter: 50 V.

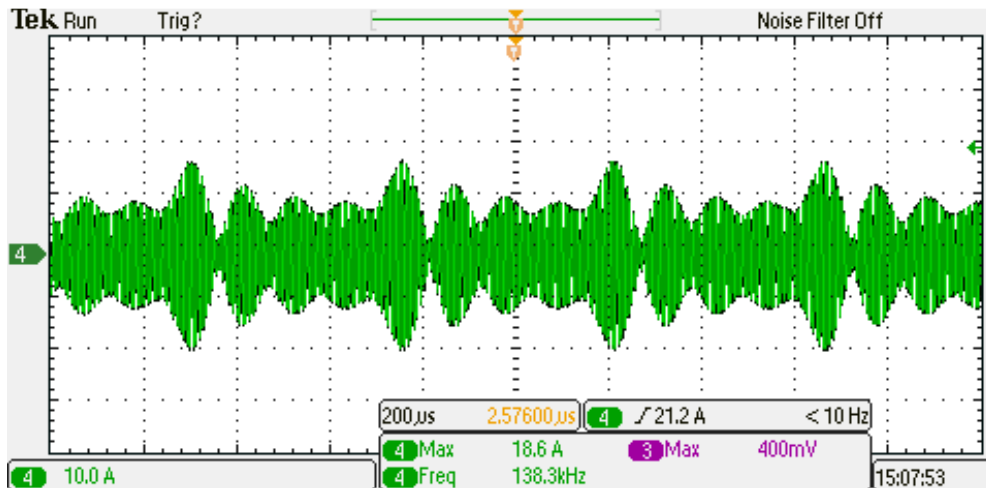


Figure 8-5 Current at work coil (138.3)

The switching frequency is lower and the supplied voltage is higher than previous test. Even so, the current value was lower, 18.6 amps was the maximum value. This means that the frequency is below than the resonant one.

Test 3:

Next figure shows the work coil current applying next conditions:

- Switching frequency: 148 KHz.
- Voltage supplied to converter: 32 V.

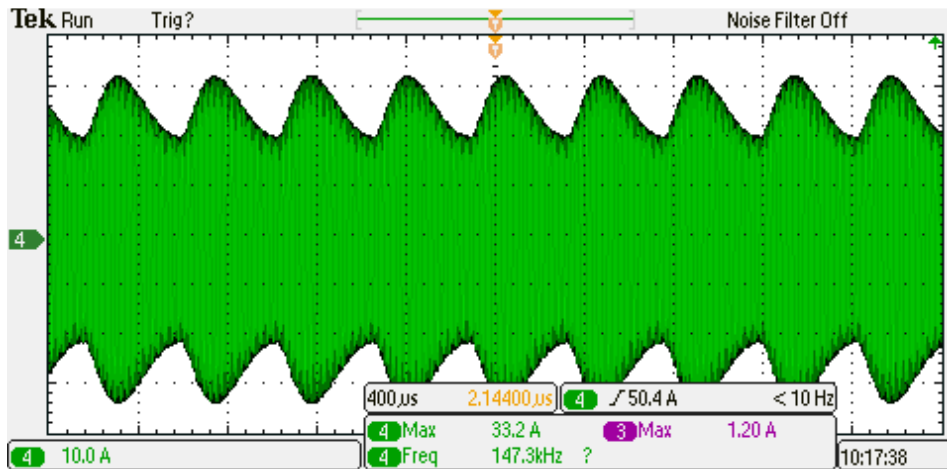


Figure 8-6 Current at work coil (148 KHz)

The work coil presented smooth current profile at these conditions and the current values are higher than previous tests. Although there is still the presence of oscillations which means that this is not the resonant frequency, this frequency is closed to the resonant one.

Test 4:

Next figure shows the work coil current applying next conditions:

- Switching frequency: 149.3 KHz.
- Voltage supplied to converter: 36 V.

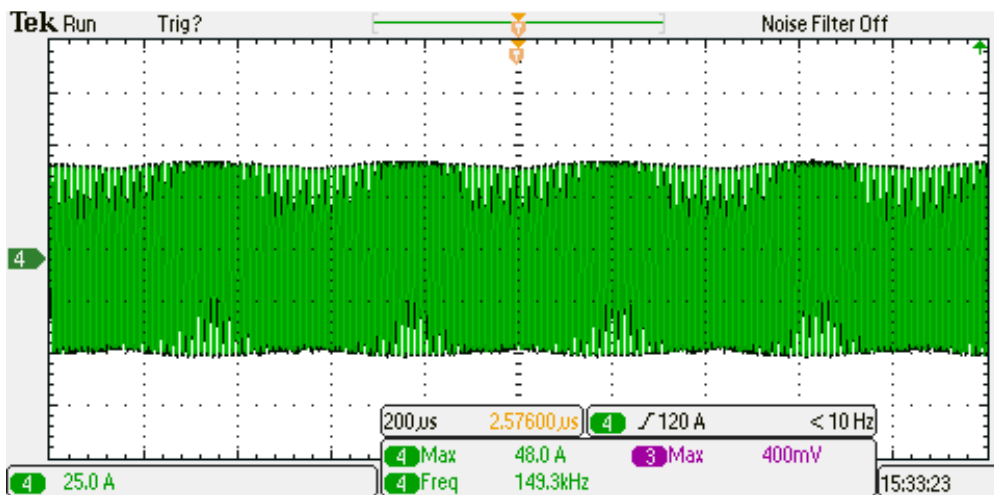


Figure 8-7 Current at work coil (149.3KHz)

As can be seen the current profile does not present oscillations and the gain of the current is higher in comparison to previous tests. Applying only 36 volts, the peak current at the work coil was 48 amps.

Next figure shows the waveform at the work coil with more definition.

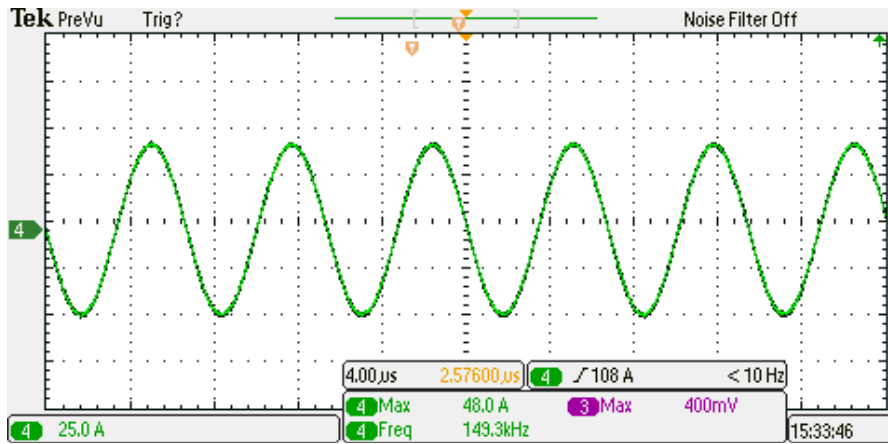


Figure 8-8 Detailed current at work coil (149.3KHz)

The waveform is purely sinusoidal, as is expected within resonant circuit.

### 8.2.1. Frequency deviation - Explanation.

The explanation of this deviation of 10 KHz respect to the expected one is due to the component which formed the circuit were not exactly as simulated ones. The value of the capacitance at resonant tank was a slightly higher because there are fixed values of capacitance in the market. The simulated capacitance value at resonant tank was 900 nF and the capacitance installed in the setup was 957 nF. Moreover the work coil was not placed with disposition which was calculated, i.e. the inductance value was calculated and measured as 1.4 µF and this value was given only when the inductor legs were straight. In order to accomplished safety reason, the disposition of the work coil was change and the legs were bound to allow the plastic cage cover the entire setup. This disposition of the work coil caused a slightly decrement of its inductance value. Therefore, these small changes related to the capacitance value as well as inductance value caused a deviation of the resonant frequency.

The new value of the work coil is given by the next expression:

$$L = \frac{1}{(2\pi f)^2 * C} = \frac{1}{(2\pi * 140\text{KHz})^2 * 957\text{nF}} = 1.2 \mu\text{H} \quad (8.1)$$

### 8.2.2. Validation of new frequency with laboratory parameters

In order to validate the explanation about the change at the resonant frequency, the real system was simulated in LTspice. Next figure shows the schematic of the simulations and after that is presented the parameter values at the setup and the calculated at the work coil including the parasitic resistance.

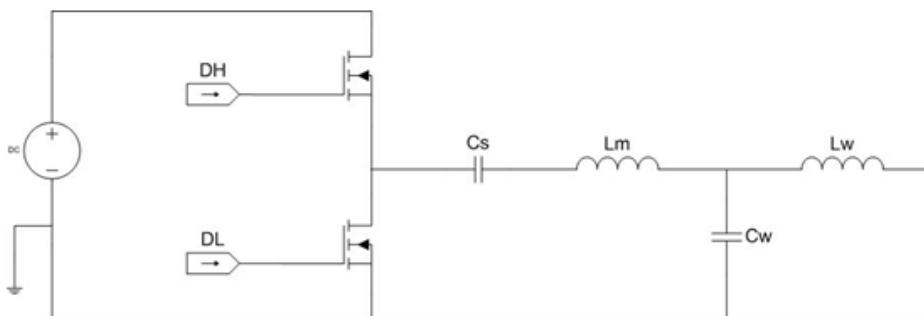


Figure 8-9 simulated schematic

	Intrinsic value	Parasitic resistance
<b>Cs</b>	396 nF	407 $\mu\Omega$
<b>Lm</b>	34 nH	1 $\Omega$
<b>Cw</b>	957 nF	174 $\mu\Omega$
<b>Lw</b>	1.2 $\mu\text{H}$	5 m $\Omega$

Table 8.1 Parameter values of the components at the simulation

Next figure shows the simulation of the current applying 149.3 KHz and 36 volts at the converter terminals in order to compare the final test with the simulations.

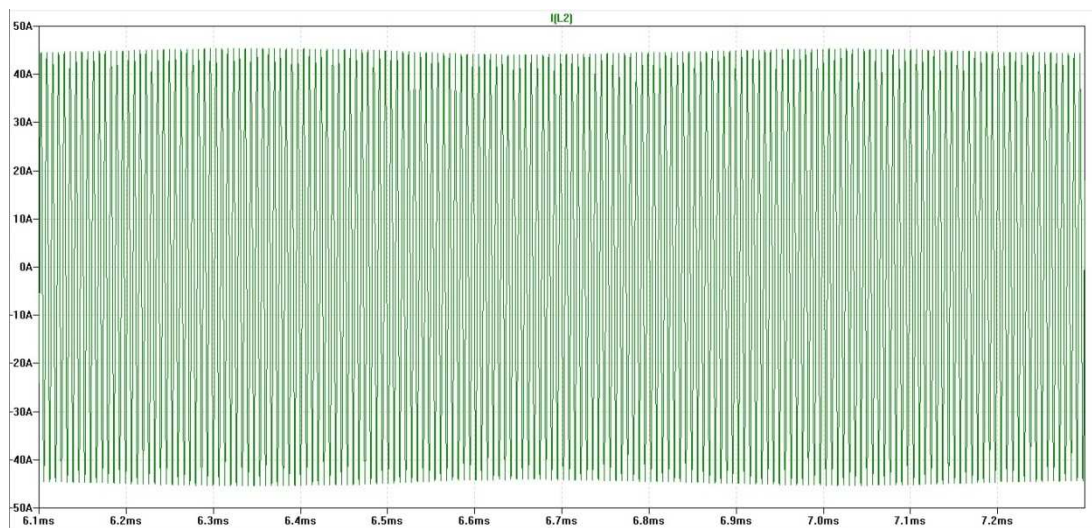


Figure 8-10 Simulated current at work coil

The peak value reached at the simulation was 46 amps, which is 2 amps of difference from the real setup. Being a resonant circuit this simulation validates all the explanations about the change in the resonant frequency.

## 9. Conclusions and future work

*This chapter presents the conclusions and future work may be interesting to develop further the thesis.*

The proposed half bridge converter with resonant tank has been tested in simulation and implemented the setup in the laboratory. The development of the setup has been completely successful since it has been achieved the goals of the thesis. Moreover, the problems encountered during the development of present thesis and the adopted solutions have been documented.

The digital control designed in the microcontroller was implemented successfully and the frequency signals that feed the power mosfets worked at the proper values.

Furthermore, the crowbar circuit protection has been designed and tested in the laboratory with positive result. The converter will be protected in case of malfunction events.

Finally, it should be said that the lack of time did not allow running more test in the laboratory. Running test applying higher voltage between the converter terminals should be interesting in order to study the behavior of the converter and especially the higher current that could be reached at the work coil.

### 9.1. Future work

- Study of the interaction between the work coil and different piece of metals that can be placed inside the patient with localized tumor.
- After study previous point, test the setup in small animals.

---

## Bibliography

---

1. Riadh W. Y. Habash, Rajeev Bansal, Daniel Krewski, Hafid T. Alhafid. "Thermal therapy-Part 2". Critical reviews in biomedical engineering.
2. I. Nagano, H. Nagae, Y. Shiozaki et al. "Development of a portable cancer treatment system using induction heating- A new weapon for killing the cancer".
3. Riadh W. Y. Habash, Rajeev Bansal, Daniel Krewski, Hafid T. Alhafid. "Thermal therapy-1". Critical reviews in biomedical engineering.
4. Seyer Nasr Tabatabaei, Sylvain Martel. "Hyperthermia via AC electromagnetic field and magnetic nanoparticle integrated in micro-carriers navigable in blood vessels".
5. Riadh W. Y. Habash, Rajeev Bansal, Daniel Krewski, Hafid T. Alhafid. "Thermal therapy-Part 4". Critical reviews in biomedical engineering.
6. Guojun Ma, Guotai Jiang. "Review of tumor hyperthermi technique in biomedical engineering frontier.
7. Press, Bronzino Joseph. "The biomedical engineering handbook". ISBN:978.0849385940. CRC and (1999), 2 Edition.
8. Segerstrom S, Miller G. Psychological stress and the human immune system: A meta-analytic study of 30 years of inquiry. Psychological Bulletin 2004 and 130(4):601–630.
9. Semiconductor., Induction heating systme topology. Review. Application note\_9012. Fairchild.
10. Ned Mohan et al. Power electronics. Converters, applications and design. ISBN:978-0471226932. Edition 3, 2002.
11. Richard Burnett, "Induction\_heating".
12. Soe Sandar, Han phyo and Nyein Soe. "Design, calculation and performance testing of heating coil in induction surface hardening machine".
14. A. Merello, A. Rugginenti and M. Graso. "Using monolithic high voltage gate drivers". International Rectifier.
15. Silicon N-Channel MOS (DTMOS II). TK40J60U. Toshiba\_Mosfet, Datasheet.
16. Ned Mohan et al. Power electronics. Converters, applications and design.
17. IPC2221, Generic standard of printed board design.
18. Dow, Corning\_340. Datasheet.

19. Charles Phillips, Royce Harbor. Feedback control systems. ISBN: 0-13-949090-6. Prentice Hall. 2000.
20. Pei Ying Chen. "A new design method of PID controller for inverse processes with dead, time".
21. Katsuhiko Ogata. "Modern control engineering". ISBN: 978-0132273077. 3rd, Edition.
22. T.W.Martin, S.S. Ang. "Digital Control For Switching Frecuencies".
23. Katsuhiko Ogata, Discrete-Time Control Systems. ISBN:978-0130342812. 2nd Edition.1995.
24. Michael Johnson, Mohammad Moradi, PID Control: New Identification and Desing Methods, ISBN: 978-1852337025. Springer 2005.
25. "28/44 pin, High performance swith mode power supply digital signal controllers".Dspic30F1010/202X, Datasheet. Microchip.
26. Jorge Zambada. "Sinusoidal control of PMSM motors with dspic30F DSC". Application note, 1017. Microchip.
27. Randi Yates. " Fixed-Point Arithmetic, An Introduction".
28. Comparing Flotaing-Point and Fixed-Point Implementations on ADI Blackfin Processors with LabVIEW, National Instruments.
29. MPLAB COMPILER FOR PIC24 AND dsPACE DSCs, USERS GUIDE, MICROCHIP.
30. Robert Erickson, Dragan Maksimovic. "Fundamentals of power electronics". ISBN:0-7923-7270-0. 2nd, edition.2000.
31. Powder cores, Magnetics\_Datasheet. .
32. R. Clarke. "A introduction to the air cored coil". Slides from, Surrey University.
33. "Section 10, Watchdog Timer and Power Saving Modes". Microchip.
34. Thyristor theory and design consideration, Handbook, On Semiconductor.
35. High Power Silicon Controlled Rectifier, 1200volts, 63Arms, Solid State\_Datasheet.
36. Semiconductor Fuse, 6-80A, 690V. Document 35785312. Copper Bussmann,Datasheet.
37. EMC Improvement Guidelines. Application Note, Atmel.
38. Bussmann, High speed fuses. Application guide.
39. Film Capacitors. General technical information, Epcos.



## Appendix A

### List of components

Next table shows the components used for the project implementation at the laboratory. The rows in red colour represent the components used for digital control. The rows in blue colour represent the components used in order to drive the power mosfets. The rows in green colour represent the components used in the converter.

Component	Model	Amount	Price/unit (Kr)
Comparator	MAX963ESD+ IC, COMPARATOR HIGH SPEED, DUAL	2	23.34
Inverter gate	74AHCT1G04GW/T1 74AHCT SINGLE GATE, SMD, 74AHCT1G04	2	1.74
AND gate	74AHCT1G08GW 74AHCT SINGLE GATE, 74AHCT1G08, 5TSSOP	2	4.33
SR-Latch	CD4043BE IC, CMOS QUAD NOR, 4043, DIP16, 18V	1	5.15
OR gate	SN74AHCT32N LOGIC, QUAD 2IN POS-OR GATE, 14DIP	1	1.3
Inverter Schmitt Trigger	HEF40106BP IC, HEX INVERTER, SCHMITT, LOCMOS, DIP14	1	0.49
Inverter gate	HCF4069UBEY- IC, 4000 CMOS, 4069, DIP14, 5V	1	0.53
XOR gate	74AHCT1G86W5-7 GATE, XOS OR, SGL MOSFET, 50 ns, DIP-8	1	3.21
Thyristor driver	IRS4427PBF IRS4427PBF - IC, IGBT / MOSFET, 50 ns, DIP-8	1	17.29
LED red	-	2	-
Resistance	1Ω,100Ω, 133Ω,1kΩ,1M Ω, 2.7MΩ	2,2,2,2,4,2	-
Thyristor	C147D, Solid state thyristors 400V,63A,TO65	1	76.13
Capacitor	B43501-330uF,450V	2	110.61
Inverter gate	74AHCT1G04GW/T1 74AHCT SINGLE GATE, SMD, 74AHCT1G04	2	1.74
Inverter Schmitt trigger	74AHCT1G14SE-7 INVERTER, SCHMITT- TRIG, 1 IP, SOT353	1	2.87
Diode	STTH1R04QRL ULTRAFAST 400V	1	-
Capacitor	CK06BX684K, Capacitor,50V,680nF	1	-
Mosfet driver	IR21064SPBF DRIVER, MOSFET HIGH/LOW, SMD, 21064	2	38.63
Dspic30F1010			33.69
Demo board			400
Power mosfet	TK40J60U -MOSFET, N CH, 600V, 40A,TO220SIS	2	123.30
Heat sink	WA-T247-101E TO-247	2	-
Capacitor	BFC237514333 Pulse Film Capacitors 33000pF 5% 630volts	40	10.61
Capacitor	BFC237514274 Pulse Film Capacitors .27uF 5% 630volts	5	26.41

HF Litz wire 1 meter	-	1	-
Powder core	-	2	-
LEM LA-25-NP	-	-	188.38
LEM 505-S	-	-	-
<b>Approximation of total price</b>			1214 Kr

---

## Appendix B

### Selecting capacitors for inverter

---

*This appendix shows the characteristics of the chosen capacitors and why are suitable for the operating conditions. This appendix is based on datasheet capacitors and (39).*

---

There are different kinds of capacitors in the market, but not all of them are appropriate for the designed inverter. High frequency and high current are presented at the capacitors. Those specifications must be accomplished by them, otherwise the capacitors will not provide current enough, and as worst case scenario capacitors may blow because of the dielectric cannot withstand the fast variation of voltage between their terminals. So it is of paramount importance to choose the proper kind of capacitors in order to achieve satisfactory behaviour of the inverter.

MKP capacitors are suitable capacitors for operating conditions. This kind of capacitors is a subset of metalized thin film capacitors and their characteristics are:

- High frequency- high power application
- Low dissipation factor in the entire temperature range
- Low moisture absorption

Preceding characteristics are explained in next paragraphs.

#### ***c.1) High frequency- high power***

This fact will be explained by means of figures presented in the datasheet capacitor. The chosen capacitors have a value of 33 nF each one, but in order to explained clearly the figures 10 nF will be used for that explanation. Next figure shows the RSM voltage that can be applied against the frequency.

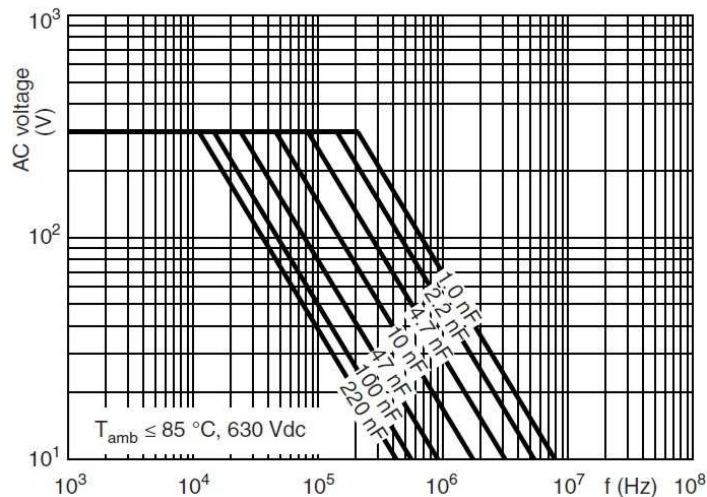


**Figure B. 1 Voltage against frequency**

As can be seen in the figure, the graph is defined by linear function, and it presents two slopes, first region is depicted as zero slope, and second region is depicted as negative slope. Taking as an example 10 nF, it is possible to notice that it can be applied 300 V<sub>RSM</sub> when applying up to 50 KHz. After this frequency the applied voltage must decrease and keep below the limit. The explanation of these limits is as follows:

Next figure shows more clear the capacitor behavior against frequency. It should be noticed that there are 3 regions, but region C is in order of MHz for chosen capacitors, so it will be considered negligible.

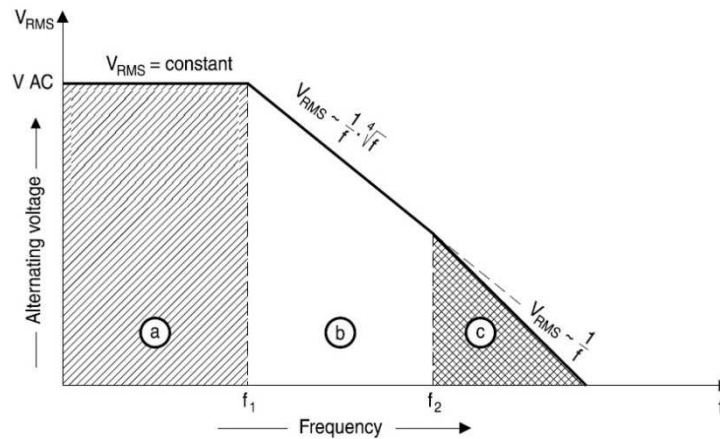


**Figure B. 2 Alternating voltage limit depending on frequency**

Region A:

Region A presents constant value of applied RMS voltage up to the frequency limit of  $f_1$ . This voltage must not be exceeded, otherwise corona discharge would start to occur and it may degrade the film metallization and the dielectric, and thus, it would change the value of the capacitance. As a worst case scenario the dielectric can be so damaged that it may blow up.

Region B:

This region presents the negative slope. From  $f_1$  to  $f_2$ , the more applied frequency, the less must be the applied voltage. This fact is related to thermal power dissipation. When increasing the frequency, the power generated increases and if the generated power exceeds the capability of the capacitor to dissipate energy, the capacitor will be destroyed. Forthcoming equations show the powers.

$$P_{gen} = V_{RMS}^2 * 2 * \pi * f * C * \tan \delta \tag{b.1}$$

Where:

$V_{RMS}$ = applied voltage

$f$ = applied frequency

$C$ = capacitance value

$\tan \delta$ = dissipation factor, which is defined by:  $\tan \delta = ESR * 2 * \pi * f * C$

So finally the equation is:

$$P_{gen} = V_{RMS}^2 * ESR * (2 * \pi * f * C)^2 \tag{b.2}$$

As can be derived from previous equations, it is not a linear relation, but it is squared, so a positive variation of frequency will cause larger power generated.

The power dissipated by capacitor is given by:

$$P_{diss} = \alpha * A * \Delta T \tag{b.3}$$

Where:

$\alpha$ = heat transfer coefficient

A= surface are of the capacitor

$\Delta T$ = self-heating or steady-state overheating attained at the hottest part of the capacitor surface in relation to the surrounding atmosphere

The heat transfer coefficient and the dissipation factor depend on technology, construction, material and geometry of each capacitor. Dissipation factor depends also on frequency and temperature.

The self-heating parameter depends mainly on the dielectric material. MKP capacitors have polypropylene as dielectric and its self heating value must not exceed 10°C. By contrast some dielectrics used in other kind of metalized capacitors can withstand larger  $\Delta T$ . For example, polyester or polyethylene naphthalene can withstand 15°C.

Therefore, safety conditions are met when  $P_{gen} \leq P_{diss}$ .

### c.1.1) Maximum Ac voltage versus temperature

Figure B-1 shows the graph for the chosen capacitor. It should be noticed that the values are given for ambient temperature lower than 85°C. In case that the ambient temperature exceeds mentioned temperature, the applied RMS voltage is derated. It is of paramount importance to take this fact into account when choosing capacitors, otherwise if the temperature is higher than expected and the capacitor was close to the limit, it may lose their properties and as worst case scenario, capacitor may blow up. See next figures.

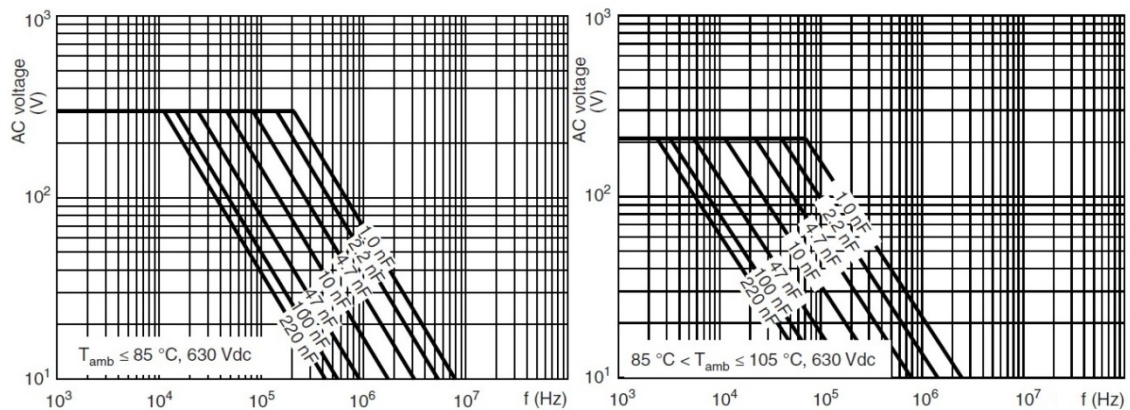


Figure B. 3 Variation of voltage and frequency depending on temperature

As can be seen at region A, when the ambient temperature is lower than 85°C the maximum allowable RMS voltage is 300 volts, and when the temperature is higher than 85°C the maximum allowable RMS voltage is 200 volts. Moreover, transition change between region A and region B is also derated when the temperature increases above the 85°C. Taking as a reference 10 nF, the change between regions occurs at 50 KHz when  $T_{amb} < 85^\circ C$  and when  $T_{amb} > 85^\circ C$  the change between region occurs at 12 KHz.

### c.2) Low dissipation factor in the entire temperature range

Next figure shows the variation of the dissipation factor against temperature for different kind of film capacitors. MKT and MFT use as dielectric polyethylene terephthalate, MKP and MFP use as dielectric polypropylene and MKN uses as dielectric polyethylene naphthalene.

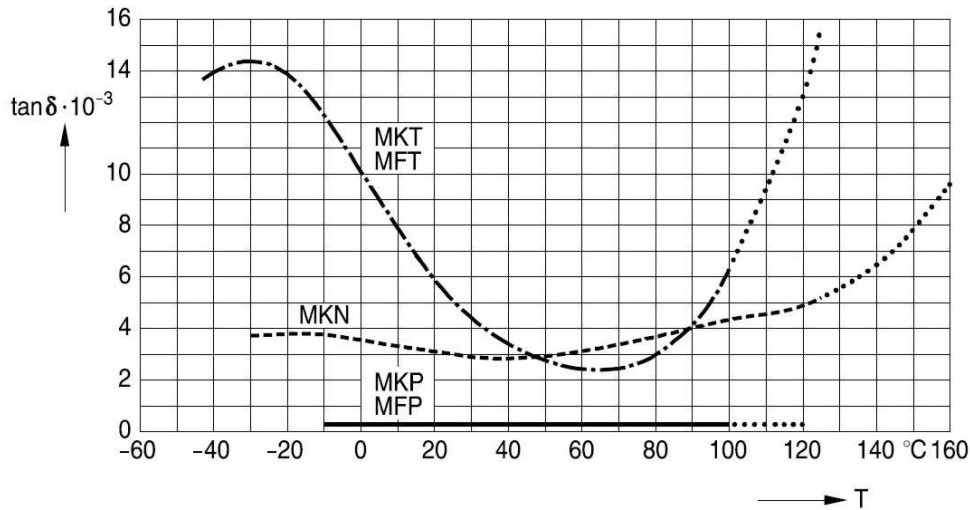


Figure B. 4 Dissipation factor for different dielectrics

It should be noticed that for MKP and MFP there is no variation of the dissipation factor in their entire temperature range. By contrast, the other dielectrics show that the temperature really affects their dissipation factor, especially for MKT and MFT.

**c.3) Low moisture absorption**

The MKP capacitors and MFP does not present large variation of their capacitance when the humidity increases. The maximum variation is presented at 80% of humidity, being less than 0.5%. By contrast, the other capacitors present variation up to 3%. See next figure.

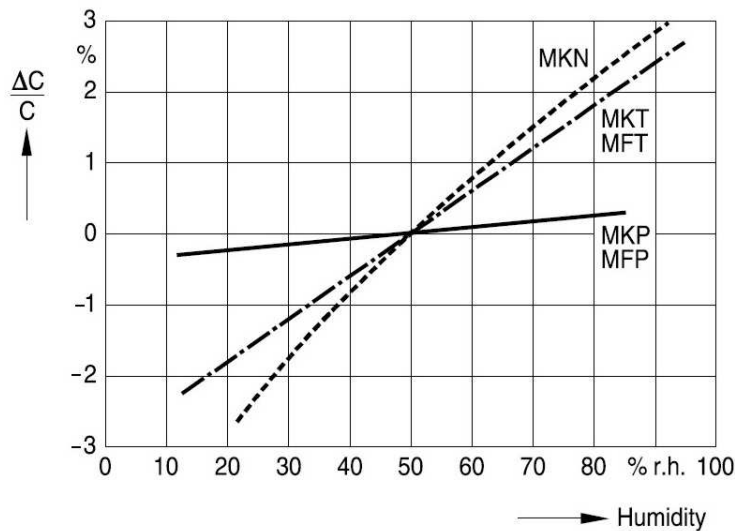


Figure B. 5 Moisture absorption for different dielectrics

**c.4) Conclusions**

In this appendix was explained different facts that must be taking into account when choosing capacitor. MKP and MFP were the only suitable capacitors for the developed application. Although MFP was also suitable, it is commonly used for application for higher current pulse than MKP. Even MFP could be used for this application it leads to an oversize of the component, and thus, an unnecessary cost increment.

---

## Appendix C

### Laboratory experiment. DC-link capacitors

---

*The aim of these small experiments is to test the behavior of film capacitors and electrolytic capacitors at DC-link.*

---

Before explaining the results in the laboratory, it should be explained the importance of the DC-link, especially when the switching frequency at the converter is high.

First, DC-link can supply larger current pulses than voltage supply but the most important fact for specifications of the designed converter is to make short the current path from drain at high side mosfet to ground. The reason is explained as follows:

In next figure is depicted the power supply, cables which connect power supply to half bridge, and the half bridge.

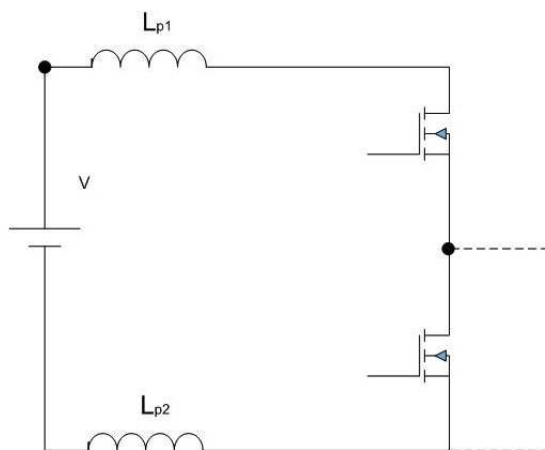


**Figure C. 1 Equivalent circuit with parasitic inductance**

As can be seen, the cables present parasitic inductance and this value depends on the length of the cable. In the laboratory the available cables have associated parasitic inductance of approximately 15nH/cm, since their length is 1 meter; their associated parasitic inductance is 1.5  $\mu$ H. Therefore,  $L_{p1}$  and  $L_{p2}$  will be 1.5  $\mu$ H each one. The circuit will also present parasitic inductance at the half bridge topology, but it has been eliminated from this explanation, since the effect of that inductance will be present whether DC-link is mounted or not.

The circuit is defined by 2<sup>nd</sup> Kirchhoff's law as follows:

$$V_x = V_{dc} - (V_{Lp1} + V_{Lp2}) \quad (C.1)$$

Where:

$V_x$ = voltage at the load

$V_{dc}$ = voltage provided by power supply

$V_{Lp1}, L_{p2}$ = voltage at parasitic inductances

The current will be supplied by the power supply when high side mosfet is on. The transient voltage at the terminals of high side mosfet had rise/fall time of 20ns. Assuming that current supplied is 5 amps, the voltage at the parasitic inductance is:

$$V_{Lp1} = L_{p1} * \frac{di}{dt} = L_{p1} * \frac{\Delta i}{\Delta t} = 1.5 * 10^{-6} * \frac{0 - 5}{20 * 10^{-9}} = -375 \text{ V} \quad (C.2)$$

So the voltage at the load will be:

$$V_x = 300 - (375 - 375) = 1050 \text{ V} \quad (\text{C.3})$$

As can be seen there will be a voltage overshoot of 1050 V, which will destroy the mosfets.

DC-link will supply the current need at the converter. Since DC-link is placed close to high side mosfet, the distance is reduced, and thus, the parasitic inductance is also reduced. See next figure.

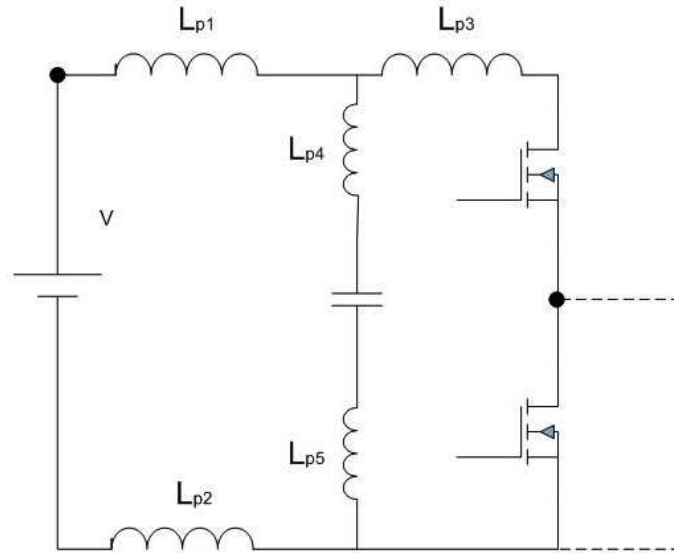


Figure C. 2 Equivalent circuit with parasitic inductance and DC-Link

Assuming the distance from DC-link to high side mosfet of 3 cm, the parasitic inductance will be 45nH. Moreover the total parasitic inductance at the capacitor legs will be approximately 30nH. The voltage at the load will be given by:

$$V_x = 300 - \left( 45 * 10^{-9} * \frac{0 - 5}{20 * 10^{-9}} + 30 * 10^{-9} * \frac{0 - 5}{20 * 10^{-9}} \right) = 318.75 \text{ V} \quad (\text{C.4})$$

So as was derived, the absence of DC-link will cause an overshoot of 750 V and the presence of DC-link will cause an overshoot of 18.75 V.

Laboratory experiment:

The experiment was run with the setup depicted in the next figure.

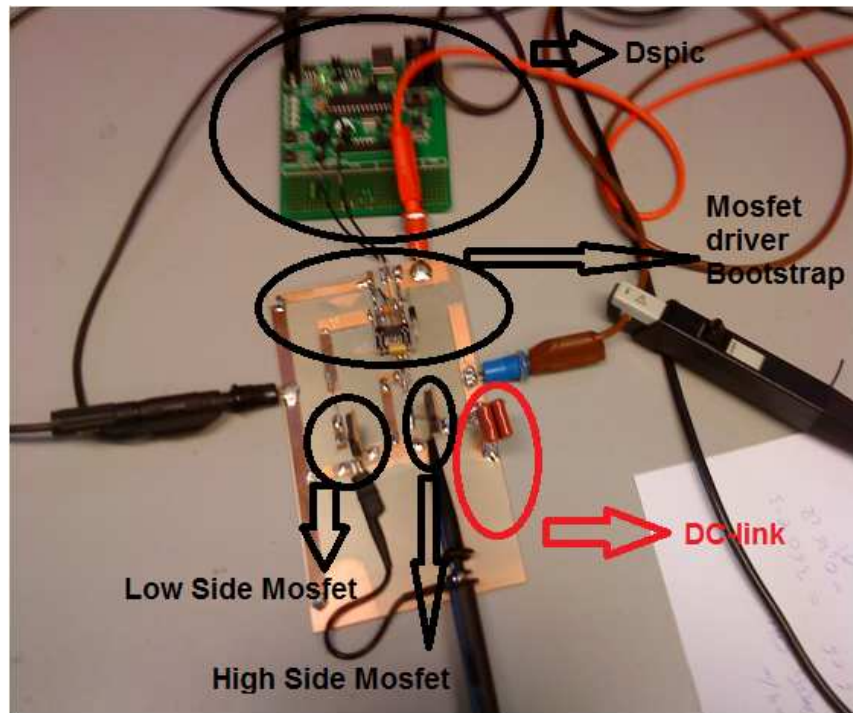


Figure C. 3 Setup built in the laboratory

The applied voltage to mosfet driver was 18 volts, and the applied voltage at the input of the half bridge was 9.1 volts. As measurements, voltage was taken from high side mosfet to drain-source. However, the current probe was placed at the legs of the capacitors under test..

In order to compare properly the behavior of the two kinds of capacitors; the capacitors were chosen with similar electrical characteristics. Therefore, two pair of metalized thin film capacitors and two pair of electrolytic capacitors was chosen. The equivalent capacitance value was 1  $\mu$ F and the maximum allowable voltage that can withstand was 50 volts.

**c.1 Testing capacitors.**

Forthcoming figures show the behaviour of metalized film capacitor and electrolytic capacitor respectively. Current probe was placed at the legs of the capacitors.

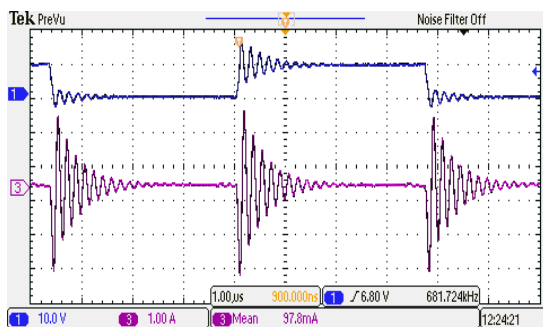


Figure C. 4 Voltage and current with thin film capacitor

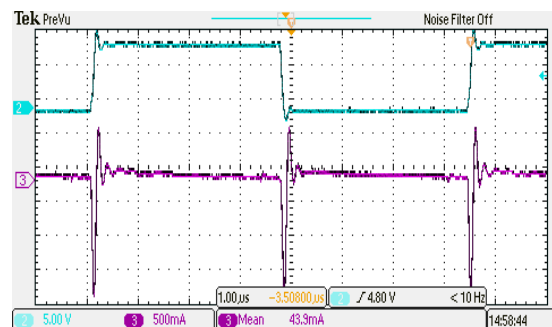


Figure C. 5 Voltage and current with electrolytic capacitor

Ideally the voltage profile and current profile should be a clean waveform, i.e. the waveforms do not present any oscillations. However, the results obtained in these experiments are far from previous notation due to the presence of parasitic inductance related to cable, PCB tracks and capacitor legs. The presence of these parasitic inductances together with capacitor gives as a result the generation of oscillations at the voltage and current profile. The period of the frequency is approximately 5 cycles per 1  $\mu$ s, so the resonant frequency is 5MHz.

From previous figures can be derived that film capacitor provides more current (2.5 A) than electrolytic capacitor (lower than 2 A). Moreover the oscillation at electrolytic capacitor is damped after 40 ns and the film capacitor is damped after 2  $\mu$ s. The reason both cases is due to the ESR, i.e. for first case, the greater the resistance, the less available current, and in second case, when a resonant circuit has a resistance, the voltage and current are damped proportionally to the resistance value.

---

## Appendix D

### Dspic program

---

*In this appendix is shown the implemented microcontroller program.*

---

The code programmed is shown below:

```
#include "p30f1010.h"

/* Configuration Bit Settings */
_FOSCSEL(FRC_PLL)
_FOSC(CSW_FSCM_OFF & FRC_HI_RANGE & OSC2_CLKO)
_FPOR(PWRT_128)
_FGS(CODE_PROT_OFF)
_FBS(BSS_NO_FLASH)
typedef signed int SFRAC16;
#define SWITCH2 (!PORTFbits.RF6) // Declaration of SWITCH S2
// Use this MACRO when using floats to initialize signed 16-bit fractional
#define SFloat_To_SFrac16(Float_Value) \
    ((Float_Value < 0.0) ? (SFRAC16)(32768 * (Float_Value) - 0.5) \
    : (SFRAC16)(32767 * (Float_Value) + 0.5))

unsigned int i=0; // Back-up variable for the SWITCH S2
void InitADC(void); // Declaration of all functions
void InitPWM(void);
void InitUserInt(void);
void PIDControl (void);
void PWM (void);

SFRAC16 Meas_Current, Ref_Current; // Actual and Desired Current
```

```
SFRAC16 ControlOutput = 0;           // Controller output, used as a voltage output,
SFRAC16 Frequency;
```

```
// PID gains used by the controller.
```

```
SFRAC16 Kp = SFloat_To_SFrac16(0.19);           // P Gain
```

```
SFRAC16 Ki = SFloat_To_SFrac16(0.19);           // I Gain
```

```
SFRAC16 Kd = SFloat_To_SFrac16(0.000);           // D Gain
```

```
// Constants used by the PID controller, since a MAC operation is used, the
```

```
// PID structure is changed
```

```
SFRAC16 ControlDifference[3] \
```

```
    __attribute__((__space__(xmemory), __aligned__(4)));
```

```
SFRAC16 PIDCoefficients[3] \
```

```
    __attribute__((__space__(ymemory), __aligned__(4)));
```

```
/******
```

```
Function:          void __attribute__((__interrupt__)) _INT0Interrupt(void)
```

```
*****/
```

```
void __attribute__((interrupt , no_auto_psv)) _INT2Interrupt (void)
```

```
{
```

```
    IFS1bits.INT2IF=0;           // Clear the flag for the INT2
```

```
    i=i+1;
```

```
    if (i==1)
```

```
    {
```

```
        PTCONbits.PTEN=1;
```

```
        ADCONbits.ADON = 1;
```

```
    }
```

```
    if (i==2)
```

```

    {
        ADCONbits.ADON = 0;    // Stop the PWM module
        PTCONbits.PTEN = 0;   // Stop PWM
        i=0;                   // Reset the counter
    }
}

/*****
Function:          void __attribute__((__interrupt__)) _ADCInterrupt(void)
*****/

void __attribute__((interrupt , auto_psv)) _ADCInterrupt (void)
{
    IFS0bits.ADIF = 0;        // Clear ADC Interrupt Flag
    IFS2bits.ADCP2IF=0;      // Clear ADC Pair 2 Interrupt Flag
    ADSTATbits.P2RDY= 0;    // Clear the register of the conversion of the buffer
    // The Control adaptation
    Meas_Current=(ADCBUF4)*(3.8701);
    Ref_Current=(ADCBUF5)*(8.17667);
    PIDControl();
}

/*****
Function:          int main (void)
*****/

int main (void)
{
    __builtin_write_OSCCONL(4); // Enable write in FRC Sequence enable bit
    OSCTUN=0x0007;
    InitUserInt();           // Initialize User Interface I/Os
    InitADC();               // Initialize ADC to be fractional
}

```

```

InitPWM();                // Configuration of the PWM module: 140kHz

ControlDifference[0] = 0;           // Error at K(most recent)
ControlDifference[1] = 0;           // Error at K-1
ControlDifference[2] = 0;           // Error at K-2 (least recent)

// Implementation of the discrete control
PIDCoefficients[0] = Kp+Ki+Kd;     // Modified coefficient for using MACs
PIDCoefficients[1] = -(Kp + 2*Kd); // Modified coefficient for using MACs
PIDCoefficients[2] = (Kd);         // Modified coefficient for using MACs
ADCPC1bits.SWTRG2=1;

while(i==0){}

// Wait for SWITCH S2 to be pulsed

while(1){}

}

```

/\*\*\*\*\*\*

Function: void InitPWM(void)

Overview: InitPWM, initializes the PWM as follows:

1. FPWM = 140000 Hz
2. Complementary PWMs
3. Set Duty Cycle to 0.5 for complementary
4. Set ADC to be triggered by PWM module
5. Configure deadtime to be 240 ns

\*\*\*\*\*/

```
void InitPWM(void)
```

```
{
```

```

    Frequency=(14.55*64)/0.140;    // Hexadecimal value for desired frequency
    PTCONbits.EIPU=1;              // Enable immediate Period updates
    PTPER=Frequency;               // Primary time base register of 140 kHz

```

```

MDC=PTPER/2;           // Duty cycle of 50%
PWMCON1=0x0101;       // Configuration PWM register
PHASE1=0x0000;        // PWM phase –shift register
DTR1=0x00F2;          // Dead time of 240 nS
ALTDTR1=0x00F2;       // The same dead time but in the complementary
IOCON1=0xC001;        // Complementary PWM mode

TRGCON1bits.TRGDIV = 0; // Trigger on every event
TRGCON1bits.TRGSTRT= 0; // Start the counting at the start

TRIG1 = 200;           // Trigger event at 0.214 usec from start of the PWM cycle
SEVTCMP = 1;           // Enable triggering for ADC
PTCONbits.PTEN = 1;    // Start PWM
return;
}

```

/\*\*\*\*\*\*

Function: void PWM(void)

Overview: Here the values of the new frequency are updated:

1. FPWM
2. Complementary PWMs
3. Set Duty Cycle to 0.5 for complementary
4. Set ADC to be triggered by PWM special trigger
5. Configure deadtime to be 500 ns

\*\*\*\*\*/

```
void PWM(void)
```

```
{
```

```
PTPER=(0x1E24 + ControlOutput); // Update the PWM frequency
```

```
MDC=PTPER/2;
```

```

DTR1=0x00F2;

ALTDTR1=0x00F2;

return;

}

/*****

Function:          void InitUserInt(void)
*****/

void InitUserInt(void)
{
    TRISF = 0xFFFF;           // PORTF are inputs
    TRISB = 0x0000;           // PORTB are inputs
    PORTFbits.RF6=0;          // SWITCH2 is initialize to zero
    IFS1bits.INT2IF=0;         // Clear the flag of the SWITCH S2 interrupt
    INTCON2bits.INT2EP=0;      // Interrupt on positive edge
    IEC1bits.INT2IE=1;         // External interrupt enable it
    IPC4bits.INT2IP=0x0007;    // External interrupt is the most important

    return;
}

/*****

```

Function: void InitADC(void)

Overview: Below is the code required to setup the ADC registers for:

1. 1 channel conversion (in this case RB2/AN2)
2. PWM trigger starts conversion
3. Pot is connected to CH0 and RB2/AN2
4. The data format will be signed fractional

```

*****/

void InitADC(void)

```

```

{
    ADCONbits.ADSIDL = 0;           // Operate in Idle Mode
    ADCONbits.FORM = 1;           // Fractional mode
    ADCONbits.GSWTRG = 1;        // Global software trigger bit
    ADCONbits.EIE = 0;           // Disable early interrupt
    ADCONbits.ORDER = 1;         // Odd channel first
    ADCONbits.SEQSAMP = 1;       // Sequential sampling enable
    ADCONbits.ADCS = 7;          // Clock divider is set for Fadc/16

    ADSTAT=0x0000;               // Clear the ADSTAT register
    ADSTATbits.P2RDY=0;          // Clear the ADSTAT pair bits

    ADPCFG = 0x0030;             // AN4 and AN5 are inputs
    ADCPC1bits.IRQEN2=1;         // Enable the interruption
    ADCPC1bits.SWTRG2=1;        // Trigger Source Selection for convert pair control
    ADCPC1bits.TRGSRC2=0x4;      // PWM trigger

    // Set the interrupt configuration

    IFS0bits.ADIF = 0;           // Clear ISR flag
    IEC0bits.ADIE = 1;           // Enable the ADC interrupts
    IPC2bits.ADIP = 0x0005;      //Set ADC Interrupt Priority

    return;
}

/*****

Function:          PIDControl(void)

*****/

void PIDControl(void)

```

```

{
// Declaration of the pointers

SFRAC16 *ControlDifferencePtr = ControlDifference;

SFRAC16 *PIDCoefficientsPtr = PIDCoefficients;

SFRAC16 x_prefetch;

SFRAC16 y_prefetch;

    register int reg_a asm("A");
    register int reg_b asm("B");

    reg_a = __builtin_lac(Ref_Current,0);
    reg_b = __builtin_lac(Meas_Current,0);
    reg_a = __builtin_subab();

    *ControlDifferencePtr = __builtin_sac(reg_a,0);

    reg_a = __builtin_movsac(&ControlDifferencePtr, &x_prefetch, 2,
        &PIDCoefficientsPtr, &y_prefetch, 2, 0);
    reg_a = __builtin_lac(ControlOutput, 0);

    reg_a = __builtin_mac(x_prefetch, y_prefetch,
        &ControlDifferencePtr, &x_prefetch, 2,
        &PIDCoefficientsPtr, &y_prefetch, 2, 0);
    reg_a = __builtin_mac(x_prefetch, y_prefetch,
        &ControlDifferencePtr, &x_prefetch, 2,
        &PIDCoefficientsPtr, &y_prefetch, 2, 0);
    reg_a = __builtin_mac(x_prefetch,y_prefetch,
        &ControlDifferencePtr, &x_prefetch, 2,

```

```
        &PIDCoefficientsPtr, &y_prefetch, 2, 0);  
  
// Charge the final value of the accumulator  
    ControlOutput = __builtin_sac(reg_a, 0);  
  
// Store last 2 errors  
    ControlDifference[2] = ControlDifference[1];  
    ControlDifference[1] = ControlDifference[0];  
  
    PWM();  
    return;  
}
```

---

## Appendix E

### Inductor design

---

*In this appendix is shown the implemented code in order to obtain a optimized value of the inductors..*

---

The program developed for the calculation of the size of the air coil inductor is shown below:

```
format long e
clear all
clc

c=7.1e-3;           %Thickness of the wire used
Wa=pi*(c^2)/2;     %Wire section

I=141.42;          %Approximated current value in RMS
a=0;

L=1.435e-6;        %Value of the inductance

%There are two loops: taking values for the number of turns from
1 to 10, different values of wideness are calculated

%for difference values of diameters. N:Number of turns;
a:Diameter of the workcoil; b:Wideness of the workcoil

%In the end, a matrix with the values is obtained
for N=1:1:10
    for i=1:1:10          %Size of the turns in m
        Va=linspace(50e-3,60e-3,10);
        %Vector with the possible diameters of the inductor
        a=Va(i);
        b=((0.001*N^2*((a/2)^2))/(254*L))-((114/254)*a);
        %Wideness of the workcoil
        Vb(N,i)=b;
        if b>(0.8*(a/2))          %Application of the constrains
            Vbval(N,i)=b;
        end
    end
end
```

```

else
    Vbval(N,i)=0;
end

%The constrains are applied with if/else loops
if (c*N)>b           %The thickness of the wire multiple
                    %by the number of turns has to be
                    %bigger than the wideness of the
                    %inductor

    Vcval(N,i)=0;   %The value is not valid
    Vbc(N,i)=0;

else
    Vcval(N,i)=1;   %The value is valid
    Vbc(N,i)=b;

end

%Vbc is the final vector that satisfies all the constrains
if Vbc(N,i)==0;
    Vlong(N,i)=0;
else
    long=(a*pi).*N;           %Amount of wire need
    Vlong(N,i)=long;
end

if Vbc(N,i)==0
    VPcu(N,i)=0;
else
    Pcu=((Ro*N)*(a*pi)*I^2)/Wa;           %Total losses.
    VPcu(N,i)=Pcu;
end

end

end

%The shortest wideness value

```

```

minb_past=100;
row_b=0;
column_b=0;
for i=1:1:10
    [minb_actual,I]=min(Vbval(i,:));
    if minb_actual<=minb_past && minb_actual>0
        minb_past=minb_actual;
        row_b=i;
        column_b=I;
    else
    end
    b=minb_past;
    values_b=[row_b column_b b];
end
%%The lowest power losses
minPcu_past=10000;
row_Pcu=0;
column_Pcu=0;
Ro=1.724e-8;
for i=1:1:10
    [minPcu_actual,I]=min(VPcu(i,:));
    if minPcu_actual<=minPcu_past
        minPcu_past=minPcu_actual;
        row_Pcu=i;
        column_Pcu=I;
    else
    end
    Pcu=minPcu_past;
    values_Pcu=[row_Pcu column_Pcu Pcu];
end
%%The shortest value of wire length

```

```

minlong_past=100;
row_long=0;
column_long=0;
for i=1:1:10
    [minlong_actual,I]=min(Vlong(i,:));
    if minlong_actual<=minlong_past && minlong_actual>0
        minlong_past=minlong_actual;
        row_long=i;
        column_long=I;
    else
    end
    long=minlong_past;
    values_long=[row_long column_long long];
end
plot(Vbc, 'b+:');
grid on;
hold on;
plot(Vlong, 'r+:');
%According to the plot the smallest value is for Vbc(6,3)

```